DISCRETE ELEMENT MODELLING OF SOIL - PILE INTERACTION WITH EMPHASIS ON SOIL CHARACTERISTICS AND PILE INSTALLATION METHODOLOGY

by

Ahmet Talha Gezgin

B.S., Civil Engineering, Boğaziçi University, 2012

M.S., Civil Engineering, Boğaziçi University, 2015

Submitted to the Institute for Graduate Studies in
Science and Engineering in partial fulfillment of
the requirements for the degree of
Doctor of Philosophy

Graduate Program in Civil Engineering

Boğaziçi University

2021

ACKNOWLEDGEMENTS

I appreciate my supervisor Assoc. Prof. Özer Çinicioğlu for his enormous support, endless patience, and sincere encouragement. Without his guidance, motivating attitudes, and critical help, this thesis work would not have been possible. When I was still at my bachelor's study, I remember the day I knocked at his door to share with him the passion that I had for becoming an academician. Since that day, I am always feeling lucky to have him as my mentor in this path.

Besides my supervisor, I would like to thank the rest of my thesis committee. The constructive discussions during multiple progress meetings contributed significantly to the scientific aspects of this dissertation.

I am also indebted to the financial support of The Scientific and Technological Research Council of Turkey (TUBITAK). I was honored to have a fellowship from BIDEB 2211-A program. Moreover, I was served as project coordinator for ARDEB 1002 (Short Term R&D Funding Program with project number 119M849).

I would like to extend my special thanks to Behzad Soltanbeigi for his unquestioning support. Our friendly and long discussions made this journey fruitful for me. I still remember the very first day that he instructed me with DEM technique and its background. Aside from the scientific side, our friendship has been an invaluable asset for me in the past couple of years.

I also truly appreciate the support from my colleagues at Boğaziçi University: Sedat Semih Çağlayan, Işık Ateş Kıral, Emirhan Sancak and Uğurcan Erginağ. Our long-lasting friendship will be always remembered for me. Additionally, my sincere gratefulness goes to my one of best friends Osman, who was accompanying me since the first the I entered Boğazici University. I spent more than 14 years at Boğazici University and at this moment I feel sad to say goodbye to this magnificent place. However, I will be always honored to be a "Boğaziçili", and this will help me to open

new and beautiful chapters in my life.

The last three years of my PhD were even more meaningful after meeting my wife Hilal. I had up and downs and she was all the time there to calm me. I remember in the early days of our relationship, I was overwhelmed with the pressure and doubtful thoughts regarding my PhD. Hilal turned to be my angel of hope and helped to overcome my dubious feelings within this rigorous path. Moreover, Hilal's parents were always supportive and helped me to walk joyfully through these hassles.

Last but not least, with all my heart and soul, I would like to present the biggest thanks to my family. My parents Aynur and Mustafa, did their best to support me in all stages of my life and they never lost their faith in me. Years ago I give them my word and now I am sure I have made them proud. My brothers, Fatih Mehmet and Ömer Hakan supported and encouraged me throughout all these years. We were housemates for many years with my brothers, where we established our second home far from our parents. I am in debt for every single day that we spent together as a family in Istanbul. I also send my regards to the soul of my two grandmothers and two grandfathers.

ABSTRACT

DISCRETE ELEMENT MODELLING OF SOIL - PILE INTERACTION WITH EMPHASIS ON SOIL CHARACTERISTICS AND PILE INSTALLATION METHODOLOGY

Soil-pile interaction is a complex geotechnical problem that requires rigorous multi-scale analyses. However, it is challenging to understand the micro aspects of this problem with either experimental approaches or continuum-based numerical models. On the other hand, the discrete element method (DEM) provides a powerful medium for modelling soils as particulate materials and can be used to examine soil-pile interaction at multi-scale. Accordingly, this dissertation aims to investigate soil-pile interaction with DEM modelling. For this purpose, three different subjects are discussed in this dissertation. Initially, a parametrical study has been conducted to clarify the influence of soil properties on pile penetration resistance. Later on, this study tackles the problem of computational cost; it is well known that one limiting aspect of DEM is its high computational demand. Regardingly, this dissertation also aims to clarify the validity of three techniques that are utilized to reduce computational time. In this respect, the appropriate parameters for DEM models are validated using the experimental results of a previous study. Lastly, this dissertation focuses on soil-pile interaction considering the effects of pile installation. Both jacked and replacement piles are installed into each sample and the response of the granular assembly is assessed in detail. Eventually, the jacked and replacement piles are subjected to vertical loading tests to determine their bearing capacity. The results obtained during pile construction and loading stages suggest that installation technique, in addition to soil density state and particle shape, also has a considerable effect on soil-pile interaction.

ÖZET

ZEMİN ÖZELLİKLERİNİN ETKİSİNDE ZEMİN - KAZIK ETKİLEŞİMİNİN VE KAZIK İMALAT METODOLOJİSİNİN AYRIK ELEMANLAR YÖNTEMİ İLE MODELLENMESİ

Zemin-kazık etkileşimi, titiz çok ölçekli analizler gerektiren karmaşık bir geoteknik problemidir. Bununla birlikte, bu problemin mikro yönlerini deneysel yaklaşımlar veya sürekli-tabanlı sayısal modellerle anlamak zordur. Öte yandan, ayrık eleman yöntemi (DEM), zeminleri tanecikli malzemeler olarak modellemek için güçlü bir ortam sağlar ve zemin-kazık etkileşimini çok ölçekli olarak incelemek için kullanılabilir. Buna göre, bu tez, DEM modellemesi ile zemin-kazık etkileşimini araştırmayı amaçlamaktadır. Bu amaçla tezde üç farklı konu ele alınmıştır. İlk olarak, zemin özelliklerinin kazık penetrasyon direnci üzerindeki etkisini netleştirmek için parametrik bir çalışma yapılmıştır. Daha sonra, bu çalışma hesaplama maliyeti sorununu ele almaktadır; DEM'in sınırlayıcı yönlerinden birinin yüksek hesaplama talebi olduğu iyi bilinmektedir. Bununla ilgili olarak, tezin ikinci kısmı, hesaplama süresini azaltmak için kullanılan üç tekniğin geçerliliğini açıklığa kavuşturmayı amaçlamaktadır. Hesaplama süresini azaltma yaklaşımlarının simülasyonundan önce, doğrulanmış bir DEM modeli için uygun model parametreleri, önceki bir çalışmanın deneysel sonuçları kullanılarak belirlenmiştir. Ayrıca bu çalışma kazık yerleştirme yöntemlerinin etkileri açısından zemin-kazık etkileşimine odaklanmaktadır. Her bir numuneye hem itme kazıklar hem de fore kazıklar yerleştirilmiş ve granüler malzemenin tepkisi ayrıntılı olarak değerlendirilmiştir. Son olarak, itme kazıklar ve fore kazıklar üzerinde taşıma kapasitelerini belirlemek için dikey yükleme testleri yapılmıştır. Kazık imalat ve yükleme süreçlerinde elde edilen sonuçlar gösteriyor ki, zemin sıkılık durumu ve tanecik şekillerine ek olarak kazık imalat yöntemlerinin de zemin - kazık etkileşimi üzerinde büyük bir etkisi bulunmaktadır.

TABLE OF CONTENTS

ACKNOWLEDGEMENTS iii
ABSTRACT v
ÖZET vi
LIST OF FIGURES x
LIST OF TABLES xv
LIST OF SYMBOLS xvi
LIST OF ACRONYMS/ABBREVIATIONS xix
1. INTRODUCTION 1
1.1. Aims and Objectives 2
1.2. Dissertation Structure 4
2. BACKGROUND 6
2.1. Literature Survey 6
2.1.1. Experimental Studies on Soil-Pile Interaction 6
2.1.1.1. Field Tests 6
2.1.1.2. Calibration Chamber Tests 8
2.1.1.3. Centrifuge Tests 9
2.1.2. Numerical Studies 11
2.1.2.1. Finite Element Method (FEM) 11
2.1.2.2. Discrete Element Method (DEM) 13
2.2. Technical Framework of Discrete Element Method (DEM) 21
2.3. Drawbacks of Using DEM for Soil-Pile Interaction: High Computational Cost 25
3. INFLUENCE OF SOIL CHARACTERISTICS ON PILE PENETRATION . 27
3.1. Methodology 27
3.1.1. General Information 27
3.1.2. Sample Preparation 29
3.1.3. Pile Penetration Procedure 30
3.2. Consideration of Boundary Effect 32
3.3. Test Program 35

3.4. Results and Discussions 37
3.4.1. Effect of Particle Stiffness on Penetration Resistance 37
3.4.2. Effect of Void Ratio on Penetration Resistance 39
3.4.3. Effect of Inter-Particle Friction on Penetration Resistance . . . 42
3.4.4. Effect of Particle Size on Penetration Resistance 44
3.4.5. Effect of Particle Size Distribution on Penetration Resistance . . 46
3.4.6. Effect of Particle Shape on Penetration Resistance 51
3.4.7. Effect of Rolling Friction on Penetration Resistance 53
4. VALIDATION OF DEM MODELING OF PENETRATION IN GRANULAR MATERIALS AND METHODS TO REDUCE COMPUTATIONAL TIME . 56
4.1. DEM Model and Validation 56
4.1.1. General Description of Experiments Used for Validation of DEM Models 56
4.1.2. Validation Procedure 58
4.2. Methods to Reduce Computational Time 61
4.2.1. Using a Quarter of the System in DEM 63
4.2.2. Using an Up-Scaled DEM Model 64
4.2.3. Using Particle Refinement Method during Sample Preparation . 66
5. MULTI-SCALE ANALYSIS OF DEPENDENCY OF SOIL - PILE INTERACTION CHARACTERISTICS ON PILE INSTALLATION TECHNIQUE . . 70
5.1. Methodology 70
5.1.1. General Model Setup 70
5.1.2. DEM Simulations Program 73
5.1.3. DEM Model Setup of Pile Installation 74
5.1.3.1. Jacked Pile 74
5.1.3.2. Replacement Pile 75
5.1.4. DEM Model of Vertical Pile Load Tests 76
5.2. Results and Discussions 77
5.2.1. Pile Installation Stage 77
5.2.1.1. Jacked Piles 77
5.2.1.2. Replacement Piles 81
5.2.2. Pile Vertical Loading Stage 83

5.2.2.1. Jacked Piles 84
5.2.2.2. Replacement Piles 86
5.2.2.3. Soil Response based on Installation Methods 87
6. SUMMARY 90
6.1. Influence of Soil Characteristics on Pile Penetration 90
6.2. Validation of Dem Modeling of Penetration in Granular Materials and Methods to Reduce Computational Time 91
6.3. Multi-scale Analysis of Dependency of Soil - Pile Interaction Characteristics on Pile Installation Technique 93
7. CONCLUSION 97
REFERENCES 98

LIST OF FIGURES

Figure 2.1. Calculation cycle of DEM simulations (Gezgin *et al.*, 2021). 23

Figure 3.1. Set-up of the simulation of pile penetration. 28

Figure 3.2. DEM model: (a) before pile penetration; (b) after pile penetration. 30

Figure 3.3. Various temporal averaging of original data of penetration resistance. 32

Figure 3.4. Investigation of boundary effect for loose models with different mold depths; force chain networks at halfway and full penetration a) H_c =22.5 cm b) H_c =30 cm c) H_c =45 cm and d) comparison of penetration resistances for all mold depths (G_p = 5 x 10^8 Pa, e = 0.7, d_p = 10 mm). 33

Figure 3.5. Investigation of boundary effect for dense models with different mold depths; force chain networks at halfway and full penetration a) H_c =22.5 cm b) H_c =30 cm c) H_c =45 cm and d) comparison of penetration resistances for all mold depths (G_p = 5 x 10^8 Pa, e = 0.7, d_p = 10 mm). 34

Figure 3.6. Investigation of boundary effect for 30 cm and 45 cm deep molds; force chain networks at full penetration and comparison of penetration resistances: for loose model with e = 0.67 (a and c) and for dense model with e = 0.56 (b and d) (G_p = 5 x 10^8 Pa, d_p = 7.5 mm.) 35

Figure 3.7. Influence of particle shear modulus on penetration resistance. . . . 39

Figure 3.8. Influence of void ratio and soil fabric on penetration resistance: (a) average coordination numbers; (b) force chain networks at halfway and full penetration for model 7 prepared by air pluviation; (c) force chain networks at halfway and full penetration for model 8 prepared by loading-unloading; (d) comparison of penetration resistances for models 4, 6, 7 and 8. 42

Figure 3.9. Effect of coefficient of inter-particle friction on penetration resistance. 43

Figure 3.10. Effect of particle size on penetration resistance. 46

Figure 3.11. Different PSDs used in the models. 47

Figure 3.12. Effect of PSD on penetration resistance (* at the densest state). . 50

Figure 3.13. Particle aspect ratio. 51

Figure 3.14. Effect of particle shape on penetration resistance. 53

Figure 3.15. Comparison of the effects of rolling friction against particle shape on penetration resistance. 55

Figure 4.1. Upper and lower boundaries of the normalized penetration resistance forces in the experiments conducted by Feng *et al.* (2019). . 58

Figure 4.2. DEM model of a cylindrical object penetration (a) normal view (b) top view. 59

Figure 4.3. Comparison of resistance forces obtained from the models with different coefficients of rolling friction and experiment boundaries. . . 61

Figure 4.4. DEM model of penetration of the cylinder penetration with only a quarter of the sample (a) normal view (b) top view. 63

Figure 4.5. Comparison of resistance forces obtained from the models in which sample is full and a quarter, respectively. 64

Figure 4.6. Using Particle Refinement Method during Sample Preparation. . . 66

Figure 4.7. Application of refinement method (a) before penetration (b) after penetration. 68

Figure 4.8. Effect of particle refinement method on penetration resistance. . . 69

Figure 5.1. Soil sample prepared using particle refinement method (top view). 72

Figure 5.2. Features of DEM models used for investigation of influences of pile installation methods. 74

Figure 5.3. Installation steps of jacked piles. 75

Figure 5.4. Installation steps of replacement piles. 76

Figure 5.5. Penetration resistances in Model 34 [spherical - dense], Model 35 [non-spherical - dense], and Model 36 [non-spherical - loose] in terms of (a) total resistance (b) end bearing (c) shaft friction. . . . 78

Figure 5.6. Variations in average coordination numbers during penetration stage (a) Model 34 [spherical - dense] (b) Model 35 [non-spherical - dense] (c) Model 36 [non-spherical - loose]. 80

Figure 5.7. Contacts between the particles before and immediately after penetration in (a) Model 34 [spherical - dense] (b) Model 35 [non-spherical - dense] (c) Model 36 [non-spherical - loose]. 81

Figure 5.8. Variations in average coordination numbers during installation stage of replacement piles in (a) Model 37 [spherical - dense] (b) Model 38 [non-spherical - dense] (c) Model 39 [non-spherical - loose]. . . . 82

Figure 5.9. Contacts between the particles before and immediately after installation in (a) Model 37 [spherical - dense] (b) Model 38 [non-spherical - dense] (c) Model 39 [non-spherical - loose]. 83

Figure 5.10. Jacked pile load test results, that show total resistance, end bearing, and shaft friction, in a) Model 34 (spherical - dense) b) Model 35 (non-spherical - dense) c) Model 36 (non-spherical - loose). 85

Figure 5.11. Comparison of load test results for jacked piles in Model 34 (spherical - dense), Model 35 (non-spherical - dense), and Model 36 (non-spherical - loose) in terms of a) total resistance b) end bearing c) shaft friction. 85

Figure 5.12. Replacement pile load test results, that show total resistance, end bearing and shaft friction in a) Model 37 (spherical - dense) b) Model 38 (non-spherical - dense) c) Model 39 (non-spherical - loose). 86

Figure 5.13. Comparison of load test results for replacement piles in Model 37 (spherical - dense), Model 38 (non-spherical - dense), and Model 39 (non-spherical - loose) in terms of a) total resistance b) end bearing c) shaft friction. 87

Figure 5.14. Effect of installation method (jacked and replacement piles) in terms of end bearing for a) dense sample with spherical particles (Models 34 & 37) b) dense sample non-spherical particles (Models 35 & 38) c) loose sample with non-spherical particles (Models 36 & 39). 88

Figure 5.15. Effect of installation method (jacked and replacement piles) in terms of shaft friction for a) dense sample with spherical particles (Models 34 & 37) b) dense sample non-spherical particles (Models 35 & 38) c) loose sample with non-spherical particles (Models 36 & 39). 89

LIST OF TABLES

Table 3.1. Dimensions of the chamber and the pile in the DEM models. . . . 28

Table 3.2. A summary table with all values of the parameters used in the DEM models. 29

Table 3.3. Properties defined in each model of the test program. 36

Table 3.4. Parameters of the PSD. 48

Table 3.5. Properties of models related with particle size distribution (PSD). 51

Table 4.1. DEM material properties used in the all simulations. 59

Table 4.2. DEM model properties used in the validation stage. 60

Table 4.3. Features of DEM models generating for validation. 61

Table 4.4. Details of DEM models generated for reduction of computational time. 62

Table 4.5. Dimensions in Model 32. 67

Table 5.1. Dimensions in Models 34 - 39. 73

LIST OF SYMBOLS

B	Pile diameter
B_o	Object diameter
C_c	Coefficient of curvature
C_u	Coefficient of uniformity
D_{10}	Diameter corresponding to 10% finer by weight
D_{30}	Diameter corresponding to 30% finer by weight
D_{50}	Average particle diameter
D_{60}	Diameter corresponding to 60% finer by the weight
D_c	Chamber Diameter
D_p	Pile length in soil
d_{max}	Major axis length of a clump
d_{min}	Minor axis length of a clump
d_p	Particle diameter
e	Void ratio
e_r	Coefficient of restitution
E_i	Young's modulus of each sphere in contact
E^*	Equivalent Young's modulus
F	Penetration resistance
F_n	Normal force
F_n^d	Damping force
F_t	Tangential force
G_p	Particle's shear modulus
G_p^*	Equivalent shear modulus
g	Gravitational acceleration
H_c	Chamber height
h	Penetration depth
h_n	Normalized penetration depth
m^*	Equivalent mass
n	Porosity

p_n	Normalized penetration resistance
R^*	Equivalent radius
R_c	Width of quarter of sample
R_{c1}	Width of first zone
R_{c2}	Width of second zone
R_{c3}	Width of third zone
R_{c4}	Width of fourth zone
R_i	Width of each sphere in contact
R_o	Object radius
R_{pile}	Pile radius
S_o	Section area of object
S_n	Normal stiffness
S_t	Tangential stiffness
T_R	Rayleigh time step
W_c	Chamber width
ϑ_c	Upper limit velocity for quasi-static penetration
ϑ_{object}	Object velocity
ϑ_{pile}	Pile velocity
$\overrightarrow{\vartheta_n^{rel}}$	Relative normal velocity
$\overrightarrow{\vartheta_t^{rel}}$	Relative tangential velocity
β	Damping coefficient
δ_n	Normal overlap
δ_t	Tangential overlap
μ_r	Rolling friction coefficient
$\mu_{(s,particle)}$	Inter-particle static friction coefficient
$\mu_{(s,object)}$	Coefficient of static friction between sand particles and object
$\mu_{(s,pile)}$	Coefficient of static friction between sand particles and pile
ν_p	Particle Poission's ratio
π	Pi
ρ_p	Particle density

τ	Torque
Ψ	Packing fraction
ω	Unit angular velocity vector object at a contact point

LIST OF ACRONYMS/ABBREVIATIONS

2D	Two Dimensional
3D	Three Dimensional
AR	Aspect Ratio
CFA	Continuous Flight Auger
CPT	Cone Penetration Test
DEM	Discrete Element Method
PSD	Particle Size Distribution

1. INTRODUCTION

An important role of geotechnical engineering is to ensure the safe transfer of structural loads to the ground. For transferring these loads, depending on soil properties and load characteristics, different types of foundation systems can be designed (e.g. shallow and deep foundations). Piles are classified as deep foundation systems and are constructed whenever shallow foundations do not satisfy the necessary design criteria. However, unlike shallow foundations, pile construction significantly alters the engineering properties of soils. Unfortunately, the impact of pile construction on soil is uncertain and depends on many factors. Additionally, it is not possible to obtain soil samples from the vicinity of piles for testing. As a result, soil properties used in analytical calculations are assumed based on the presumed influence of pile construction on the soil. Evidently, this practice is far from ideal since the accuracies of analytical pile design methods are dependent on the correct determination of representative soil properties. That is why the investigation of the impact of pile construction on soil response is very important.

Soil - pile interaction was investigated by different researchers, using field tests (Adejumo and Boiko 2013; Gavin *et al.* 2013; Li *et al.* 2019a; Qin *et al.* 2017; Tan and Lin 2013), laboratory tests (Ni *et al.* 2010; Yang *et al.* 2014; Yin *et al.* 2018; Zarrabi and Eslami 2016), and numerical analyses based on finite element method (FEM) (Broere and Van Tol 2006; Jin *et al.* 2018; Khoubani and Ahmadi 2014; Phuong *et al.* 2016; Pucker and Grabe 2012; Tolooiyan and Gavin 2013; Wu and Yamamoto 2014). Among these, field tests are considered the most accurate since they benefit from the exact similitude of all possible factors, such as stress distribution, particle morphology, size, and number. However, they suffer from high costs, and additionally; they do not allow the observation of particle size effects and inter-particle interactions. Small-scale modelling and especially centrifuge modelling is a more economical substitute to full-scale testing. But also with small-scale models, it is still not possible to examine particle level mechanisms that dominate behavior. On the other hand, conventional numerical analysis based on constitutive models of soil behavior offers a possible alternative for

studying the alteration of soil with pile penetration. However, the reliance on advanced constitutive models on numerous parameters that can be obtained by tedious testing further complicates their use. Furthermore, even with powerful constitutive models, identification of particle to particle and particle to structure interaction is very difficult. At this point, the discrete element method (DEM) provides a powerful medium for numerical modelling of soils as particulate materials. DEM requires only basic physical rules to simulate soil behavior rather than constitutive models. Thus, with DEM, even the most complex mechanisms of pile-soil interaction can be modelled using a small set of fundamental physical and mechanical rules. In DEM, the granular medium is considered as an assembly of discrete interacting particles. Eventually, the exact location, velocity, and forces at contacts for each particle are tracked in small time steps. More explanations in detail and basic formulations are given in Section 2.2.

This dissertation aims to investigate the multi-scale response of granular soils at pile construction stage and during loading tests. In this respect, DEM is used for simulations of cohesionless soils with different properties (i.e. particle stiffness, particle size, particle size distribution, particle shape, inter-particle friction, rolling friction, sample void ratio). Firstly, the differently prepared samples were subjected to pile penetration and soil response is examined. Secondly, novel techniques were employed to decrease the computational cost of the DEM simulations. Then, using these techniques, the samples with different soil density states and particle shapes were prepared. At the end of the sample preparation process, the jacked and replacement piles were installed into these samples, and subsequently subjected to vertical loading tests. Lastly, the soil responses to the pile installation and loading process were separately interpreted based on soil density state, particle shape, and pile installation method. Overall, the conducted analyses will provide a deeper insight into the soil-pile interaction problem.

1.1. Aims and Objectives

This dissertation covers the effect of soil properties on penetration resistance, the techniques for computational time saving, and the influence of pile installation methods. The reasoning for topic selection and the respective triggered objectives for

each part of this study are briefly discussed below.

Soil response to pile penetration has both macro- and micro-mechanical aspects. At both scales, the properties of the particles and their interactions with each other control overall behaviour. With a wide possibility of varying soil characteristics, DEM enables a detailed examination of particle-scale effects during pile penetration. Consequently, the initial phase of this study attempts to clarify the dependency of penetration resistance on soil particle properties through carrying out a comprehensive parametric study.

DEM provides a powerful framework for modelling soils as particulate materials and can be used to investigate soil-pile interaction. However, such models are computationally demanding and need extensive optimization, which in turn requires an understanding of the influences of soil characteristics on the mechanics. Correspondingly, two different optimization approaches are employed within this study to reduce computational costs. Firstly, soil particle scale properties that affect computational cost were assessed (i.e. particle stiffness, particle size, and particle shape). Successively, three different model preparation techniques were used to reduce computational time in DEM simulations. These techniques are based on decreasing the total number of particles and increasing particle sizes by keeping the ratio of the pile to particle diameter constant.

In practice, generally, the pile performance is assessed based on its bearing capacity at the end of the installation stage. However, by knowing the changes that are occurring in the surrounding soil due to different pile installation methods, it is possible to elaborately characterize the soil-pile interaction during loading. Accordingly, various soil samples were simulated and subjected to jacked and replacement pile installation techniques. The analyses include the assessment of soil responses at the beginning, during, and at the end of two installation processes. At each stage, the effects of microscale parameters on pile's macro behavior and monitored. Additionally, performing vertical bearing capacity tests on the jacked and replacement piles, the influences of installation method on the end bearing capacity and the shaft resistances of the piles

are examined.

1.2. Dissertation Structure

This dissertation is composed of six chapters and presents a comprehensive numerical analysis framework that is performed to investigate the multi-scale mechanism of soil-pile interaction. The dissertation is organized as follows:

Chapter 1 presents an introduction that includes the problem definition, the aims, and the objectives in this study. It also mentions the importance of the issue and the various investigation methods. Additionally, a brief description of each chapter is also given.

Chapter 2 presents a literature survey of the previous studies about soil-pile interaction and pile installation mechanisms. These studies are classified according to the methods of analysis. Especially the studies in which DEM is used are summarized in detail to show the capability of this technique. Additionally, the theoretical background of DEM simulation and its formulation are briefly described.

Chapter 3 discusses the influences of various soil characteristics on pile penetration resistances. Here, the focus is especially on the effects of particle-based properties and the advantages of using DEM simulations for examining soil-pile interaction are demonstrated.

Chapter 4 firstly outlines the procedure to obtain a validated DEM model using the experimental results. Additionally, novel techniques to reduce computational cost of DEM simulations are explained, and the results are discussed comparatively.

Chapter 5 clarifies the multi-scale influences of different pile installation methods on soil-pile interaction. Firstly, various soil samples with different density states and particle shapes are subjected to pile installation process with two different techniques (i.e. jacked and replacement). Then, vertical loading tests are conducted on installed

piles. Consequently, soil response to pile installation and pile bearing capacity are separately examined to understand the influences of soil density, particle shape, and installation method.

Chapter 6 summarizes results of analyses, observations and recommendations regarding pile installation and sample properties.

Chapter 7 presents a conclusion for the dissertation.

2. BACKGROUND

Investigation of soil-pile interaction requires multi-scale analyses utilizing both the experimental and numerical approaches. Accordingly, this chapter summarizes previous studies on soil-pile interaction by classifying them as either experimental or numerical. In the review of numerical studies, the focus is mostly on studies that used discrete element method. Additionally, the technical framework of discrete element modelling is presented in this chapter.

2.1. Literature Survey

2.1.1. Experimental Studies on Soil-Pile Interaction

2.1.1.1. Field Tests. Cone Penetration Test (CPT) is the most popular field test that is used to interpret soil-pile interaction. CPT involves the penetration of a cone tipped rod into the ground at constant velocity. Both cone and shaft resistances can be measured during penetration via mounted sensors. Owing to the similarities between the mechanisms prevalent in pile driving and CPT testing, CPT results are frequently used in the prediction of bearing capacities of driven piles (Abu-Farsakh and Titi 2004). Schneider *et al.* (2008) examined seven CPT-based design techniques, that include the conventional American Petroleum Institute (API) approach, for the calculation of the axial capacity of driven piles.

In addition to driven piles, field tests are also conducted to investigate the soil-pile interaction mechanism for alternative pile installation techniques. These studies also consider pile geometries other than the conventional spherical shape. As an example, Zhang and Wang (2009) conducted field tests to examine the effects of installation in case of jacked and driven H-piles. Their study involved three test piles that were a jacked pile, a driven extended pile that is installed using both jacking and driving techniques, and a reference driven pile. The authors presented the results obtained for both jacked and driven piles in terms of penetration resistances, residual forces

developed after installation, and static and dynamic load tests. Using these results, influences of the installation method were investigated in different aspects.

Gavin *et al.* (2013) conducted static load tests on two continuous flight auger (CFA) piles of similar lengths but different diameters that were installed into dense sand. They applied various load test procedures such as maintained load test and constant rate of penetration by considering creep effect. They measured the base pressure and the base settlement response to that in each loading test. They aimed to observe the influence of pile diameter and normalized pile length (i.e. the ratio of length to diameter) on the mobilized base pressure. Since these piles were not at the same diameter, the authors normalized base settlement by pile diameter to render piles - stiffness responses and base resistances comparable. After the loading tests, they realized that creep had an effect on the base pressures measured in maintained load tests and its effect decreased with an increase in loading velocity. They also revealed that normalized pile length and diameter do not have an effect on mobilized pressure-settlement responses of CFA piles.

Wang *et al.* (2021) investigated earth pressures at the pile-soil interface for jacked piles in silty soil and silty clay. They jacked two pre-stressed high-strength concrete (PHC) pipe piles that have the same diameter (400 mm) but different lengths (12 m and 22 m) in the project. Before the construction, earth pressure sensors were installed on the piles to measure earth pressures during jacking. This way, the authors observed the change in earth pressure at the pile-soil interface due to the penetration of the PHC pipe pile. The test results showed that the earth pressure gradually decreases as moving away from the pile base to the top. They also revealed that the pile length affected the earth pressures at the pile-soil interface and should be considered. In addition, it was realized that soil strength at a certain depth decreased as pile penetration depth increased due to soil distortion during the pile jacking. This decrease led to an attenuation of lateral pressure.

2.1.1.2. Calibration Chamber Tests. One of the most efficient ways to correlate CPT results and soil parameters is to conduct calibration chamber tests. In these tests, soil conditions such as soil type, density and porosity, and stress states in vertical and horizontal directions can be controlled. However, boundary conditions in calibration chamber tests are different from those in the field, such that the radial boundaries are not flexible. For that reason, the penetration resistance measured in the chamber tests may differ from that obtained from the field tests (Yu and Mitchell 1998).

Schnaid and Houlsby (1991) performed a study to investigate the effect of the chamber size using the results of both the chamber tests and field tests obtained from the literature. They deduced that the chamber size affected the tip penetration resistance for all sand densities. However, the influence was more significant, especially for dense soils.

Salgado *et al.* (1998) proposed a penetration resistance theory to quantify chamber size effect. To develop the theory, for each soil property, they compare the results obtained from both the field test and the chamber test when all soil conditions were the same. Then, they presented a parametric study about the influence of soil properties and stress states on the chamber size effect. This study showed that the chamber size effect becomes more intense with increasing relative density and stress state and with decreasing confining stress.

White and Bolton (2004) used a novel image-based technique that is particle image velocimetry (PIV) to measure the displacement and strain paths developed due to the plane-strain pile installation in a surcharged calibration chamber. They could observe the displacement trajectories of soil elements, full-field displacement, and stain paths and fields using the PIV technique. In this way, they examined the effects of soil type, pile breadth, soil initial state, and the use of a driving shoe.

Arshad *et al.* (2014) used a similar technique that is the digital image correlation (DIC) to observe soil-cone interaction in the silica sand with different crushability levels. They conducted a series of CPTs in a half-circular chamber to acquire the images

that were taken during the cone penetration for implementing the DIC technique. They measured the cone resistances and obtained the soil displacement fields that resulted from the penetration process by analyzing captured successive images. The results of the resistance measurement and image processing via DIC indicated that soil displacement around the rod was dependent on soil density and degree of particle crushability.

2.1.1.3. Centrifuge Tests. Centrifuge modelling is an economical substitute to full-scale testing since centrifuge tests can enable the stress states that are the same as it in field tests. The full-scale stresses are replicated by increasing the gravitational forces on the model. According to Bolton *et al.* (1999), the repeatability and reliability of cone penetration tests in the centrifuge are very promising. They revealed the main influences of density and stress on penetration resistances obtained from centrifuge tests. A series of centrifuge tests were conducted by varying some test factors that are boundary condition, particle size, geometry effect, and test locations.

Klotz and Coop (2001) conducted a series of model pile tests in a centrifuge, in which the pile penetrating two types of sands with different particle strengths. Based on the results, the researchers concluded that the design approaches that are functions of just relative density are not sufficient to correctly determine pile capacity. The results showed that pile capacity is dependent on both density and stress level of, the combination of which is referred to as "in situ state". For that reason, they quantified in situ state of each sample before pile installation. They also found that the state parameter (Ψ) should be quantified as a function of ratio of stresses. The authors also compared penetration resistances that were determined as functions of in situ-state for considered sand types. White and Lehane (2004) performed a series of pile installation tests in a drum centrifuge. The authors examined the distribution of horizontal stress that acted on the shaft during installation and cyclic loading. In this way, they aimed to investigate friction fatigue that referred to the decrease in ultimate shaft friction due to pile penetration to deeper levels. They installed the piles using different methods that were monotonic, jacked, and pseudo-dynamic to examine the

effect of cycling loading during penetration. After installation, they performed different types of load tests with different modes including compression, cyclic compression, and cyclic compression-tension. The test results showed that the main reason for friction fatigue is cyclic history. It was seen that there is no friction fatigue during monotonic installation while cyclic installation led to a considerable decrease in shaft resistance and cyclic loading also caused a degradation of horizontal effective stress.

Liu and Lehane (2012) investigated the influence of particle shape on tip resistance by conducting a series of centrifuge CPTs. These tests were conducted in four uniformly graded samples with different particle shapes. They performed the cone penetration tests at three different levels of centrifugal acceleration and two different relative densities. The test results indicated that the particle shape had a significant effect on the CPT tip resistance of a granular assembly at a given stress level and relative density. In addition, the authors suggested considering the effect of particles shape on the friction angles (peak and critical state) for the estimation of the relative density of soil from data of cone penetration test.

Mo *et al.* (2015) conducted a series of cone penetration tests in layered soils. The authors focused on the examination of penetration into layered soils. Therefore, they prepared six different samples in total. Two of these samples were soils with uniform density so that the tests conducted in them were used as a reference for the other sample tests. Layered soil samples were classified into two groups. They are two-layer samples, loose over dense and dense over loose, and "sandwich" samples, dense-loose-dense and loose-dense-loose. During the penetration, they pushed the half-rod and the full-rod into a 180^o axisymmetric container. The half-rod was used to observe the induced soil deformation while using the full-one to measure penetration resistance. The authors interpreted the penetration results and soil deformations by relating them to soil density and soil layering. They compared the observed soil deformations with previous test data to investigate the influence of the axisymmetric condition. They also indicated that the influences of soil layering on both soil deformation and penetration resistance are dependent on the relative properties of soil layers.

2.1.2. Numerical Studies

2.1.2.1. Finite Element Method (FEM). Finite element method (FEM) that incorporated the first small-strain models were used to study the bearing capacity of piles for cohesive soils in several studies such as Griffiths (1982), Sloan and Randolph (1982), and De Borst and Vermeer (1984). In these studies, the vertical loadings were performed on the piles that introduced the pre-bored holes in an in-situ stress state. Thus, the build-up stresses around the cones were ignored.

However, these models are insufficient to simulate pile penetration mechanisms because it is a boundary value problem (BVP) that requires the capability for modelling large deformations and the sliding between soil and pile. Therefore, realistic modelling of pile penetration with FEM is difficult. For successful modelling, various approximations of pile penetration are employed. Sheng *et al.* (2005) used an alternative numerical approach to model the installation and loading of a pile. This approach, based on a Lagrangian multiplier method, involves the capability of simulating large-deformations and frictional contacts, therefore suitable of simulating soil-pile interaction.

Nevertheless, this approach requires determining the next location of boundary nodes at the end of each step. For large strain finite element modelling without a need for frequent re-meshing, Susila and Hryciw (2003) utilized an auto-adaptive re-meshing method. They used Mohr-Coulomb's theory to model the sand-cone interaction while selecting the non-associative Drucker-Prager constitutive model to simulate the sand behavior. In this way, the authors could simulate the sand-cone interaction during the penetration with results that were very compatible with experimental and analytical studies in the literature.

Tolooiyan and Gavin (2011) determined the cone penetration resistances using two commercial finite element packages that utilize different approaches. The authors used Plaxis to adopt spherical cavity expansion analyses while using Abaqus/Explicit to perform an auto-adaptive re-meshing method that is called ALE combining the

properties of pure Lagrangian analysis and pure Eulerian analysis. The ALE technique provides the mesh for independently moving, therefore, enables a high quality of mesh even under large deformation. In the cavity expansion approach, they used Mohr-Coulomb and Hardening Soil as the stiffness models. The results showed that the Hardening Soil model enabled better estimates of the cone penetration resistance. On the other hand, they also employed the ALE method, a more direct technique to simulate cone penetration test, using Abaqus. Although the Druker-Prager model used in the ALE method is a relatively simple soil model, it could also provide excellent predictions of the cone penetration resistance without unacceptable mesh deformation.

Qiu *et al.* (2011) also aimed to solve the pile jacking problem that is a boundary value problem containing larger deformations using a Coupled Eulerian-Lagrangian (CEL) approach. The authors firstly conducted a benchmark test based on a strip footing problem to reveal the validity of the selected approach. Then, they applied this approach to a more complex geotechnical boundary value problem that is pile penetration. They showed the capability of the CEL method to simulate the pile penetration problem by obtaining results compatible with the classical finite element models.

Hamann *et al.* (2015) adopt a similar approach to investigate the pile penetration mechanism for fully saturated soil in partially drain conditions. The authors employed a numerical approach to model the soil as a two-phase medium. They applied this approach to both a classical finite element analysis in a Lagrangian formulation and a Coupled Eulerian-Lagrangian (CEL) method. Using this approach in different methods in finite element modelling, the results were compared. In this study, they also examined the effects of both the installation process and the permeability on the soil surrounding the pile.

Zhang *et al.* (2013) presented a novel study about pile penetration in crushable soils. They proposed a new formula to calculate the end bearing capacity of piles that penetrate the crushable soils. With this formula, it was possible to consider the breakage crushability of the particles and evaluate the particle size distribution (PSD). The

authors integrated this formula using the finite element modelling to investigate pile penetration mechanism. Then, they validated predictions of particle size distributions due to breakage of the particles surrounding and end-bearing capacity of the pile using the experimental results. As the next step, they also carried out a parametric study to quantify the influences of particle crushing on the pile bearing capacity.

2.1.2.2. Discrete Element Method (DEM). Discrete element method (DEM) provides a powerful medium for numerical modelling of soils as particulate materials. Originally, this method was developed by Cundall and Strack (1979) for analyzing problems considering rocks that involve large displacement contact problems. DEM requires only basic physical rules to simulate soil behaviour rather than constitutive models. Thus, with DEM, even the most complex mechanisms of pile-soil interaction can be modelled using a small set of fundamental physical and mechanical rules.

Huang and Ma (1994) firstly used this alternative tool to investigate the pile penetration mechanism. They developed a numerical technique based on the coupled DEM and boundary element method (BEM) model. The sandy soil was modeled as an assembly of circular disks since the 2D DEM model was used in the study. As a result of their study, it is observed that the penetration mechanism was affected by the loading history.

Lobo-Guerrero and Vallejo (2005) aimed to visualize the penetration resistance developed in driven piles. They used crushable particles in 2D DEM models simulating pile penetration mechanisms. The particles were generated as circular disks which are allowed to break if the failure criterion is fulfilled. They compared the results of two different simulations of which the only one contained crushable particles. The results indicated that the sample with weaker particles showed lower penetration resistance because breakage and rearrangement of the particles led to stress relaxation. In their next study, Lobo-Guerrero and Vallejo (2007) investigated the influences of pile tip shape on the penetration resistance developed in the soils with crushable particles using 2D DEM simulations that are the same as their previous study. For this purpose, they

used three types of pile tip shapes that are flat ended, open ended and triangular tip. They asserted that the pile tip shape had considerable effect on both the penetration resistance and particle breakage. According to Lobo-Guerrero and Vallejo (2007), flat ended piles give the higher penetration resistances than open ended piles and piles with triangular tips.

Jiang *et al.* (2006, 2007, 2008) carried out 2D DEM analyses to simulate penetration tests in the sandy soil. Granular medium in the simulations was generated using uncrushable circular disks under an amplified gravity field of 1000g. Additionally, they designed K0 lateral stress boundaries to eliminate possible boundary effects. In these studies, the standard penetrometers were pushed into the granular medium. Jiang *et al.* (2006) showed the clear influences of interface friction between the soil and the penetrometer on the penetration mechanism. In addition, Jiang *et al.* (2007) revealed that considerable changes in both magnitudes and directions of stresses are observed in the soil surrounding the penetrometer. Then, Jiang *et al.* (2008) investigated the failure mechanisms observed during the penetration and, the classical and non-classical kinematic fields of the penetration tests.

In the studies related to the DEM modelling of penetration tests, three-dimensional models are also used. Arroyo *et al.* (2011) firstly reported 3D DEM simulations of a penetration test. They claimed that the quantitative comparison of the results of 2D DEM simulations with the experimental results was difficult. Accordingly, Arroyo *et al.* (2011) generated a virtual calibration chamber in the 3D DEM model and simulated the cone penetration tests in sands that are at different initial densities and subjected to various isotropic stresses. Using this virtual calibration chamber, they obtained macro-scale results quantitatively compatible with the physical experiments. Butlanska *et al.* (2014) used the DEM model that was in the study of Arroyo *et al.* (2011) to examine the results of the virtual penetration tests at meso- and micro-scale. They used particle displacements and distributions of contact forces, and stress and strain fields to observe the soil response to the penetration at the micro- and meso-scale, respectively. Butlanska *et al.* (2014) also investigated the influences of radial boundary conditions, initial average density, initial stress state, and particle rotation

inertia. It should be also noted that in the studies of both Arroyo *et al.* (2011) and Butlanska *et al.* (2014), particle rotation was inhibited to develop a rolling resistance between the spherical particles.

One of the significant limitations of DEM is the high computational cost that directly related to the number of particles in models. Accordingly, McDowell *et al.* (2012) aimed to show the validity of some techniques to reduce computational time. For this purpose, firstly, they used only a segment of the chamber and the cone penetrometer. This method is technically applicable because the pile (and cone) penetration is the axisymmetric problem. In this way, they achieved an acceptable computational cost. In addition, they used the particle refinement method in which smaller particles are near the cone penetrometer while larger ones are further away. Thus, a higher number of particles in contact with the cone was obtained using fewer particles than would be required without this method. They compared the cone penetration resistance obtained from the simulation where both of the time-saving methods were adopted with that obtained using an entire chamber filled with only small particles. The results were very compatible with each other. Additionally, they investigated the particle shape effect on the cone penetration resistance. They used two different particle shapes that are the single sphere and the two-ball clump of equivalent volume. The comparison showed that clump particles lead to higher resistance than the spherical ones.

Falagush *et al.* (2015) performed a study by adopting the methods to reduce the computational time that was also used in the study of McDowell *et al.* (2012). They first investigated the effect of sample preparation on penetration resistance. Here, they prepared two different samples using the deposition and compaction method and the radius expansion method, respectively. The comparison result showed that there is no effect of sample preparation on the penetration resistance. Then they gave constant mass to each particle although the particles were at different sizes in order to decrease the computational cost. So, they noticed that this did not significantly affect the tip resistance. They also examined the influences of initial sample porosity, mean effective stress, and particle friction coefficient on the resistance. According to their findings, a lower initial sample porosity, higher mean effective stress, and higher particle friction

coefficient individually lead to an increase in the penetration resistance.

Jiang *et al.* (2014) used DEM simulations to investigate the inclined cone penetration mechanism. In their study, they simulate a series of cone penetration tests using the cone inclined at different angles. In these test simulations, both the frictional and frictionless penetrometers are used to observe the effect of friction. The results indicated that the friction had important influences only on soils adjacent to the cone side and tip. In addition, it was seen that the tip resistance increased with cone friction and inclination angle measured from the vertical direction. They also realized that the soil on the side the penetrometer that inclined towards was exposed to compaction while the soil on the opposite side showed a dilatant behavior. In the simulations, different failure mechanisms were successfully observed during the penetration. However, it was realized that the friction had a stronger influence on the failure mechanism on the opposite side the penetrometer inclined towards.

Zhang and Wang (2015) aimed to investigate penetration mechanisms in both macro-mechanical and micro-mechanical aspects. For this purpose, they generated a 3D DEM model for simulating a centrifuge model pile using the calibrated parameters and the appropriate contact model. According to Zhang and Wang (2015), a calibrated rolling resistance should be applied at the spherical particle contacts. It is not sufficient that particle rotation is not allowed to create a rolling resistance. As a result of their investigation, they found the simulation results to be compatible with the results of the centrifuge test in terms of both the base and shaft resistance. In addition, they revealed the micromechanical indication of the shear band developed using the movement of associated particles and contact force distribution.

It is also possible to simulate pile penetration mechanism in cohesive granular assemblies using DEM. As an example, Janda and Ooi (2016) used DEM to model cone penetration in cohesive solids as well as unconfined compression tests. They used a visco-elastic-plastic frictional adhesive contact model. They purposed to investigate the capabilities of this contact model to reproduce the cone penetration resistance qualitatively. To better interpret the results, they implemented the temporal averaging

on the instantaneous data of the penetration resistance. At the end of the simulations, it was observed that the penetration resistance increased until a certain depth, then it remained around a constant value that represents a typical steady-state response. They also asserted that the contact model that was used in the study was capable of capturing the effect of consolidation stress history of cohesive soils on the penetration resistance. In addition, they examined the effect of the contact model parameters on penetration resistance. It was noticed that higher unloading-reloading stiffness, an indicator of contact plasticity, and higher adhesive stiffness led to an increase in the penetration resistance. They also investigate the influence of the coefficient of sliding friction on the resistance. The results showed that the higher friction causes more resistance until a threshold value. For a higher friction coefficient, its influence on penetration resistance saturated. Lastly, they revealed that there was a linear relationship between the limiting penetration resistance and undrained shear strength.

DEM simulations are also used to investigate dynamic penetration problems in addition to the monotonic pile penetration mechanism. Tran *et al.* (2016) performed 2D DEM simulations of the penetration tests in both constant velocity and impact conditions. In impact conditions, impacts are applied on the top of the rod and penetration distance and tip resistance are measured. Then, Tran *et al.* (2016) qualitatively compared the mechanical response of the samples to the penetration with the experimental results because they were aware that an assembly of disks could not behave as same as a real granular soil. They aimed only to describe soil behavior under the penetration rather than to quantitatively link the simulation results with the experimental ones. They also investigated the effect of penetration rate on both constant velocity and impact conditions. It was seen that the sample behaviour transitioned from quasi-static regime to dense flow regime when the rod velocity was higher than a certain level. In constant velocity condition, when the rod penetrated with an excessive velocity, the assembly showed a greater resistance to the penetration. In impact condition, an increase in impact velocity caused a higher variation in the tip force. In addition, the authors compared the tip forces obtained from constant and impact velocity penetrations. According to the observation, the rod velocities were equal in impact and constant velocity conditions at the beginning of the penetration. However,

the velocity progressively reduced as the rod penetrated the assembly in the impact test. Therefore, the tip force in the impact condition is lower than that in the constant velocity condition.

Duan *et al.* (2018) used discrete element modelling for a purpose that is unlike those of the other studies. The authors studied the influences of the installation method on pile behavior by adopting 2D DEM models. Driven and bored piles (one for each pile type) were simulated so that they had the same geometry as each other. These piles were installed into a granular medium that was simulated under an amplified gravity field of 100g. For DEM simulation of driven pile installation, the author pushed the pile a stepwise increase of vertical load level until the desired depth was reached. After each load increment, they cycled the system until the equilibrium condition. On the other hand, they followed another procedure to install the bored pile. In the installation process of the bored pile, they firstly deleted the granular particles in the region that was planned as the pile location. Then, the pile was put in the granular assembly. As the final step, the model continued to cycle until equilibrium. Then, the installation stage was completed for the pile types. After the installation stage for each pile type was completed, the load tests were applied on both the driven and bored piles. According to the simulation results, it was seen that the ultimate shaft resistance of the driven pile was considerably higher than that of the bored pile. Additionally, they observed that the bored pile experienced relatively large settlements while the driven pile resisted settlements during the loading tests. Another observation presented in this study was that soil friction was effective after a certain depth for the bored pile whereas the friction had influence even at the beginning of penetration for the driven pile.

DEM is also a useful tool for the investigation of the behavior of open-ended piles. Consequently, Guo and Yu (2016) used discrete element modelling to analyze soil plug mechanisms for open-ended pipe piles. They built a soil column inside a pipe pile as a simulation of the plug generated during the penetration process. According to the simulation results, firstly, a higher internal unit shear resistance was developed due to the arching effect. In addition, a uniform porosity distribution of the sample could not

be observed after the installation of the open-ended pile. It was seen that the sample was denser at the bottom due to the compaction effect on the particles, and was looser near the soil-pile interface because the particles slid along the inner of the pipe wall. The authors also revealed that the coefficient of friction between the soil and the pile is a critical parameter for plug resistance.

Li *et al.* (2019) performed another study about the investigation of open-ended piles based on discrete element modelling. They adopted a 2D DEM model to examine the soil plug mechanism during penetration and loading processes at both micro-scale and macro-scale. The authors firstly assessed the macro-mechanical aspect of sand plug behavior in terms of the porosity and stress state. It was seen that the distribution of porosity along the soil plug showed that a dense zone which is half pile diameter in length was formed at the pile tip. In addition, they observed a significant load transfer at the base of the soil plug. In the examination of the micro-mechanical aspect, it was revealed that the particles moved inside the pipe during the penetration process and formed the soil plug which moved as a block. However, as the pile was penetrating, the flow rate of the soil mass inside the pile slowed down due to the increase in resistance accumulation. The authors also investigated the arching mechanism in the soil plug by interpreting the distribution of particle contact force and the principle stress rotation. Liu *et al.* (2019) presented a study about the responses of open-ended piles at different diameters during the installation stage using 2D DEM models. These models, which are similar to those used by Duan *et al.* (2018), were generated using the circular disks under an amplified gravity field of 100g to simulate deep foundations. Three open-ended piles that had equal wall thickness and length are created with different outer diameters. They realized that the development of shear zones could be explicitly demonstrated by observing the relative displacement of the particles. In addition, it was seen that the dominant plugged modes (fully or partly) continuously exchanged during the penetration, and this continuous exchange was more apparent in the pile with the smaller diameter. The authors revealed that the majority of penetration resistance was developed as pile base resistance, the sum of plug resistance and annulus resistance, and the base contribution to the total resistance also increased as the pile diameter was increasing. It was also observed that the unit lateral resistance started to decrease

at a specific penetration depth since horizontal effective stress acting on the shaft was reduced.

DEM also allows investigating the installation and performance of screw piles. Chen *et al.* (2018) studied axially loaded screw piles using different methods. They utilized discrete element modelling as a numerical method in addition to experimental tests and digital image correlation. The authors performed two-dimensional DEM simulations in the numerical part of the study. The pile capacity was calculated by considering vertical components of the base resistance, the shaft frictions, and the screw section reactions. A control pile that is a type of shaft pile was also simulated to reveal the effect of the screw section of the pile. The control pile and the screw pile were subjected to the same conditions and the load-displacement curves were obtained. These curves were compared with the model test results also conducted by the authors. They observed that the simulation and test results were compatible for both the control and screw piles. They also compared the results obtained for these piles with each other. The comparison showed that screw-shaft piles had a higher capacity to carry vertical load than the control ones. They also examined the contact forces acting on the base, shaft, and screw sections of the pile, separately. In the subsequent study, Chen *et al.* (2020) investigated behaviour of partially-screwed shafts using both the experiments and the 2D DEM simulations. As a first step, they conducted static load tests to observe soil-pile interaction and the bearing capacity. Then, the authors used the results of the experiments to validate a DEM model. This DEM model was set to examine soil-pile interactions at micro-scale. In addition, the influences of significant geometric characteristics that are length of screw section, pitch, and shaft diameter on bearing capacity and load transfer of piles were investigated using the DEM simulations. According to the results, the lowermost thread and the screw section had a significant effect on the pile bearing capacity. The authors also suggested an optimum pile geometry that enabled soil-pile interaction at the maximum level and increased the pile performance.

Shi *et al.* (2019) performed a study about screw pile penetration using 3D DEM simulations. The authors focused on the drilling velocity ratio that is the ratio of

rotational velocity to penetration velocity. They simulated a loose granular assembly using a particle refinement method to decrease the number of total particles, therefore, the computational cost. The DEM model of a mini screw pile was validated using the experimental model test results. Then, Shi *et al.* (2019) adopted a series of DEM models with different drilling velocity ratios. They aimed to investigate the variation of stress distribution in the granular material, particle displacement around the pile, and changes in the void ratio of the sample at various drilling velocity ratios. Accordingly, it was first seen that a higher drilling velocity ratio led to a decrease in the driven force. They also observed that the soil particles around the pile moved upward away from the screw at the high drilling velocity ratio. On the other hand, the particle movement was downward away from the pile if the drilling velocity ratio is lower than the critical velocity. In addition, it was shown that the change in the void ratio of assembly due to the pile penetration was dependent on the drilling velocity ratio. The lower velocity ratio caused a significant decrease in void ratio around the pile. However, it was observed that this reduction in the void ratio decreased with an increase the drilling velocity ratio.

2.2. Technical Framework of Discrete Element Method (DEM)

DEM is a numerical technique that can simulate individual grains in a particulate system. In order to simulate the particle interaction with its surrounding, this method employs Newton's laws of motion. DEM determines the location of particles within small time-steps, and based on a contact model, it calculates the forces among contacting particles. Using this force, it is possible to update the acceleration of each particle, which is then integrated to determine the particle's velocity and displacement.

The initial step in DEM is to generate the geometry of the system, where particles can overlap while maintaining inter-particle contact. The fundamental idea of DEM is based on two different physical laws: Newton's second law, applied to the particles, and force-displacement law at the contacts. DEM performs repeated calculations using such these basic physical laws. Firstly, the contact forces of the particles are calculated from their displacements using the force-displacement law. Considering both the con-

tact forces and body forces acting on the particle, the total normal and shear forces acting on each particle are separately determined at each time-step. Following the calculation of the contact forces, Newton's second law of motion is applied every individual particle. Between two succeeding time-steps, the accelerations of all particles are calculated based on particle masses and the forces acting. Particles - new velocities and displacements are determined with double integration of acceleration over each time step.

For particle i, the equation of motion is given by

$$m_i \left(\frac{d^2 x_i}{dt^2} \right) = f_i + m_i g \tag{2.1}$$

where m_i is the mass of the particle, t is time, x_i is its position, g is the acceleration due to gravity and f_i is the force acting on the particle due to particle contacts as defined by

$$f_i = \sum f_i^c. \tag{2.2}$$

The rotational motion equation for particle i is calculated using

$$I_i \left(\frac{d\omega_i}{dt} \right) = T_i \tag{2.3}$$

where I_i is the moment of inertia for particle i, ω_i is its angular velocity and T_i is the total torque acting, which is defined by Equation (2.4) where l_i is the branch vector of particle i, defined by Equation (2.4) and Equation (2.5) are represented as follows:

$$T_i = \sum l_i^c * f_i^c \tag{2.4}$$

and

$$I_i = r_i - r. \tag{2.5}$$

The principles of DEM theory for calculating the positions and forces of all individual particles are explained in detail by C. O'Sullivan (O'Sullivan 2011). The summary of the calculation cycle of DEM is given in Figure 2.1.

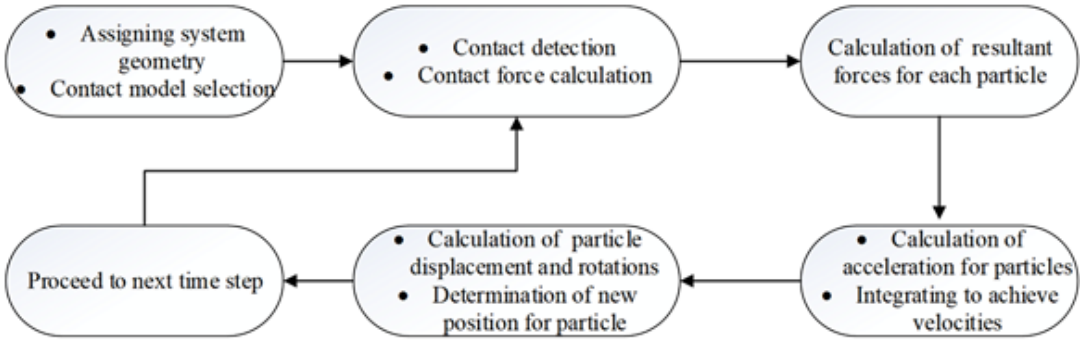


Figure 2.1. Calculation cycle of DEM simulations (Gezgin *et al.*, 2021).

In DEM, particles are subjected to force transmission from surrounding contacting particles, whereas, in reality, particles can be affected by the disturbance propagation from particles located further away. The time-step in DEM is calculated based on a percentage of Rayleigh wave speed (the time taken for a Rayleigh wave to pass a sphere with a certain radius and material properties). This time limitation ensures the fact that energy cannot propagate to a particle from beyond its immediate neighboring. Rayleigh is calculated using

$$T_R = \frac{\pi d_p \sqrt{\rho_p / G_p}}{0.3262 v_p + 1.7532} \tag{2.6}$$

where d_p, ρ_p, G_p and ν_p are the particle's diameter, density, shear modulus, and Poisson's ratio, respectively.

Hertz-Mindlin (no-slip) is used in this study, which is one the most commonly used contact models in DEM. The normal force (F_n) in this contact model is determined using

$$F_n = \frac{4}{3} E^* \sqrt{R^*} . \delta_n^{2/3} \tag{2.7}$$

where δ_n is the normal overlap, and R^* and E^* are referred to as equivalent radius and equivalent Young's modulus that are calculated using

$$\frac{1}{E^*} = \frac{\left(1 - v_{pi}^2\right)}{E_i} + \frac{\left(1 - v_{pj}^2\right)}{E_j} \tag{2.8}$$

and

$$\frac{1}{R^*} = \frac{1}{R_i} + \frac{1}{R_j} \tag{2.9}$$

with E_i, ν_{pi}, R_i being Young Modulus, Poisson ratio, and radius of each sphere in contact. Additionally, a damping force is embedded in the contact model. The normal component of the damping force (F_n^d) is obtained from

$$F_n^d = -2\sqrt{\frac{5}{6}}\beta\sqrt{S_n m^*}.\overrightarrow{v_n^{rel}} \tag{2.10}$$

where ($\overrightarrow{\vartheta_n^{rel}}$) is relative normal velocity. Equivalent mass (m^*), normal stiffness (S_n) damping coefficient (β) are calculated using

$$m^* = \left(\frac{1}{m_i} + \frac{1}{m_j}\right)^{-1} \tag{2.11}$$

$$S_n = 2E^*\sqrt{\delta_n R^*} \tag{2.12}$$

and

$$\beta = \frac{\ln e_r}{\sqrt{\ln^2 e_r + \pi^2}} \tag{2.13}$$

with e_r the coefficient of restitution. Similarly, it is possible to obtain the tangential force (F_t) through tangential overlap (δ_t) and tangential stiffness (S_t) using

$$F_t = -S_t\delta_t \tag{2.14}$$

and

$$S_t = 8{G_p}^*\sqrt{\delta_n R^*} \tag{2.15}$$

with G_p^* being as equivalent shear modulus calculated using

$$\frac{1}{{G_p}^*} = \frac{1}{G_{pi}} + \frac{1}{G_{pj}}. \tag{2.16}$$

The tangential damping force is determined using

$$F_t^d = -2\sqrt{\frac{5}{6}}\beta\sqrt{S_t m^*}.\overrightarrow{\nu_t^{rel}} \tag{2.17}$$

with $\overrightarrow{\nu_t^{rel}}$ being relative tangential velocity. Note that the tangential force has a maximum limit this is equal to Coulomb friction as $\mu_{(s,particle)}F_n$, where $\mu_{(s,particle)}$ is the coefficient of static friction.

The material properties that are needed as an input for DEM simulation in EDEM software are briefly discussed here. The values for the Poisson's ratio, Shear/Young's modulus, and Solids Density must be entered into the relevant fields. Additionally, based on calibration, the values of coefficients of restitution, static friction, and rolling friction can be applied to the simulated particles. These coefficients can be assigned separately for particle-particle and particle-geometry contacts.

2.3. Drawbacks of Using DEM for Soil-Pile Interaction: High Computational Cost

Although, DEM is superior for modelling penetration problems in granular media, it does suffer from one major drawback: its high computational cost. The modelling of an extremely great number of particles and their interactions for a period of time demands dauntingly significant amount of computational resources. This limitation forces researchers to look for ways to reduce computational cost. One option is to use

two-dimensional models (Lobo-Guerrero and Vallejo, 2007; Jiang *et al.*, 2014; Wang and Zhao, 2014; Liu and Wang, 2016; Tran *et al.*, 2016; Duan *et al.*, 2017; Duan *et al.*, 2018; Esposito *et al.*, 2018; Li *et al.*, 2019b). Although, this approach is successful in decreasing computational cost, the usefulness of its results for understanding granular behavior is highly debated as the system is comprised of infinitely long bars that have widely different kinematic constraints from real granular materials (Falagush *et al.*, 2015a). Therefore, 2D DEM is not a suitable option for investigating a profoundly axisymmetric mechanism as pile penetration. That is why, irrespective of its substantial computational cost, three-dimensional DEM modelling is gaining popularity for observing soil-pile interaction (Arroyo *et al.*, 2011; Butlanska *et al.*, 2014; Zhang and Wang, 2015; Falagush *et al.*, 2015a; Janda and Ooi, 2016; Chen *et al.*, 2018; Shi *et al.*, 2019; Zhao *et al.*, 2019). Meanwhile researchers using 3D DEM face a major optimization problem; reducing the computational cost without significantly compromising model quality. This involves the determination and calibration of model and particle properties. The properties of soils (void ratio, particle size, particle shape, particle size distribution, inter-particle static friction, etc.) and structural members (pile-particle static friction, pile size, penetration velocity of the pile, mold size, etc.) influence both DEM model similitude and computational cost, therefore require optimization.

3. INFLUENCE OF SOIL CHARACTERISTICS ON PILE PENETRATION

This chapter aims to investigate the effects of soil properties on pile penetration resistances. For this aim, a series of pile penetration models are designed using three-dimensional discrete element models. Structural parameters such as model dimensions and pile properties were kept constant while soil characteristics were varied one at a time. This allowed uncoupled observation of the influences of individual soil characteristics including stiffness, inter-particle friction, rolling friction, average size, shape, packing density, and grain size distribution. as also explained by Gezgin *et al.* (2020). It is believed that obtained results will provide deeper insight into soil-pile interaction problem.

Granular materials in this study are generally described as "soil". That is because it is planned to investigate soil response with respect to the penetration process in terms of geotechnical perspective. Although the particle sizes are not as small as the sand grains, there is no obstacle for referring to these materials as "soil", since it is a general term that is used to define all gravels, sands, and clays. Additionally, the penetrating rod is called as "pile" to define it from a geotechnical aspect. Considering the particle size and rod diameter in this study, it can be deduced that the DEM simulations present various examples of the penetration process that includes small-diameter piles and soils with gravel particles. Conceptually, the discussed subject is rod penetration into a granular assembly.

3.1. Methodology

3.1.1. General Information

In this study, commercial DEM software EDEM (2018) is used for modelling pile penetration problem. The model involves a cylindrical chamber that contains grains

and a bar element that simulates the pile as illustrated in Figure 3.1. The assembly of particles in the chamber represents a dry and cohesionless soil model. Dimensions of the model chamber and the model pile are given in Table 3.1. The ratio of chamber diameter to pile diameter (D_c/B) is 16.67. This diameter ratio is selected following the work of Falagush *et al.* (2015). DEM requires a contact model for calculating interaction forces and particle displacements. In this study, Hertz-Mindlin model is defined as the contact model in all simulations. Additionally, definition and input of several parameters are necessary for simulating pile penetration. Since the main purpose of this study is to investigate the sensitivity of DEM pile penetration model to grain and model characteristics, input parameters are varied as shown in Table 3.2.

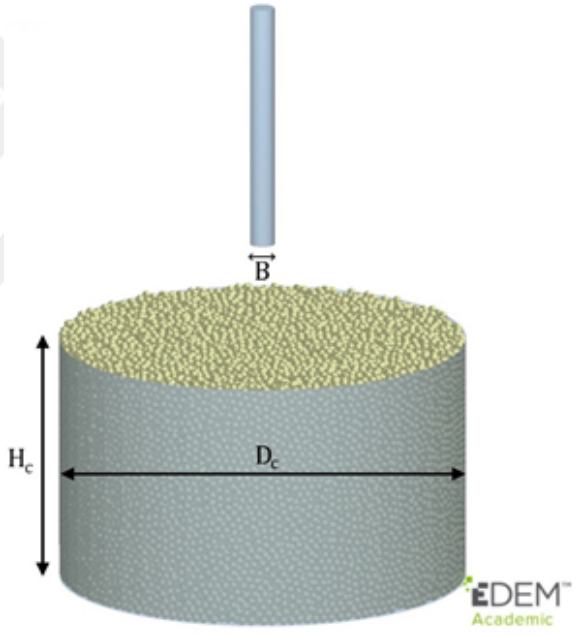


Figure 3.1. Set-up of the simulation of pile penetration.

Table 3.1. Dimensions of the chamber and the pile in the DEM models.

Dimension	**Units**	**Value**
Chamber diameter, D_c	mm	500
Chamber height, H_c	mm	225, 300, 450
Pile diameter, B	mm	30

Table 3.2. A summary table with all values of the parameters used in the DEM models.

Parameters	**Units**	**All values in use**
Particle density, ρ_p	kg/m^3	2650
Poisson's ratio, ν_p	-	0.2
Particle shear modulus, G_p	Pa	10^7, 5x10^7, 10^8, 5x10^8, 10^9
Average particle diameter, D_{50}	mm	7.5, 8.75, 10
Coefficient of Uniformity, C_u	-	1, 1.5, 2
Aspect Ratio, AR	-	0.714, 0.833, 1
Inter-particle static friction coefficient, $\mu_{(s,particle)}$	-	0.1, 0.3, 0.5, 0.7, 0.9
Rolling friction coefficient, μ_r	-	0, 0.05, 0.1, 0.2
Pile velocity, ϑ_{pile}	mm/s	35
Coefficient of static friction between soil particles and pile, $\mu_{(s,pile)}$	-	0.45
Coefficient of restitution, e_r	-	0.01

3.1.2. Sample Preparation

In this study, soil models are dry and cohesionless. Models of soil are prepared in a cylindrical chamber with frictionless walls. The mean diameter of the particles varies from 7.5 mm to 10 mm as defined in Table 3.2. Even the smallest particle specified in this study is larger than the largest soil particle in reality, but this deviation from reality is necessary to reduce the computational cost.

DEM samples are generated using the air-pluviation method. The air-pluviation method drops particles from a constant height with a constant rate into the chamber under the action of gravity. Air-pluviation is preferred since it is reproducible and allows good control over sample density. For air-pluviation, a dynamic factory capable of producing 100,000 particles per second is created. A higher particle generation rate results in looser samples. However, an increase in rate decreases computational time

up to a threshold value after which an increase in rate increases computation time, since at very high rates particles overlap and obstruct each other within the confined space of the factory.

Accordingly, the particle generation rate in this study is selected to minimize computational demand. Using air-pluviation, the packing density of the resulting granular arrangement can be controlled by adjusting inter-particle static friction. Accordingly, in this study, samples at different void ratios are prepared by adjusting inter-particle static friction. After filling the chamber, particles are allowed to settle under gravity until the time at which kinetic energies of particles are less than 10^{-4} percent of their potential energy, as suggested by Janda & Ooi (2016). When the particle settlement stage is completed and before the commencement of pile penetration, the coefficient of static friction between particles is set to its final value (Figure 3.2a).

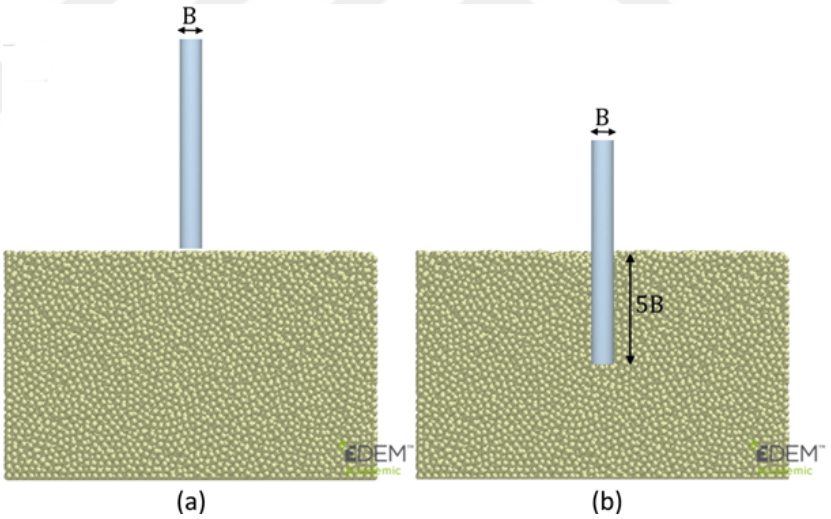


Figure 3.2. DEM model: (a) before pile penetration; (b) after pile penetration.

3.1.3. Pile Penetration Procedure

A closed-ended steel bar that is 30mm in diameter simulates the pile in each DEM model. The coefficient of the static friction between the pile and soil particles is set to 0.45 to provide a certain level of roughness to the pile. For quasi-static penetration into a granular medium, the penetration velocity, ϑ_{pile}, should be less than the upper

limit velocity for quasi-static penetration which is calculated using

$$\vartheta_c = \sqrt{2gd_p}/10 \tag{3.1}$$

where g and d_p are gravitational acceleration and grain diameter, respectively Feng *et al.* (2019). According to Feng *et al.* (2019), penetration velocity does not have any influence on resistance force as long as $\vartheta_{pile} < \vartheta_c$. The upper limit is around 38 mm/s in this study since the smallest particle is 7.5 mm in diameter. To eliminate velocity effect on resistance force, the pile penetrates at a constant velocity of 35 mm/s in all simulations. The penetration depth is equal to five times the pile diameter as indicated in Figure 3.2b, corresponding to 150 mm in this study. This ratio is chosen following the work of Duan *et al.* (2018) in which the pile penetration depth is 4.44 times the diameter.

The solid line in Figure 3.3 shows the typical variation of penetration resistance with depth. Variation of penetration resistance with depth includes instantaneous fluctuations. Since the pile penetrates a medium composed of discrete particles, the number and arrangement of particles in contact with the pile can change suddenly at every time step of the simulation, as opposed to the case of pile penetration into a continuum. The instantaneous variations in the fabric of the material that is penetrated lead to fluctuations in penetration resistance. In this study, the time step is set to 10^{-6}s. This time step is significantly small and results in a very high rate of data collection compared to experimental studies. Thus, a temporal averaging is performed on the data of penetration resistance following the suggestion of Janda and Ooi (2016). Averaging time used in this study (averaging 100 data points) can capture the general shape of the penetration resistance vs penetration depth curve while allowing comparison of the results of different models, as shown in Figure 3.3. All comparisons in this study are done using results after temporal averaging since relative differences can be more effectively identified with smoother curves.

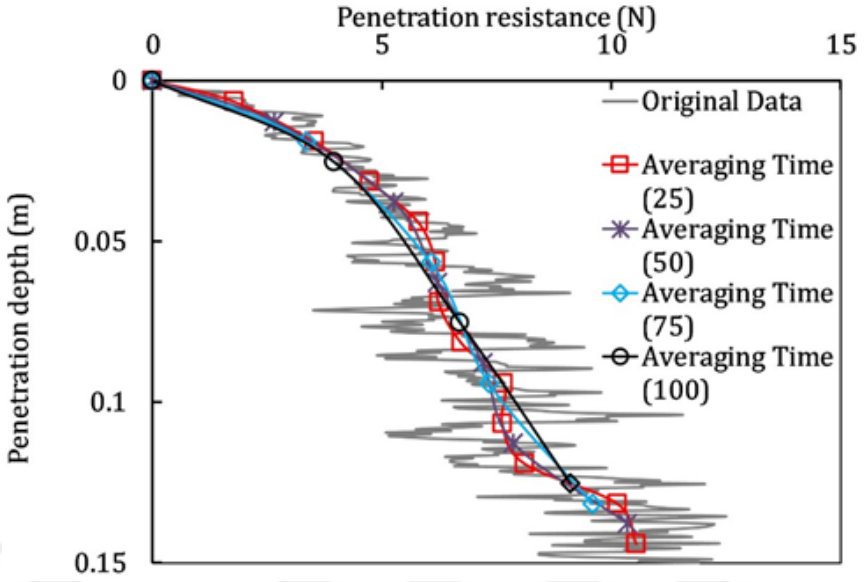


Figure 3.3. Various temporal averaging of original data of penetration resistance.

3.2. Consideration of Boundary Effect

Before proceeding with the study, it is necessary to eliminate the risk of boundary interaction. For this purpose, models with different dimensions are used to investigate possible boundary effects. Accordingly, mold depth (22.5 cm, 30 cm, and 45 cm), particle size (7.5 mm and 10 mm), and packing density (loose and dense) are varied in models and the results are compared to check whether the selected model characteristics satisfy the necessary criteria. Models prepared solely for investigating boundary effect are referred to as supplementary models and are numbered in Table 3.3 with the letter 'S'.

Figure 3.4 presents the results obtained from loosely packed models prepared with 10 mm diameter particles for three different mold depths (Models 4, S1, and S2). As observed, for each mold depth, normal force chain networks (for the rest of the paper, all force chain networks are normal force chain networks) for penetrations at the half and final distances are shown (Figure 3.4a, Figure 3.4b, Figure 3.4c). In these figures, grey lines, red lines, and black lines define weak, strong, and very strong force chains, respectively. When examined, it will be noticed that some strong chains exist at the bottom of the mold independent of the penetration effect; these are produced by

self-weights of the particles and exist even before penetration. Clearly, in the case of models with loose packing, force chain networks in none of the models connect the pile toe to the boundaries at any stage of penetration. This observation is supported by the penetration resistances measured as shown in Figure 3.4d. Apparently, the variations of penetration resistances with depth are practically the same for all loose models with 10 mm diameter particles, showing that there is indeed no boundary interaction.

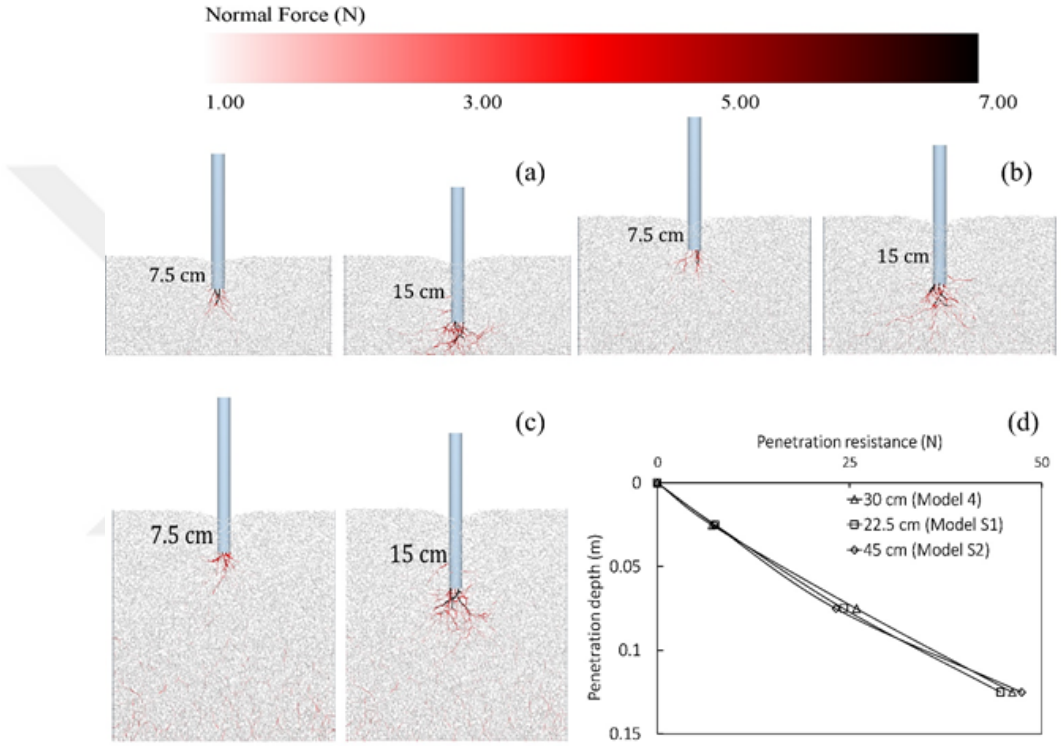


Figure 3.4. Investigation of boundary effect for loose models with different mold depths; force chain networks at halfway and full penetration a) H_c =22.5 cm b) H_c =30 cm c) H_c =45 cm and d) comparison of penetration resistances for all mold depths (G_p = 5 x 10^8 Pa, e = 0.7, d_p = 10 mm).

The same exercise is repeated with densely packed models composed of 10 mm diameter particles and the results are shown in Figure 3.5 (Models 7, S3, and S4). Evidently, for the model with 22.5 cm deep mold (Model S3), the strong force chains emanating from the pile toe reach the bottom boundary, suggesting boundary interaction. This is not the case for models with deeper molds (Models 7 and S4 with 30 cm and 45 cm respective depths). This observation is supported by the greater penetration

resistance obtained with 22.5 cm deep mold, whereas the results from the models with deeper molds agree perfectly with each other. These results suggest that using a 30 cm deep mold is sufficient to prevent boundary interaction.

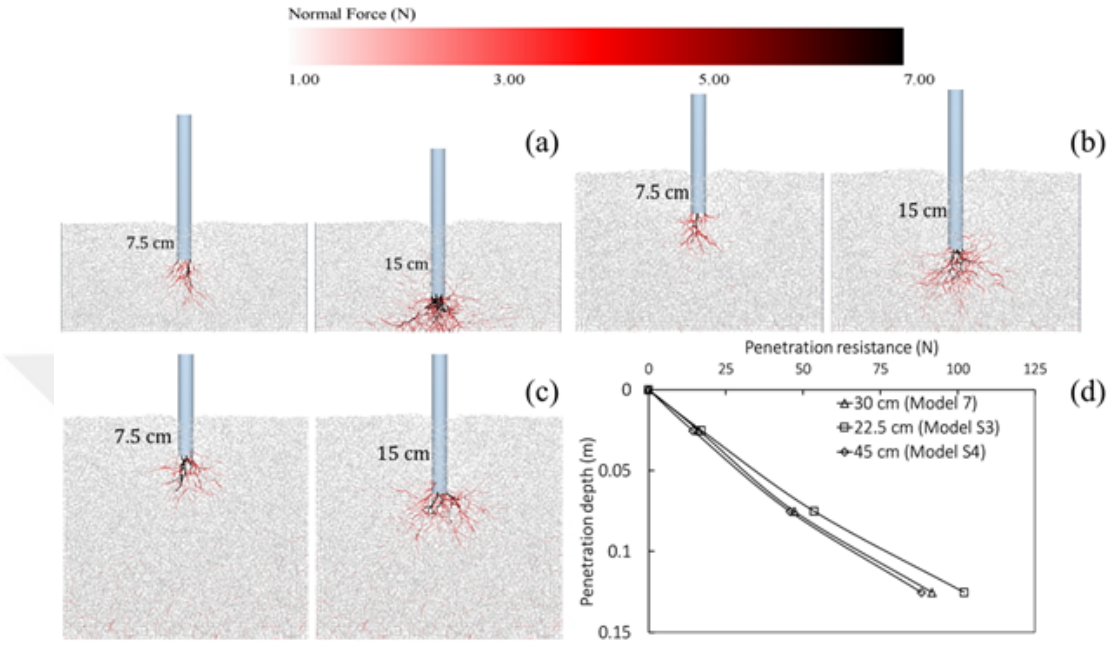


Figure 3.5. Investigation of boundary effect for dense models with different mold depths; force chain networks at halfway and full penetration a) H_c =22.5 cm b) H_c =30 cm c) H_c =45 cm and d) comparison of penetration resistances for all mold depths (G_p = 5 x 10^8 Pa, e = 0.7, d_p = 10 mm).

The maximum and minimum mean particle diameters used in this study are 10 mm and 7.5 mm, respectively. Therefore, the suitability of using a mold depth of 30 cm is considered for models made up of 7.5 mm diameter particles. Since it is already shown that 22.5 cm is not sufficient as mold depth, only 30 cm and 45 cm depths are used for comparison. Force chain networks at the end of penetration and variations of penetration resistances with depth obtained from loosely (Models 14 and S5) and densely packed models (Models S6 and S7) are shown in Figure 3.6. Clearly, for both 30 cm and 45 cm molds, there is no boundary interaction. Therefore, considering the computational cost, the smaller of these two depths (30 cm) is chosen as the model depth in this study.

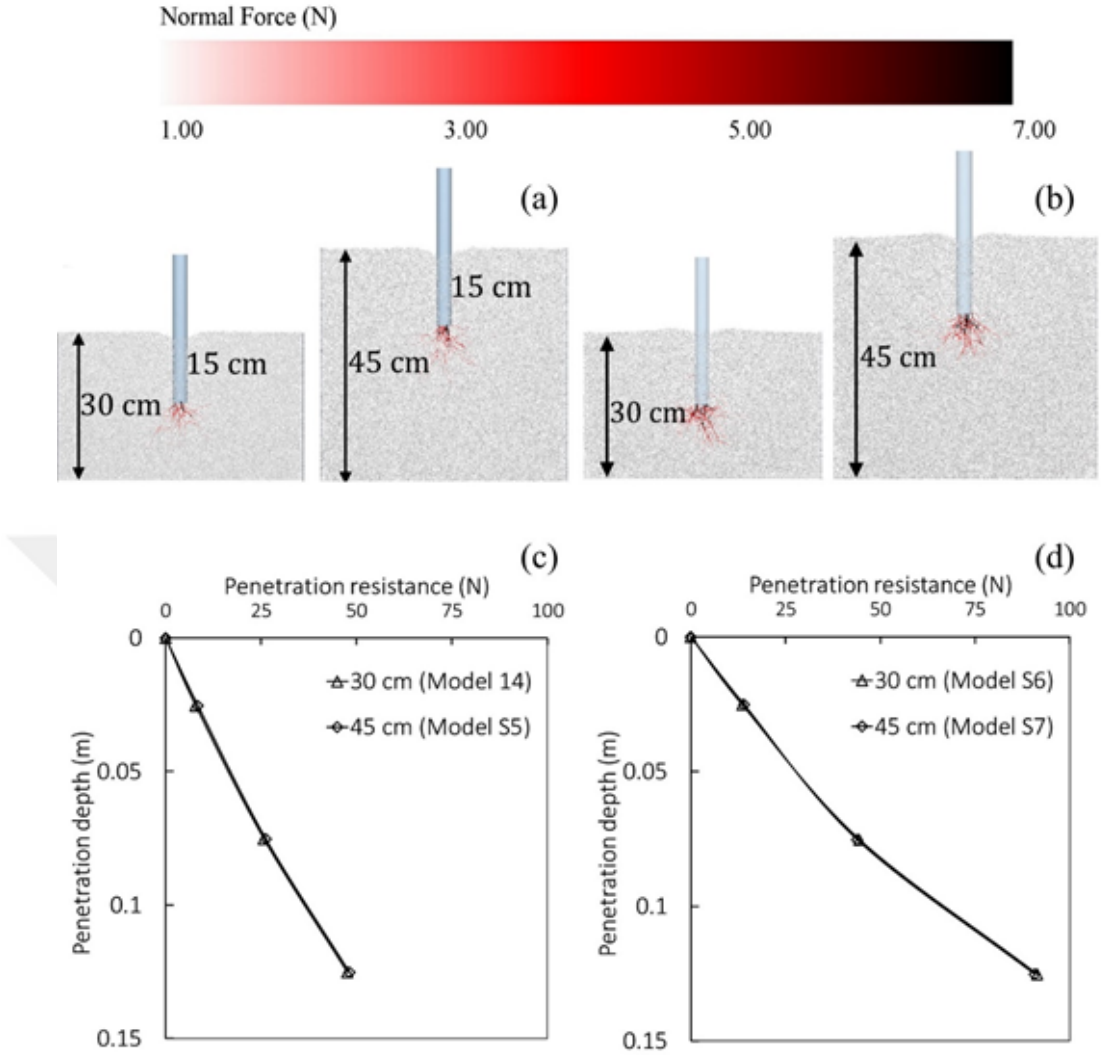


Figure 3.6. Investigation of boundary effect for 30 cm and 45 cm deep molds; force chain networks at full penetration and comparison of penetration resistances: for loose model with e = 0.67 (a and c) and for dense model with e = 0.56 (b and d) (G_p = 5 x 10^8 Pa, d_p = 7.5 mm.)

3.3. Test Program

The test program includes 23 DEM models. Parameters used in each model are given in Table 3.3. Sensitivity of DEM penetration model to following soil characteristics are examined in this study:

- Particle stiffness

- Void ratio
- Inter-particle static friction
- Particle size
- Particle size distribution
- Particle shape
- Rolling friction

In order to understand the influence of a soil characteristic, the results of the models among which the soil characteristic under investigation varies are compared with each other. In those models, the values of all parameters, apart from the parameter whose influence is under investigation in that section, are fixed. Thus, a variety of comparisons based on the penetration resistance can be achieved for different soil characteristics. In this study, reported penetration resistances are products of both shaft resistance and end bearing. Therefore, they correspond to total resistances to penetration.

Table 3.3. Properties defined in each model of the test program.

Model	H_c	G_p	$\mu_{(s,particle)}$		μ_r		e	C_c	AR	D_{50}
No	**(cm)**	**(Pa)**	**Final**	**Filling**	**Particle**	**Pile**	**(-)**	**(-)**	**(-)**	**(mm)**
1	30	10^7	0.5	0.5	0	0	0.63	1	1	10
2	30	$5x10^7$	0.5	0.5	0	0	0.68	1	1	10
3	30	10^8	0.5	0.5	0	0	0.7	1	1	10
4	30	$5x10^8$	0.5	0.5	0	0	0.7	1	1	10
5	30	10^9	0.5	0.5	0	0	0.7	1	1	10
6	30	$5x10^8$	0.5	0.25	0	0	0.67	1	1	10
7	30	$5x10^8$	0.5	0	0	0	0.59	1	1	10
8	30	$5x10^8$	0.5	0.5	0	0	0.59	1	1	10
9	30	$5x10^8$	0.1	0	0	0	0.59	1	1	10

Table 3.3. Properties defined in each model of the test program (cont.).

Model No	H_c **(cm)**	G_p **(Pa)**	$\mu_{(s,particle)}$		μ_r		e **(-)**	C_c **(-)**	AR **(-)**	D_{50} **(mm)**
			Final	**Filling**	**Particle**	**Pile**				
10	30	$5x10^8$	0.3	0	0	0	0.59	1	1	10
11	30	$5x10^8$	0.7	0	0	0	0.59	1	1	10
12	30	$5x10^8$	0.9	0	0	0	0.59	1	1	10
13	30	$5x10^8$	0.5	0.39	0	0	0.67	1	1	8.75
14	30	$5x10^8$	0.5	0.5	0	0	0.67	1	1	7.5
15	30	$5x10^8$	0.5	0	0	0	0.56	1.5	1	10
16	30	$5x10^8$	0.5	0	0	0	0.51	2	1	10
17	30	$5x10^8$	0.5	0.1	0	0	0.59	1.5	1	10
18	30	$5x10^8$	0.5	0.31	0	0	0.59	2	1	10
19	30	$5x10^8$	0.5	0.205	0	0	0.59	1	0.83	10
20	30	$5x10^8$	0.5	0.25	0	0	0.59	1	0.71	10
21	30	$5x10^8$	0.5	0	0.05	0.05	0.59	1	1	10
22	30	$5x10^8$	0.5	0	0.1	0.1	0.59	1	1	10
23	30	$5x10^8$	0.5	0	0.2	0.2	0.59	1	1	10
S1	22.5	$5x10^8$	0.5	0.5	0	0	0.7	1	1	10
S2	45	$5x10^8$	0.5	0.5	0	0	0.7	1	1	10
S3	22.5	$5x10^8$	0.5	0	0	0	0.59	1	1	10
S4	45	$5x10^8$	0.5	0	0	0	0.59	1	1	10
S5	45	$5x10^8$	0.5	0.5	0	0	0.67	1	1	7.5
S6	30	$5x10^8$	0.5	0	0	0	0.56	1	1	7.5
S7	45	$5x10^8$	0.5	0	0	0	0.56	1	1	7.5

3.4. Results and Discussions

3.4.1. Effect of Particle Stiffness on Penetration Resistance

One of the possible ways of decreasing computational cost in DEM is to reduce particle stiffness as recommended by Malone and Xu (2008). Using softer particles will result in larger critical time steps, leading to a shorter computation time (EDEM 2018). There are various methods to determine the critical time-step for DEM simulations, among which Rayleigh time-step is the most frequently used. Moreover, Zienkiewicz

and Taylor (2000) suggested that the maximum stable time step can be determined by calculating the eigenvalues of the amplification matrix. It must be noted that in this study, Rayleigh's approach is utilized to determine the critical time step. This is because time steps in DEM are determined as a percentage of the Rayleigh time step. The conventional choice for the time step is to use 20% of the Rayleigh time step (EDEM 2018; Feng *et al.* 2019). The Rayleigh time step is calculated using Equation (2.6).

As it is seen in Equation (2.6), smaller G_p will result in greater T_R values. However, excessively soft particles can cause undesirable effects on soil behaviour. This presents an optimization problem that requires the identification of the minimum particle stiffness that does not result in deviation from realistic soil response. The magnitude of minimum particle stiffness that can be used in simulations is problem-specific and can vary based on the mechanism considered. For example, Lommen *et al.* (2014) showed that using a particle shear modulus above 10^7 Pa is sufficient to get accurate results in DEM simulations of the angle of repose tests, while minimum shear modulus must at least be 10^8 Pa in case of penetration tests. Accordingly, the goal is to determine the minimum magnitude of particle shear modulus above which the results of penetration analysis do not significantly change. For this purpose, the results of the penetration simulations for which only particle stiffness is changed are compared with each other. These models are Models 1 to 5 (Table 3.3). As it is seen in Figure 3.7, the effect of the particle stiffness on penetration resistance starts to diminish once particles' shear modulus exceeds 10^8 Pa. Thus, based on the results presented in Figure 3.7, particle shear modulus that is equal to $5x10^8$ Pa is just sufficient to obtain accurate results in case of pile penetration problems. Accordingly in this study, particles' shear modulus is set to $5x10^8$ Pa in all the other models.

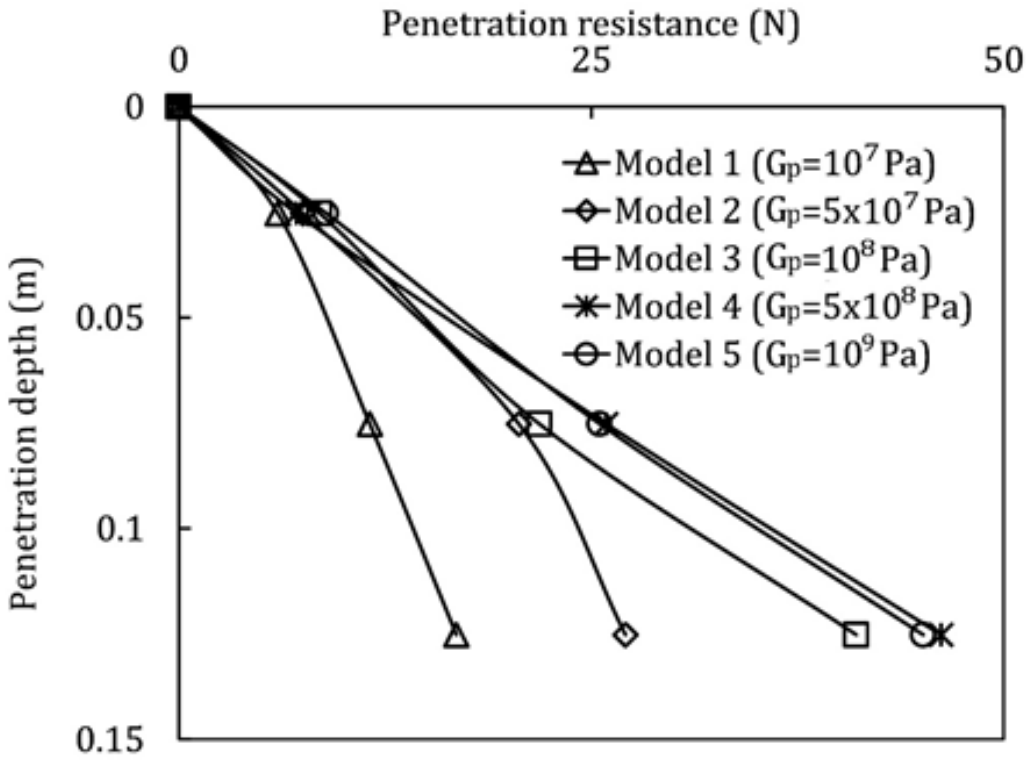


Figure 3.7. Influence of particle shear modulus on penetration resistance.

3.4.2. Effect of Void Ratio on Penetration Resistance

Soil density is one of the most critical factors that affect soils' mechanical behaviour. For dry soils, density is dependent on the arrangement grains. DEM allows the preparation of granular bodies at different densities. When soils models are prepared by pluviation, target density can be achieved by adjusting inter-particle friction. Use of smaller magnitudes of inter-particle friction during pluviation leads to smaller void ratios, resulting in denser packing. Certainly, knowledge of void ratio alone is not sufficient to determine whether an arrangement of grains is dense or loose. For a reliable evaluation of density, it is also necessary to know the loosest possible and the densest possible states and the corresponding void ratios. Influence of void ratio on penetration resistance can be ascertained by comparing the results of models that have the same characteristics, regarding shape, gradation, specific gravity and shear modulus, but different void ratios. This condition is satisfied for three different models listed in Table 3.3. These are models 4, 6, and 7. These three models are prepared

using different magnitudes of inter-particle friction during the pluviation stage. This resulted in different depositional characteristics and yielded different packing densities. The inter-particle friction coefficients during the pluviation stage are 0.5, 0.25 and 0 for Models 4, 6, and 7, respectively. This resulted in soil model void ratios that are 0.7, 0.67, and 0.59, in the same order. Once the models are ready, prior to the commencement of penetration test, inter-particle friction values are all changed to the target value, which is 0.5. Among the three models that only differ in their void ratios, Model 7 represents the densest state possible, since during the pluviation stage of this model the particles were not restricted with frictional resistance as the coefficient of the inter-particle friction was set to zero. Conversely, as explained in the previous section, soil in Model 4 corresponds to the loosest possible state because $\mu_{(s,particle)}$ was set to 0.5, which is already target value, during the pluviation stage. Thus, the soil samples in Models 4, 6 and 7 can be classified as loose, medium dense and dense, respectively.

In addition to model preparation using pluviation with adjusted inter-particle friction coefficients, it is possible to compress the granular arrangement to target void ratio by loading and unloading. For understanding the possible influence of model preparation technique on penetration resistance, a single model (Model 8) is prepared using this latter method. Model 8 is prepared initially by pluviating particles that have inter-particle friction coefficients equal to 0.5. This resulted in loose arrangement as in the case of Model 4. Later, this arrangement is compressed using a top plate and unloaded to achieve the target void ratio (e = 0.59). In their final states, Model 7 and Model 8 have the same void ratio. However, these two models have significantly different coordination numbers (Figure 3.8a). Coordination number is a micro-scale indicator, which gives information on contact density within a granular sample. It is defined as the average number of contacts per particle. Observed difference in the coordination number of Models 7 and 8 is expected, since greater number of contacts in a frictional environment will require more work input, therefore, number of contacts in frictional assemblies tend to be smaller. Evident in Figure 3.8a, loading and unloading did not cause a change in the initial coordination number. On the other hand, frictionless assemblies can freely rearrange and this results in structures with greater contact numbers. Additionally, greater coordination number leads to less intense force

networks, whereas the smaller coordination number of Model 8 results in more intense force networks (Figure 3.8b and Figure 3.8c, respectively). Clearly, this difference is due to the differences in magnitudes of force that should be carried per contact. The outcomes at the macro-scale as a result of this micro-scale mechanism are given in Figure 3.8d. Figure 3.8d compares the penetration resistances in Models 4, 6, 7, and 8 and, as expected, resistance is greater when the soil being penetrated is denser. Additionally, it is noticed that models that have the same void ratio (Models 7 and 8) yield practically the same penetration resistance, even though their coordination numbers are significantly different. This shows that macro behaviour is governed by average properties and penetration resistance is dependent on the average void ratio and stress state. This is expected, since the strength of a cohesionless assembly is a function of stress state and void ratio, as previously identified by many researchers studying the subject (Alshibli and Cil 2018; Bolton 1986; Chakraborty and Salgado 2010; Cinicioglu and Abadkon 2015; Vaid and Sasitharan 1992). Therefore, for a cohesionless granular material, stress history does not have any influence over strength (peak friction angle, critical state friction angle, and dilation angle) as long as it does not lead to cementation or granular shape changes. This is observed in the relationships proposed in Bolton's (1986) seminal work. Bolton (1986) shows that peak dilatancy angle and peak friction angle are functions of relative density and mean effective stress at failure. It is also very well known that critical state friction angle is independent of stress history since it emerges after all effects of stress history are erased. Accordingly, the results of the models can be considered applicable to problems that involve cohesionless granular materials.

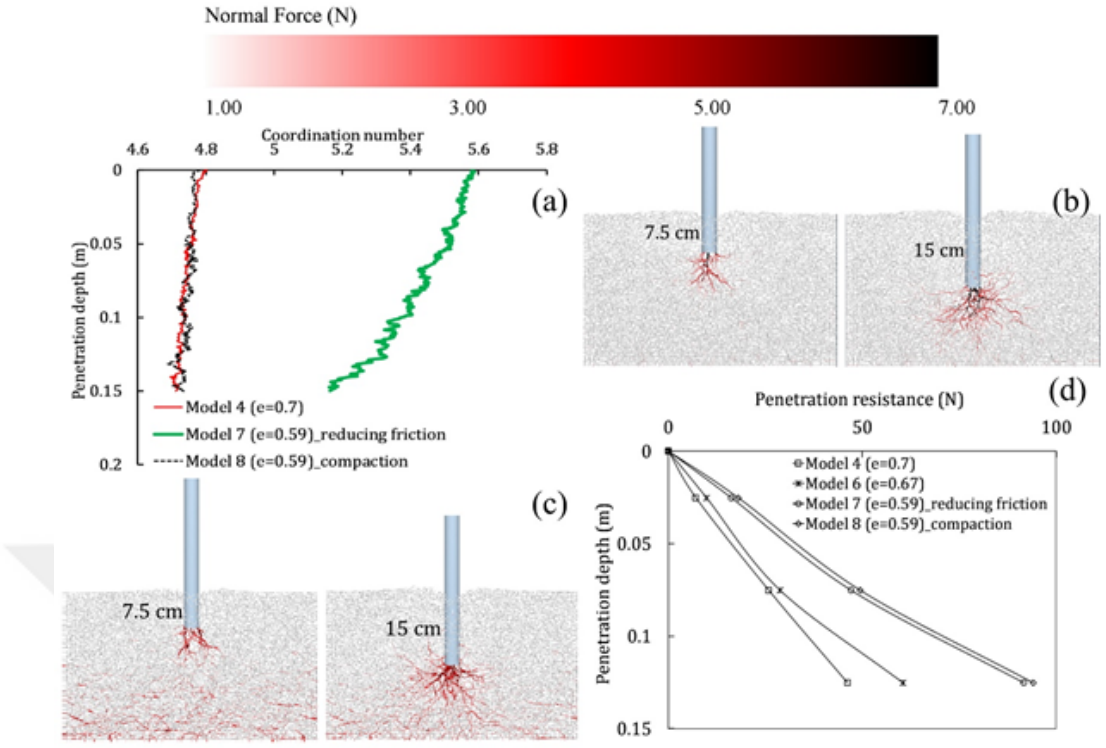


Figure 3.8. Influence of void ratio and soil fabric on penetration resistance: (a) average coordination numbers; (b) force chain networks at halfway and full penetration for model 7 prepared by air pluviation; (c) force chain networks at halfway and full penetration for model 8 prepared by loading-unloading; (d) comparison of penetration resistances for models 4, 6, 7 and 8.

3.4.3. Effect of Inter-Particle Friction on Penetration Resistance

Dry cohesionless soils consist of discrete particles that do not bond to each other. Thus, their mechanical behaviour is controlled by friction. The parameter that defines particle-to-particle interaction is inter-particle friction coefficient. Angle of repose, shear stiffness, coefficient of lateral earth pressure, peak and critical state friction angles (Barreto and O'Sullivan 2012; Chung and Ooi 2008; Gong *et al.* 2019; Yan *et al.* 2015) are just some of the mechanical characteristics of granular materials influenced by inter-particle friction. With DEM, it is possible to evaluate the influence of inter-particle friction coefficient on soil behaviour by varying its value between models. This is a necessary step in the development and validation of DEM models. The value of the inter-particle friction coefficient that results in a model that conforms with experimen-

tal results is sought in all DEM models. Accordingly, the influence of the inter-particle friction coefficient on penetration resistance is investigated. For this purpose, four soil samples (Models 9-12) that have differing inter-particle friction coefficients are prepared in addition to the sample in Model 7 while the rest of the parameters that define these models are kept the same. Information about these models is given in Table 3.3. The influence of the inter-particle friction coefficient on penetration resistance can be ascertained by comparing the results of these five models (Figure 3.9).

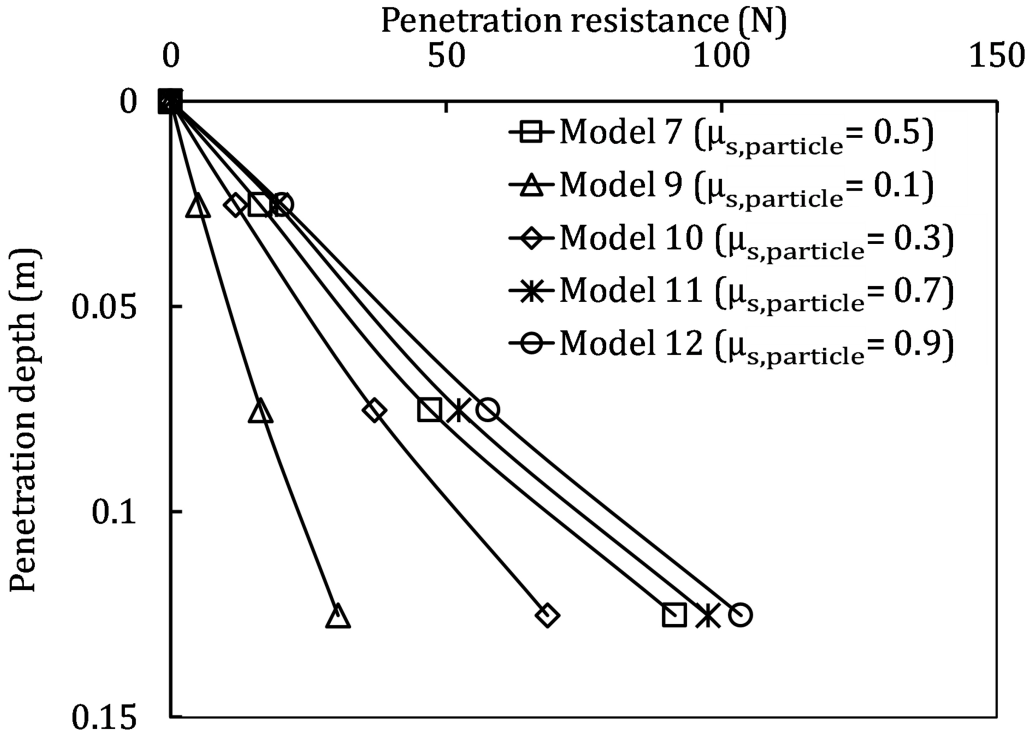


Figure 3.9. Effect of coefficient of inter-particle friction on penetration resistance.

According to Figure 3.9, an increase in inter-particle friction coefficient has a very high influence until $\mu_{(s,particle)}$ becomes 0.5. For values of $\mu_{(s,particle)}$ that are greater than 0.5, the effect of the inter-particle friction starts to saturate. Several researchers attribute this trend to the fact that inter-particle friction coefficient can have a profound effect on soil mechanical behaviour only up to a threshold value (Dai *et al.* 2016; Huang *et al.* 2014; Tran *et al.* 2016). According to Huang *et al.* (2014) and Dai *et al.* (2016), the dominance of particle sliding at particle to particle contact points starts to diminish with the increase of $\mu_{(s,particle)}$. This is because with greater values of

$\mu_{(s,particle)}$, rolling starts to become more energy-efficient than sliding. Particle rotation is free in all samples used for comparison (Models 7, 9,10,11, and 12). Obtained results are compatible with Huang *et al.* (2014) and Dai *et al.* (2016). Accordingly, it is seen that the resistance the soil shows to pile penetration can be also responsive to increases in inter-particle friction only until a limit value.

3.4.4. Effect of Particle Size on Penetration Resistance

Modeling particles at their actual sizes is the most realistic option for DEM based soil simulations. However, this is not practical in terms of computational cost, since using actual particle sizes will result in a staggeringly high number of particles, even with small-sized soil samples. Effect of particle size on total simulation time is twofold. The expected first effect is that the number of particles needed to simulate a soil sample will increase with the reduction in particle size; increase in the number of particles in simulation increases necessary computational time. Secondly, the smallest particle size in simulation is a parameter in the calculation of time step. As the smallest size becomes smaller, the Rayleigh time step also gets smaller, as seen in Equation (3.2). Smaller time steps correspond to longer simulation times as they require greater number of calculations (EDEM 2018). Therefore, it is customary to scale up particle size in DEM models in order to decrease computational cost, even at the expense of influencing soil behaviour. For that reason, it is necessary to determine the possible influences of particle upscaling on mechanical behaviour when modelling with DEM (Coetzee 2019; Lin and Wu 2012; Liu and Wang 2016; Miyai *et al.* 2019; Vangla and Latha 2015). In order to be able to observe the effect of particle size on penetration response, it is more meaningful to investigate the effect of relative particle size (B/D_{50}) rather than the particle size itself. In addition, all the input parameters apart from particle size, such as particle morphology, particle size distribution and void ratio of sample, should remain the same (Esposito *et al.* 2018; Miyai *et al.* 2019; Vangla and Latha 2015). Accordingly, two different models are generated using particles with sizes equal to 8.75 mm and 7.5 mm in diameter; these are Model 13 and Model 14 in Table 3.3, respectively. Since pile diameter remains constant in this study, (B/D_{50}) varies with the variation of particle size. (B/D_{50}) ratios in Models 6, 13 and 14 are calculated as 3, 3.43 and 4, respectively

as the pile diameter is constant at 30 mm. The aim is to prepare models composed of uniformly graded soils that have the same void ratio as that of Model 6 which would make it possible to investigate the effect of particle size only. Models that have the same void ratio, but different uniform grain sizes, are prepared by adjusting the inter-particle friction coefficients during the filling stage. When the inter-particle friction coefficients used in the filling stages of models that have successively smaller size particles are compared (specifically models 6, 13, and 14), it is noticed that higher coefficients of inter-particle friction are necessary when particle sizes are smaller to achieve the same void ratio. Eventually, the required coefficients inter-particle coefficients of friction during air-pluviation in Models 6, 13, and 14 are determined as 0.25, 0.39, and 0.5, respectively (Table 3.3). After the generation of DEM models, penetration resistances obtained from the simulations of Model 6, Model 13 and 14 (Table 3.3) are compared. According to the results shown in Figure 3.10, models with smaller particles show lower resistances to pile penetration, when all the other characteristics are the same. These findings are compatible with previous studies, such as Bolton *et al.* (1999), Feng *et al.* (2019) and Miyai *et al.* (2019). However, when the results in Figure 3.10 are examined, it is not possible to suggest a significant particle size effect. However, Bolton *et al.* (1999), Peng *et al.* (2009) and Kang *et al.* (2018) asserted that effect of particle size on penetration resistance is negligible for (B/D_{50}) values greater than 20. Based on the results in literature, it is possible to assume that penetration resistances in these tests are under the influence of particle size. But, the observed trend shown in Figure 3.10 where models with larger size particles generate greater resistance to penetration is in line with expected theoretical response. This is because when all other characteristics are the same, grains with larger sizes produce greater critical state friction angles, and therefore greater frictional resistances, as shown and explained by Dai *et al.* (2016).

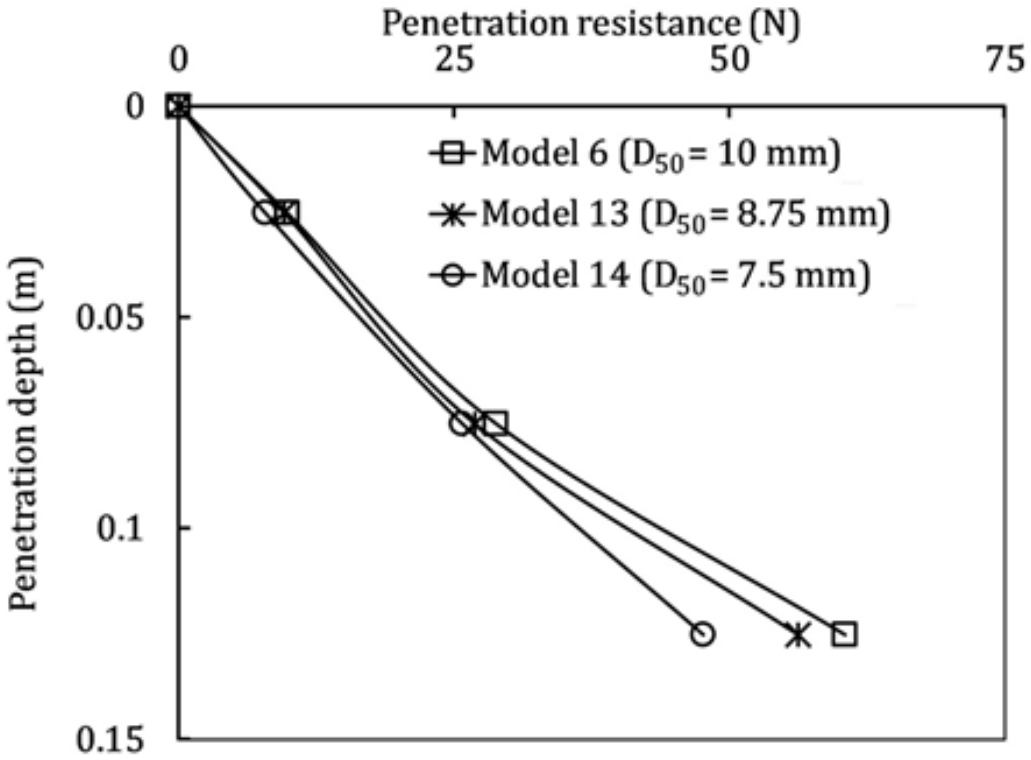


Figure 3.10. Effect of particle size on penetration resistance.

3.4.5. Effect of Particle Size Distribution on Penetration Resistance

Soil classification is the first step towards understanding possible mechanical responses and properties of soils. Especially, in case of cohesionless soils, behaviour is directly dependent on particle size distribution (PSD). Three coefficients are used to quantify the characteristics of particle size distribution curves; these are the mean particle size (D_{50}), coefficient of uniformity (C_u) and the coefficient of curvature (C_c). C_u and C_c are calculated using

$$C_u = D_{60}/D_{10} \tag{3.2}$$

and

$$C_c = D_{30}^2/\left(D_{60} \times D_{10}\right). \tag{3.3}$$

In Equation (3.2) and Equation (3.3), D_{10}, D_{30}, and D_{60} represent the diameters corresponding to 10%, 30%, and 60% finer by weight, respectively. For all the models, the magnitude of D_{50} is 10mm, except Model 13 and Model 14. Similarly, the coefficients of curvature (C_c) in all models ranged between 0.996 and 1.04, therefore it can be considered to be the same as the differences between models are insignificant. Then, among the coefficients defining the characteristics of particle size distribution curves of models in this study, C_u is the only distinguishing factor. Accordingly in this study, particle size distribution curves with three different C_u values are adopted. These are PSD_1, PSD_2, and PSD_3 with C_u values 1, 1.5, and 2, respectively (Table 3.4). The resulting PSD curves are illustrated in Figure 3.11. As seen in Figure 3.11, the mean particle sizes are the same for all PSD curves.

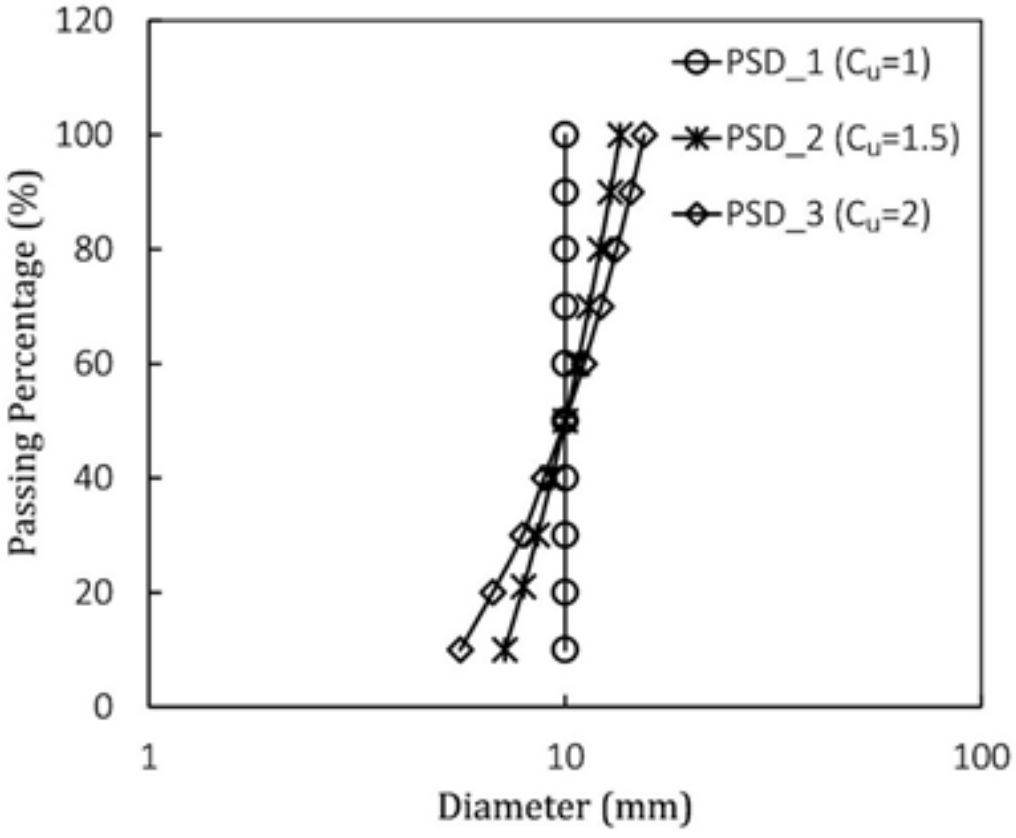


Figure 3.11. Different PSDs used in the models.

Table 3.4. Parameters of the PSD.

PSD Type	C_c (D_{60}/D_{10})	C_c $(D_{30}^2/(D_{10} \times D_{60}))$	D_{50} **(mm)**
PSD_1	1	1	10
PSD_2	1.5	1	10
PSD_3	2	1	10

The effect of particle size distribution on mechanical behaviour of soils can be classified into two aspects. Firstly, different PSD curves will result in different sample void ratios if they are prepared under the same conditions. This is because a PSD with a greater C_u corresponds to a sample with different sized particles and the smaller sized particles tend to fill voids within larger sized particles; thus, porosity (or void ratio) decreases. Secondly, samples that are collections of different-sized particles are not expected to behave the same as ones with uniform graded particles even when they are prepared at the same void ratio. Therefore, in this study, two models for each PSD curve are prepared. The first of the two models is prepared at the densest possible state by keeping inter-particle coefficient of friction zero during pluviation. For all models prepared at their densest states, void ratios might differ as a result of different PSD curves, but their relative densities are all 1. The models prepared at the densest possible state are Model 7, Model 15, and Model 16 for PSD_1, PSD_2; and PSD_3, respectively. The second of the two models is prepared with a target void ratio by adjusting the inter-particle coefficient of friction during air-pluviation; target void ratios for the second models of all PSD curves are the same for the purpose of comparison. For the models at the target void ratio, two models are prepared for PSD_2 and PSD_3 gradation curves to achieve the same void ratio as that of Model 7 (PSD_1), which is 0.59. These models are Model 17 and Model 18 for PSD_2 and PSD_3, respectively. By preparing the models at the same void ratio but with different gradations, differences in resistances to penetration in these soils will only be the product of the differences in gradation.

Eventually, five different models (Models 7, 15, 16, 17, and 18), whose details are given in Table 3.3, are used to investigate the influence of grain size distribution on penetration resistance of soils. When the results of penetration into these five models as shown in Figure 3.12 are examined, it is observed that models having PSD curves with greater C_u show higher resistances to pile penetration if they are all at their densest possible states (void ratios are 0.59, 0.56 and 0.51 for the samples with C_u= 1, 1.5 and 2, respectively). This is because each model has a different void ratio at the densest state as a result of the differences in gradation; models with smaller void ratios at densest state exhibit greater resistance to penetration as expected. On the other hand, when the samples are prepared at the same void ratio, then higher C_u values result in less resistance to penetration. Here it should be noted that coordination number does not influence resistance to penetration as previously explained in Section 3.4.2. Hence, differences in penetration resistance are caused by the differences in their relative degree of packing. Considering Figure 3.12, greater the difference of a model's void ratio from its void ratio at the densest state, less dense it's granular packing is. This is also observed by the required coefficient of inter-particle friction to achieve the target void ratio during pluviation; the required coefficients of inter-particle friction to achieve a void ratio of 0.59 are 0, 0.1, and 0.3 for Models 7, 17, and 18, respectively. Correspondingly, models that are at a looser state yielded relatively lower penetration resistances, even if they have the same void ratio. Therefore, gradation's actual impact is caused by its influence over relative degree of packing.

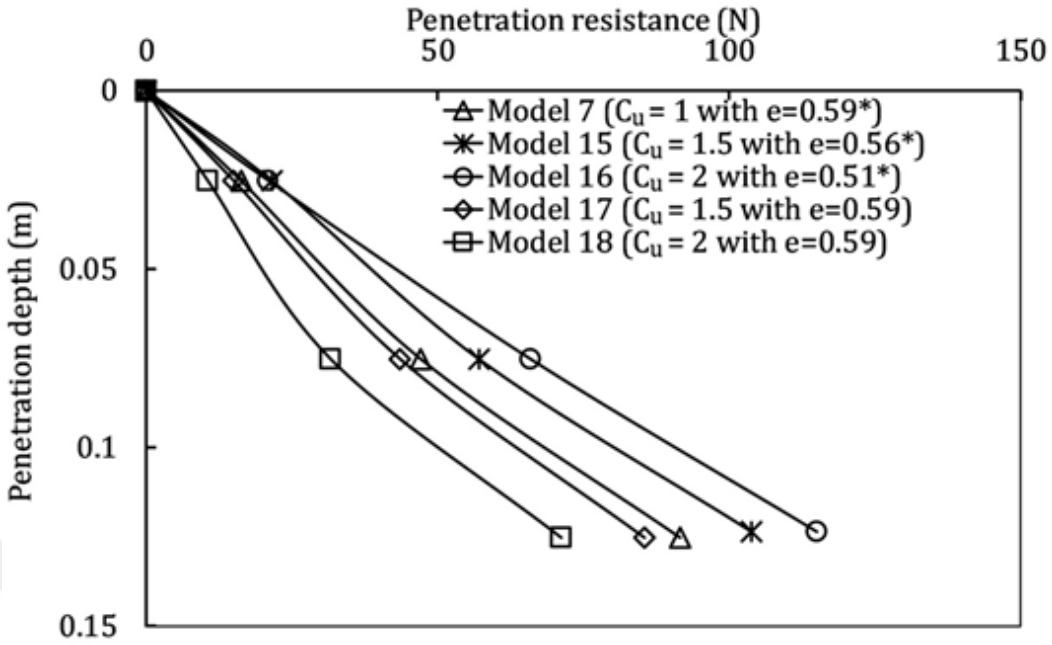


Figure 3.12. Effect of PSD on penetration resistance (* at the densest state).

Particle size distribution influences also the computational time by two different means. First, the number of particles required to achieve a certain void ratio is dependent on the particle size distribution of the assembly. Second, for models with the same D_{50} values, smallest particle diameter decreases with increasing C_u, and it is the diameter of the smallest sized particle in the assembly that is used as d_p in Equation (2.6) to calculate time step. To observe these effects, Models 7, 17, and 18 that have the same void ratio, the same D_{50} values, but different C_u magnitudes are used (Table 3.5). As it is seen in Table 3.5, PSD curve with higher C_u requires larger number of particles to achieve same void ratio if all the other characteristics of models are kept constant. In addition, an increase in C_u with a constant D_{50} leads to a decrease in the diameter of the smallest sized particle in the assembly, as shown in Table 3.5. Since computational time is proportional to the number of particles and inversely proportional to the diameter of the smallest particle in the assembly, it is clear that a model having a PSD curve with greater C_u requires relatively more computational time.

Table 3.5. Properties of models related with particle size distribution (PSD).

Model No	C_u $(D_{60/D_{10}})$	**Void ratio**	**Total Number of Particle**	D_{50} **(mm)**	**Smallest Particle Diameter (mm)**
Model 7	1	0.59	70750	10	10
Model 16	1.5	0.59	83782	10	7
Model 17	2	0.59	111624	10	5.6

3.4.6. Effect of Particle Shape on Penetration Resistance

Particle shape, an inherent soil characteristic, has a significant effect on soil behaviour. Morphology of granular materials can be quantified using shape parameters, such as aspect ratio, convexity, sphericity, roundness, and angularity (Mitchell 1993; Soltanbeigi *et al.* 2017). In this study, aspect ratio is the parameter of choice for quantifying particle shape. Aspect ratio (AR) is considered as the ratio of the minor axis length to the major axis length, as this is the preferred form in recent works, such as Jiang *et al.* (2018). To achieve aspect ratios different than 1, particles are clumped to each other. In this study, clumped particles are formed by defining two overlapped spheres. This way, particles with different aspect ratios are created as indicated in Figure 3.13.

Shape	d_{min} **(mm)**	d_{max} **(mm)**	AR (d_{min}/d_{max})
	10	10	1
	10	12	0.833
	10	14	0.714

Figure 3.13. Particle aspect ratio.

The clumps with different aspect ratios are separately used to generate the models labelled Models 19 and 20 in Table 3.3. The minor axis lengths of the clumped particles are all the same and equal to the average diameter (D_{50}) of the spherical particles in Model 7. Besides, models with particles that have different aspect ratios are prepared at the same void ratio as Model 7 by adjusting the inter-particle friction coefficient during the filling procedure. This is necessary for the considered non-spherical particles, since it is seen that the packing density is a function of aspect ratio value. Using trial and error, the coefficients of inter-particle friction in Model 19 (AR=0.833) and Model 20 (AR=0.714), which result in the same void ratio as Model 7, are determined as 0.205 and 0.25, respectively (Table 3.3). As seen for a smaller aspect ratio, a higher value of inter-particle friction must be assigned to achieve a comparable packing density. In other words, if the friction coefficient during filling is kept constant, then the models including longer particles will have higher densities. However, it must be noted that the increase in density with respect ratio is not always the case for cylindrical particles. Gan and Yu (2020) studied the variation of packing density with AR for cylindrical shape particles through DEM simulations. It is observed that the packing density, for AR <1, is increased up to around AR=0.667, and then further decrease in aspect ratio lead to a decrease in packing density. Thus, particle shape has a direct effect on soil behaviour even at the depositional stage. However, the main purpose of this study is to understand the impact of particle shape on penetration response. That is why, models composed of different shaped particles are prepared at the same void ratio. This way, it is possible to monitor the influence of particle shape uncoupled from density.

Accordingly, in Models 7, 19, and 20, all the parameters are the same, with the exception of aspect ratio. Variations of penetration resistance with depth are shown in Figure 3.14 for these three models. As it is clearly observed in Figure 3.14, even if the only difference between them is particle shape, models yield different penetration resistances. Specifically, smaller aspect ratio results in greater penetration resistance as long as the models are at the same void ratio (Figure 3.14). This is an expected outcome as deviation from sphericity hinders particles rotation capability. In other words, non-spherical particle shapes impose a partial restriction to rotation. Thus, granular structures show greater resistance to pile penetration as particles have more

elongated forms, corresponding to smaller aspect ratios.

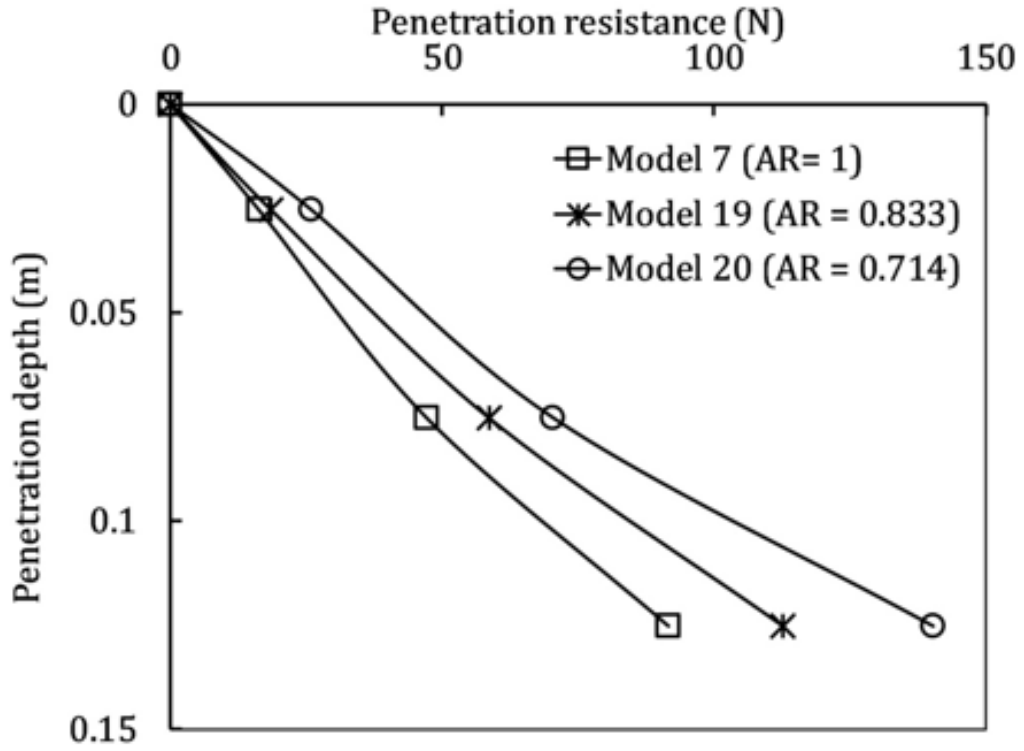


Figure 3.14. Effect of particle shape on penetration resistance.

3.4.7. Effect of Rolling Friction on Penetration Resistance

Rolling friction is defined as a torque resisting the rolling of particles. The torque is a function of normal force (F_n) and a coefficient of rolling friction (μ_r) as given in

$$\tau_i = -\mu_r F_n R_i \omega_i \tag{3.4}$$

where $R_(i)$ and ω_i are the radius of each sphere in contact and the unit angular velocity vector of the object at the contact point, respectively (EDEM 2018). Spherical particles can normally rotate without limitation. On the other hand, non-spherical shapes of particles naturally restrict rotation by increasing interlocking. Thus, rolling friction function is a numerical substitute for particle shape (Wensrich and Katterfeld 2012). Considering the computational demand, it is more advantageous to use rolling

friction as opposed to defining non-spherical particle shapes. Especially in cases when actual particle morphologies are defined in DEM, computational cost can be staggeringly high. However, the results of some studies (Esposito *et al.* 2018; McDowell *et al.* 2012) suggested that when particles are restricted or inhibited to rotate, the kinematics of the problem is not the same as when non-spherical particles are defined. Thus, it is a matter of debate whether employing rolling friction to simulate particle shape effect is appropriate or not. To investigate the influence of rolling friction on penetration simulations, three different models are created. These are Models 21, 22 and 23 and their details are given in Table 3.3. As it is seen in Table 3.3, the coefficient of rolling friction values used in this study are 0.05, 0.1 and 0.2. Models that do not include rolling friction (μ_r=0) are also added to the comparison as references. These models are Model 7, composed of spherical particles and Models 19 and 20, composed of non-spherical particles. The penetration resistances measured in Models 7, 19, 20, 21, 22, and 23 are shown in Figure 3.15. When Figure 3.15 is examined, it is noted that the trends of penetration resistance curves obtained from the models with rolling friction are significantly different than the models without. With rolling friction, the rate of increase in resistance is significantly higher in the initial stages of penetration. This high rate of increase in penetration resistance diminishes in the later stages of penetration and can be noticed from the abrupt change in the slope of the penetration resistance-depth curve. As the soil models in this study do not have a crust zone such changes in the rate of increase of penetration resistance are not reasonable. These findings are compatible with McDowell *et al.* (2012) and Esposito *et al.* (2018). Apparently, rolling friction should not be used as a substitute for particle shape. Consequently, it is advised to use as realistic particle shapes as the computational cost allows in modeling penetration problems.

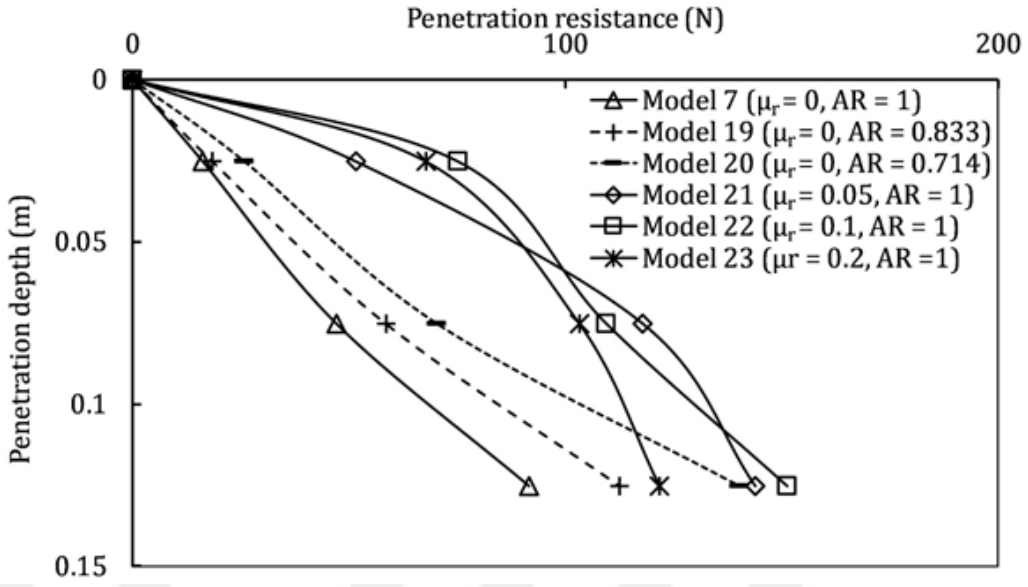


Figure 3.15. Comparison of the effects of rolling friction against particle shape on penetration resistance.

4. VALIDATION OF DEM MODELING OF PENETRATION IN GRANULAR MATERIALS AND METHODS TO REDUCE COMPUTATIONAL TIME

This chapter aims both to obtain a validated DEM model and to investigate the techniques used for reducing the computational cost. To achieve the first purpose, experimental results of a penetration study in the literature are used for the validation process. DEM models with different rolling friction coefficients are generated and the penetration resistance is obtained for each model. The resistance results are compared with the experimental ones to determine the model parameters for the validated model. As for the second purpose, three novel techniques are used for the model preparation to decrease the computational time of DEM simulations. To evaluate the validity of the approaches, the results from each of the models prepared with different techniques are compared with a similar sample that is prepared without any optimization technique.

4.1. DEM Model and Validation

4.1.1. General Description of Experiments Used for Validation of DEM Models

Here, the goal is to design a reliable DEM penetration model that is validated using experimental results. For this purpose, the results from experiments conducted by Feng *et al.* (2019) were selected as a means of verification. The model used by Feng *et al.* (2019) consists of a cylindrical object (with a diameter of 5 cm and length of 7 cm), and a cylindrical chamber (with diameter of 45 cm and depth of 21 cm) that is filled with assembly of 6 mm diameter spherical glass beads. The packing fraction (ratio of total particle volume to chamber volume) was adjusted as approximately 0.575 ($\pm$0.002). The cylindrical object penetrated the granular medium with a velocity of 0.5 mm/s, and each test is repeated five times. The resistance forces and penetration

depths were normalized using

$$p_n \equiv \frac{F}{\rho_p \times \Psi \times g \times S_o \times R_o} \tag{4.1}$$

and

$$h_n \equiv \frac{h}{R_o} \tag{4.2}$$

where F, ρ_p, Ψ, g, S, R and h are the penetration resistance, particle density, packing fraction, gravitational acceleration, section area of object, object radius, and, penetration depth, respectively (Kang *et al.*, 2018).

To clearly show the trend of the resistance along with the penetration depth, a temporal averaging is performed on the data obtained throughout the penetration following the suggestion of Janda and Ooi (2016) as explained in Section 3.1.3. According to Janda and Ooi (2016), each averaging of penetration resistance is taken for a displacement of the penetrator which is approximately 3.5 times the mean diameter of particles. In these experiments, the data were averaged at each 21 mm displacement since the bead diameter is 6 mm.

All the resistance forces are presented in a dimensionless and time-averaged form. Accordingly, the upper and lower boundaries of penetration resistance forces in the experiments conducted by Feng *et al.* (2019) are shown in Figure 4.1. These results are compared with the results obtained from the DEM simulations to determine the suitable parameters for a validated DEM model as mentioned in the following section.

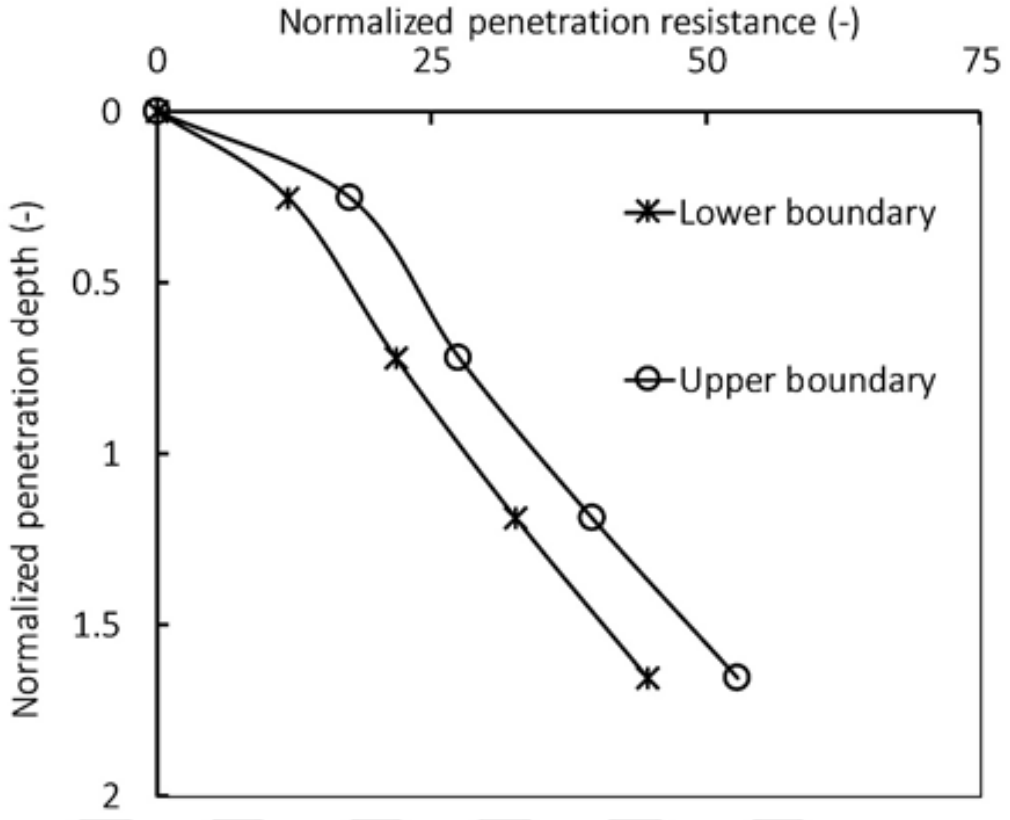


Figure 4.1. Upper and lower boundaries of the normalized penetration resistance forces in the experiments conducted by Feng *et al.* (2019).

4.1.2. Validation Procedure

In this section, the purpose is to generate a DEM model that gives compatible penetration resistance forces with the ones in the series of experiments conducted by Feng *et al.* (2019). In the generated models, the particle properties are used the same as in the study of Feng *et al.* (2019) (i.e. inter-particle friction, shape particle, particle size, particle density, and coefficient of restitution). The shear modulus for the particles is set to the same value as in the study of Gezgin *et al.* (2020). The material parameters constantly used in the validation process are given in Table 4.1.

The chamber is generated as a box rather than a cylinder in the models as shown in Figure 4.2. However, the particle diameter, the height of the granular assembly, the chamber width, and the diameter of the penetrating object are all kept the same as the

experiment conducted by Feng *et al.* (2019) as given in Table 4.2. The packing fraction of the granular medium in the DEM models generated for validation is adjusted as 0.58, which is almost the same as the one in the experiments.

Table 4.1. DEM material properties used in the all simulations.

Parameter	**Value**	**Unit**	**From**
Particle density, ρ_p	2650	kg/m^3	Feng *et al.* (2019)
Particle Poisson's ratio, ν_p	0.3	-	Feng *et al.* (2019)
Particle shear modulus, G_p	5 x 10^8	Pa	Gezgin *et al.* (2020)
Inter-particle static friction coefficient, $\mu_{(s,particle)}$	0.5	-	Feng *et al.* (2019)
Coefficient of restitution, e_r	0.8	-	Feng *et al.* (2019)
Coefficient of static friction between particles and object, $\mu_{(s,object)}$	0.3	-	Feng *et al.* (2019)

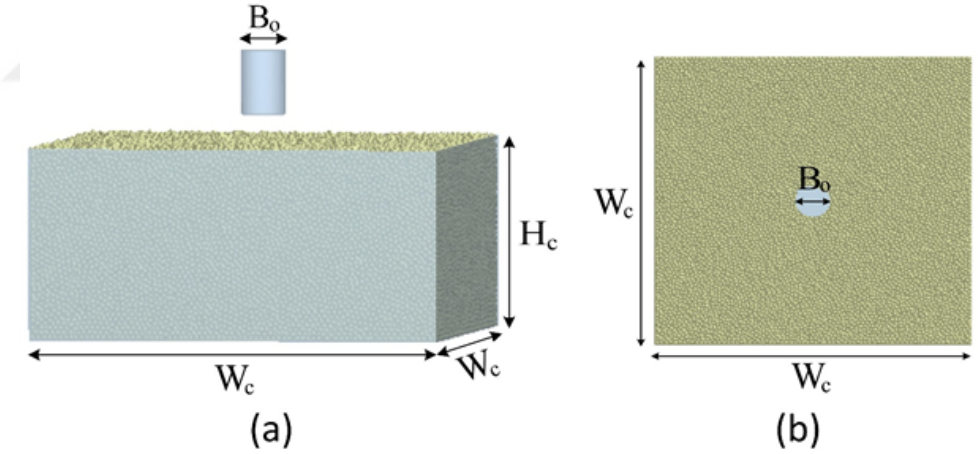


Figure 4.2. DEM model of a cylindrical object penetration (a) normal view (b) top view.

Table 4.2. DEM model properties used in the validation stage.

Parameter	**Value**	**Unit**	**From**
Chamber height, H_c	210	mm	Feng *et al.* (2019)
Chamber width, W_c	450	mm	Feng *et al.* (2019)
Object diameter, B_o	50	mm	Feng *et al.* (2019)
Velocity of the object, ϑ_{object}	30	mm/s	-
Particle diameter, d_p	6	mm	Feng *et al.* (2019)

The penetration velocity of the object in the simulations is optimized considering computational cost. Additionally, it must be noted that a too fast penetration can also affect the soil response. So, the highest velocity that does not have an effect on soil resistance to penetration should be determined for each simulation. Equation (3.1) given in Section 3.1.3 is used to calculate the maximum penetration velocity (ϑ_c). It is shown in Equation (3.1) that the limit for the velocity depends on the gravitational acceleration and the particle diameter. Since the diameter of particles in the models used for validation is 6 mm, the highest velocity that does not affect soil-object interaction is calculated as 34.3 mm/s. Thus, a velocity of 30 mm/s for the object is selected to eliminate its effect on penetration resistance with the minimum computational cost possible.

Rolling friction is selected as the variable to be used to obtain a model validated by the experiments, because it is also a parameter affecting the resistance force of the particles to penetration. Rolling friction makes rotation more difficult for the particles during penetration, as a consequence to which resistance to penetration increases. Accordingly, it is aimed to determine the coefficient of rolling friction (μ_r) which provides a compatible model. For this aim, Models 24 - 27, the details of which are given in Table 4.3, are prepared using different μ_r values. The comparison between these models is shown in Figure 4.3. According to Figure 4.3, μ_r=0.01 used in Model 26 ensures a penetration resistance compatible with the experimental results. So, Model 26 can be defined as the "validated model".

Table 4.3. Features of DEM models generating for validation.

Model No	**Coefficient of rolling friction (μ_r)**
24	0
25	0.05
26	0.01
27	0.02

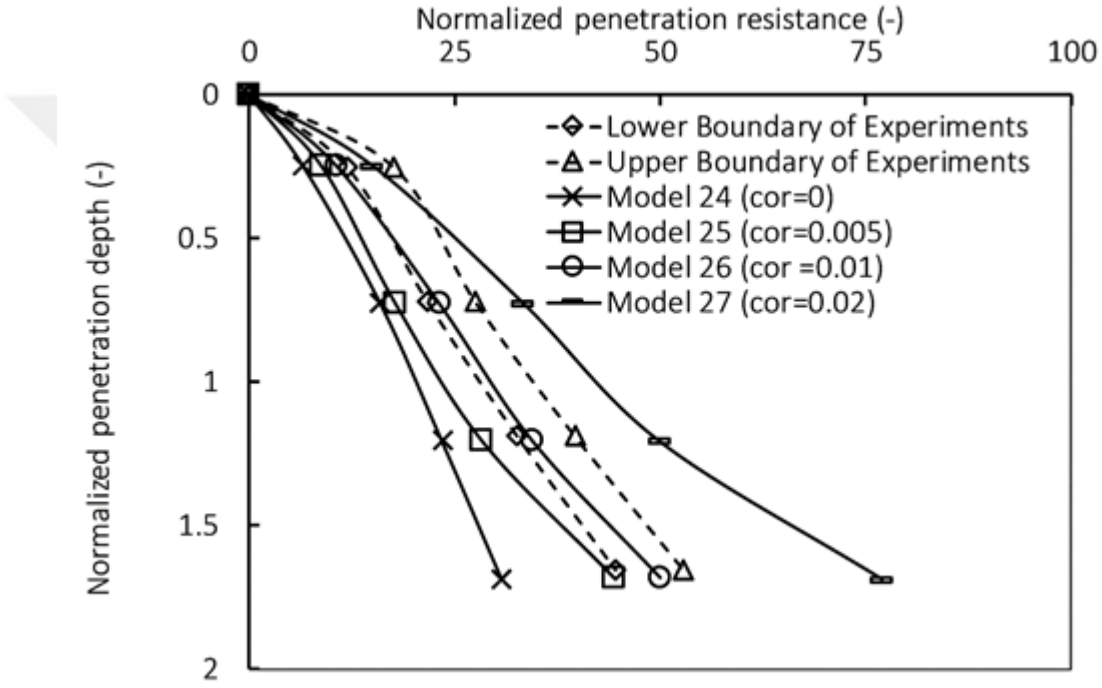


Figure 4.3. Comparison of resistance forces obtained from the models with different coefficients of rolling friction and experiment boundaries.

4.2. Methods to Reduce Computational Time

Although DEM offers several advantages for the investigation of soil response and soil-structure interaction, it also has some drawbacks. One of the most important problems is the high computational cost of simulations. Most of the solutions offered to deal with the high-cost problem usually involve reducing the number of particles (2D modelling, particle refinement method, using a quarter of the system) or increasing time step (reducing stiffness). Some techniques, such as particle upscaling, solve

the problem by both reducing the number of particles and providing larger time steps. The time step can be increased using smaller shear modulus and/or bigger particles as shown in Equation (2.6). However, some of these techniques can have undesirable effects on the simulation results. As an example, too soft particles, which have small shear modulus, can lead to deviation from realistic soil response as explained in Section 3.4.1. In addition, 2D modelling results in completely different kinematic constraints from ones obtained in 3D simulations and real granular material (Falagush *et al.* 2015a). Applying the method of particle upscaling can also negatively affect soil response in simulations if up-scaled particles are not successfully calibrated (Coetzee 2019). Hereby, the possible effect of the techniques to save on computational cost should be evaluated before applying them. Accordingly, it is aimed to investigate three methods, that are presumed to have no undesirable effect, to decrease computational time in this part of the study. Using a quarter of the system and particle refinement method, which will be explained in Sections 4.2.1 and 4.2.3, respectively, work by decreasing the number of particles. On the other hand, model upscaling, which will be mentioned in Section 4.2.2, provides an increase in the time-step by using larger particles. For all three techniques, the details of the models used for the validation purposes are given in Table 4.4.

Table 4.4. Details of DEM models generated for reduction of computational time.

Model No	H_c **(mm)**	W_c **(mm)**	d_p **(mm)**	B_o **(mm)**	ϑ_{object} **(mm/s)**	**90^o segment of the chamber**	**Refinement method**
26	210	450	6	50	30	No	No
28	210	225	6	50	30	Yes	No
29	210	112.5	3	25	24	Yes	No
30	210	450	12	100	45	Yes	No
31	210	900	24	200	60	Yes	No
32	210	562.5	6, 9, 12	100	30	Yes	Yes
33	210	562.5	6	100	30	Yes	No

4.2.1. Using a Quarter of the System in DEM

As a first technique to decrease computational cost, it was planned to consider only the particles in a 90^o segment of the granular material and the cylindrical object as in the study of Falagush *et al.* (2015a). A box rather than a cylinder is preferred as the test chamber to easily consider only a quarter of the sample and the pile as previously mentioned in Section 4.1.2. In this way, the computational cost can be excessively decreased since the total number of particles also falls to a quarter. However, firstly, it is needed to answer if only a 90° segment of the sample and the object provides sufficient accuracy of the simulation results. For this purpose, Model 28, where only a quarter of the system is considered, was generated as an alternative to Model 26. All other parameters in Model 28 are kept the same as the ones in Model 26 as given in Table 4.4. The quarter sample and the object in Model 28, before the penetration, are shown in Figure 4.4.

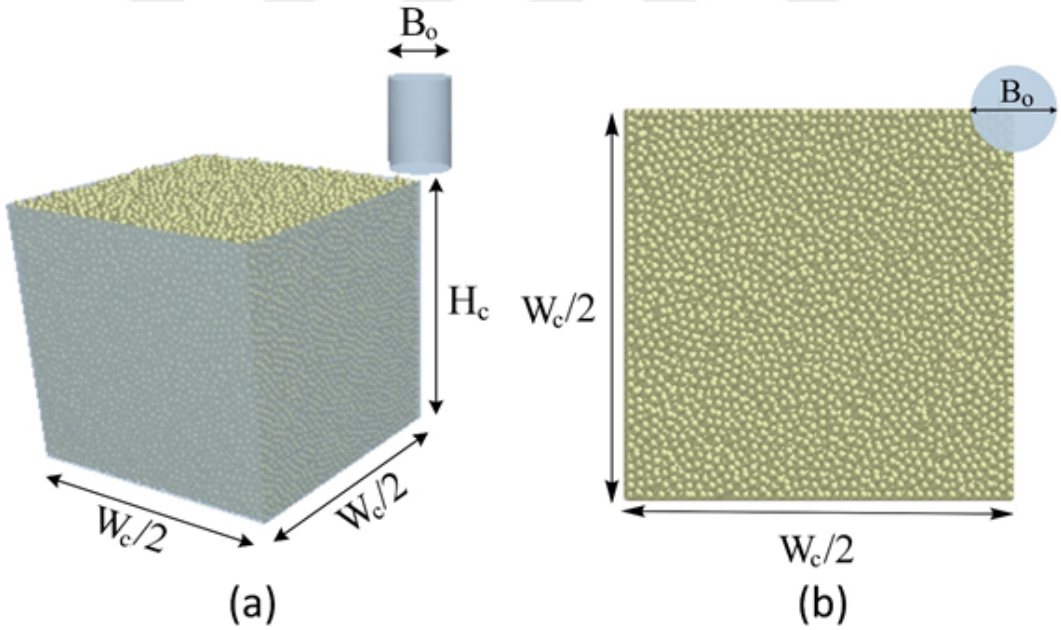


Figure 4.4. DEM model of penetration of the cylinder penetration with only a quarter of the sample (a) normal view (b) top view.

In the models involving only the particles in a 90° segment, like Model 28, the simulation results give the force acting on only a quarter of the object. It should be multiplied by four to calculate the total resistance force during the penetration, since

this is an axisymmetric problem. The results of penetration simulations in Models 26 and 28 are compared to investigate the effect of considering only a quarter of the sample and the penetrating object on the penetration resistance. The comparison result is shown in Figure 4.5. Since this method provides a compatible soil resistance with the one in the model in which it is not applied, it is also used in the models generated to investigate the effect of the methods which are explained in the following sections.

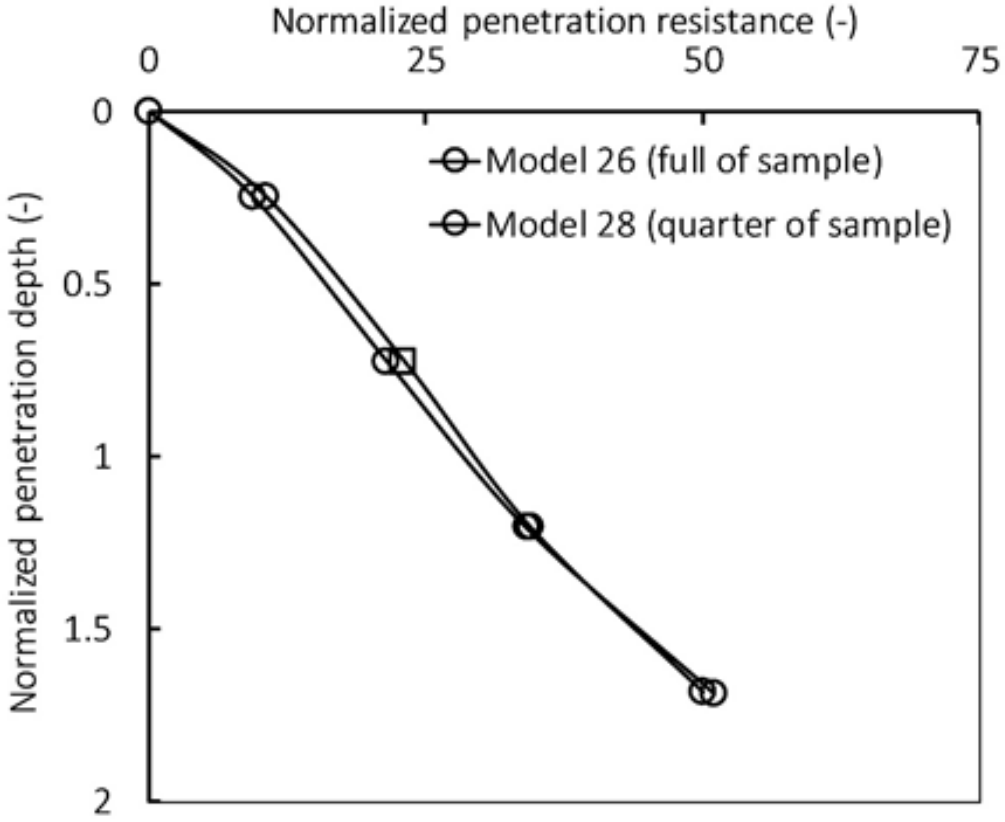


Figure 4.5. Comparison of resistance forces obtained from the models in which sample is full and a quarter, respectively.

4.2.2. Using an Up-Scaled DEM Model

One of the factors affecting the computational cost in DEM models is the smallest particle size in simulation, because it is a parameter in the calculation of the time step as shown in Equation (3.2). In other words, generating larger particles helps to decrease computational time. Therefore, the particle upscaling procedure is generally

performed in DEM models. However, the up-scaled particles need to be calibrated to represent the smaller ones in DEM models (Coetzee 2019) because particles just become larger, while the geometry sizes remain the same. On the other hand, creating an up-scaled model is different from the particle upscaling procedure. In this method, all the simulation components are up-scaled, including all particles and geometries. Thus, the ratio between the diameter of the penetrating object and the mean particle size is kept constant, unlike in the particle upscaling procedure. The interaction between the particles and the geometries can be compared by normalizing the results of the penetration simulations. Since there is a penetration problem in this study, the penetration resistance can be used as a comparison tool after making it dimensionless using Equation (4.1) and Equation (4.2). To investigate the effect of 'model scaling' on normalized penetration resistance, Models 29 - 31 (details are given in Table (**??**)) are generated in addition to Model 28. In Models 28 and 29 - 31, the ratio of the chamber width to the diameter of the cylindrical penetrating object and the ratio of the object diameter to the particle diameter are kept constant. However, since the penetration velocity is proportional to the square root of the particle diameter as shown in Equation (3.2), the allowable velocity for each particle size was calculated. The penetration velocities in Models 29 - 31 which were selected considering the maximum values are shown in Table 4.4. The normalized penetration resistances obtained in these models are compared as shown in Figure 4.6. As seen in Figure 4.6, all the normalized resistance results obtained from the models at different sizes are compatible with each other. Thus, it can be said that model upscaling is a successful procedure to decrease the computational cost.

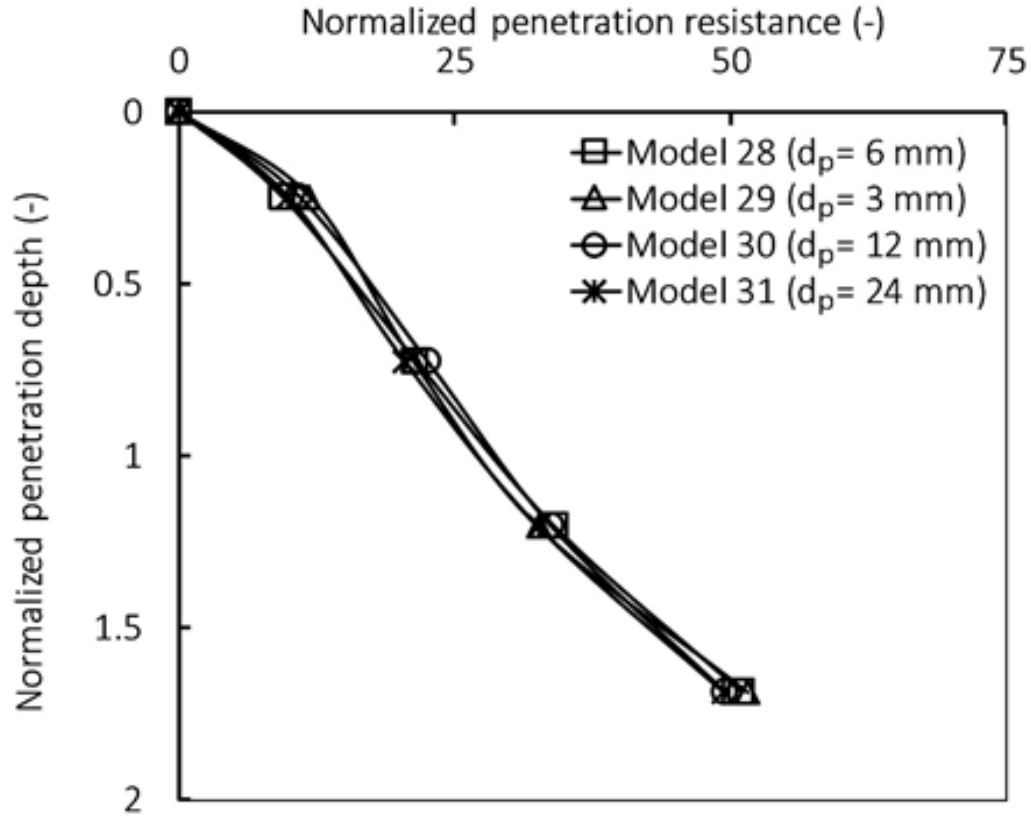


Figure 4.6. Using Particle Refinement Method during Sample Preparation.

4.2.3. Using Particle Refinement Method during Sample Preparation

One of the factors influencing the computational cost in DEM models is the number of particles used to fill the chamber. Filling only in a 90° segment of the chamber is a way to decrease the cost, as it is mentioned in Section 4.2.1. Moreover, there is another technique to achieve shorter computational time by reducing the number of particles, it is called as particle refinement method. It is based on the fact that the particles in the vicinity of the penetrating object are smaller than those further away (McDowell *et al.* 2012). In this way, the same number of particles in contact with the penetrating object can be achieved with less number of particles as shown in Model 32, the details are given in Table 4.4. Model 32, in which the refinement method is adopted, involves the particles at different sizes which are 6 mm, 9 mm and, 12 mm, respectively. These particle sizes are selected following the work of McDowell *et al.* (2012). For applying this method, the model is divided into zones as an initial step.

Each of these zones is filled with different size particles as shown in Figure 4.7a. Frictionless walls are used to separate the zones from each other during the filling stage. The width of the zone surrounding the penetrating object must be sufficiently large to satisfy transmission of the forces from the pile to the other zones. According to Sharif *et al.* (2019), the width of the core zone should be at least 2.5 times the penetrator radius. Widths of the other zones are determined based on the ratio of particle diameter in the considered zone to d_p in the core zone. Width of all the zones (R_{c1}, R_{c2} and, R_{c3}) and the equations used for their calculations are given in Table 4.5. It is important for this method that the porosity should be the same for all the zones (McDowell *et al.*, 2012; Zhao *et al.*, 2019). In this study, the porosity for all the zones is achieved as 0.4.

Table 4.5. Dimensions in Model 32.

Parameter	**Calculation step**	**Value (mm)**
d_p in Zone 1	-	6
d_p in Zone 2	-	9
d_p in Zone 3	-	12
R_o	-	50
R_{c1}	2.5*R_o	125
R_{c2}	$R_{c1} * \left(\frac{d_p \ in \ Zone \ 2}{d_p \ in \ Zone \ 1}\right)$	187.5
R_{c3}	$R_{c1} * \left(\frac{d_p \ in \ Zone \ 3}{d_p \ in \ Zone \ 1}\right)$	250

After the sample preparation, the separating walls are deleted and the particles are allowed to assume their final positions under the action of gravity. Then, the penetrating object penetrates the sample prepared using the particle refinement method as shown in Figure 4.7a. Due to the penetration, the particles can migrate from the initial boundaries as shown in Figure 4.7b.

Model 33 is created to investigate the validity of the refinement method applied in Model 32. For this aim, all the model properties are kept constant as shown in Table 4.4. The unique difference between Models 32 and 33 is that the sample in Model 33

includes only 6 mm particles. The penetration resistances obtained from Models 32 and 33 are compared as shown in Figure 4.8. As it is seen in Figure 4.8, there is no considerable difference between the resistance results of Models 32 and 33. The results supports that this method can be used to reduce computational time, while achieving similar resistance forces.

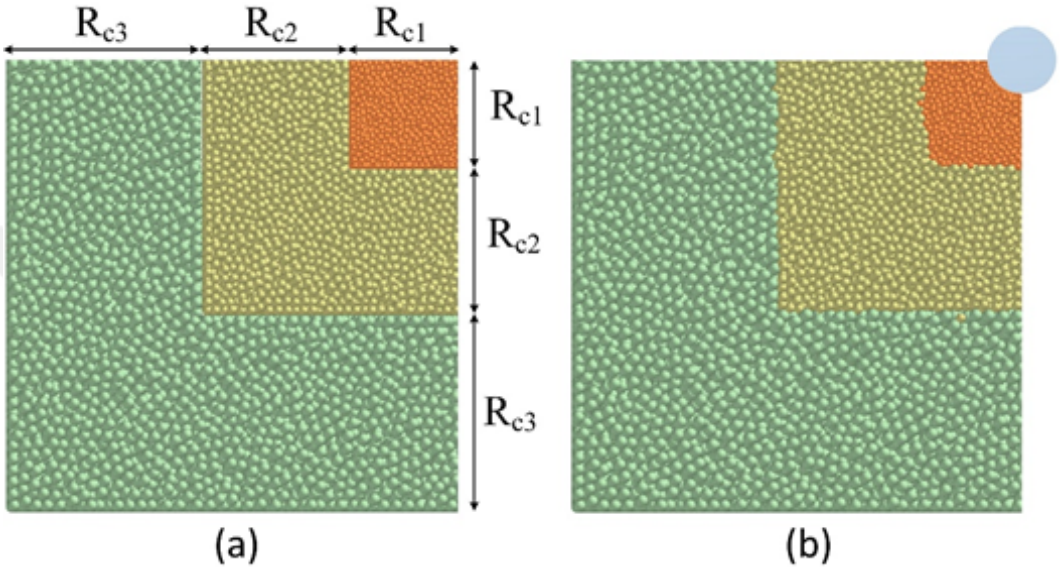


Figure 4.7. Application of refinement method (a) before penetration (b) after penetration.

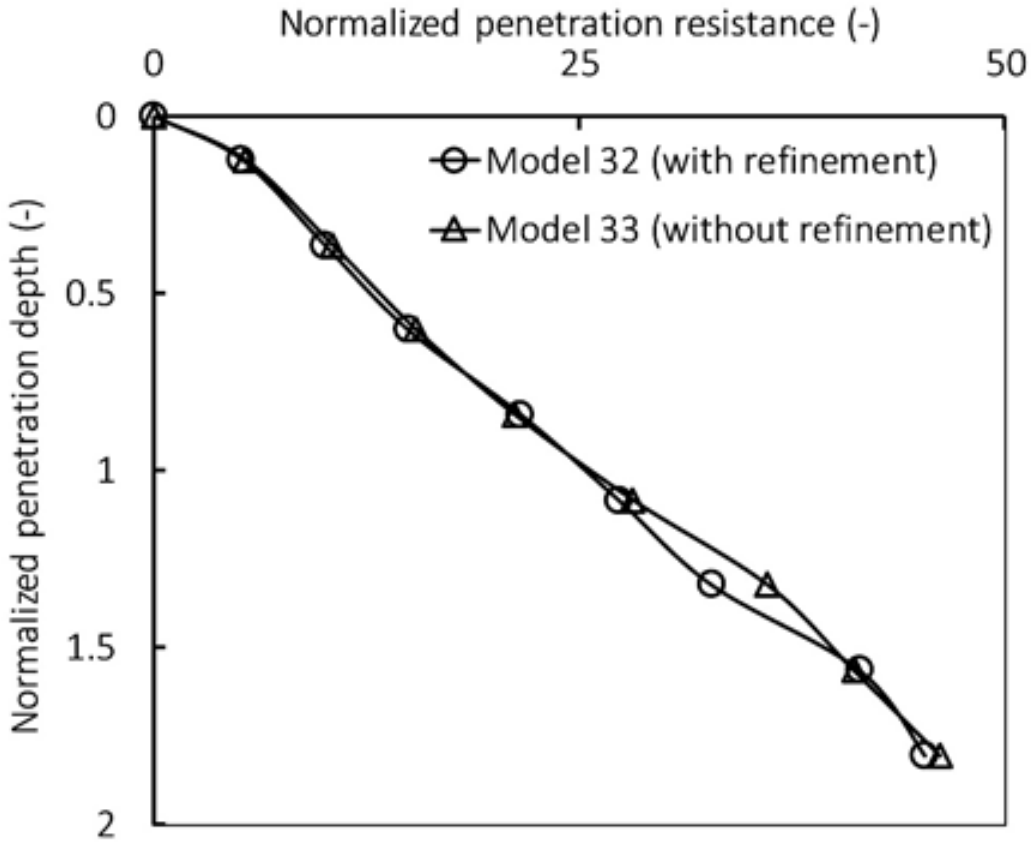


Figure 4.8. Effect of particle refinement method on penetration resistance.

5. MULTI-SCALE ANALYSIS OF DEPENDENCY OF SOIL - PILE INTERACTION CHARACTERISTICS ON PILE INSTALLATION TECHNIQUE

This chapter firstly aims to investigate the influences of the particle shape and soil density state on the response of the surrounding soil for both jacked and replacement piles. The effect of the pile installation method on soil response is also examined for different particle shapes and soil densities. These influences are observed in the stages of pile construction and vertical loading, separately. To understand the influence of particle shape, two types of dense samples are prepared using spherical particles with an aspect ratio (AR) = 1 and non-spherical particles with AR= 0.67. For investigation of the effect of soil density state, the non-spherical samples (AR= 0.67) at the loose state are additionally prepared to compare with the dense ones. In these samples, both jacked and replacement piles are constructed and then exposed to vertical loading tests.

5.1. Methodology

5.1.1. General Model Setup

The DEM models involve a box chamber filled with the particles and a pile. The granular packing in the chamber represents cohesionless soil. It is important to notice that the granular material and the rod are called “soil” and “pile”, respectively, because it is aimed to interpret the results of penetration and loading processes in terms of geotechnical perspective as explained in Chapter 3. The interactions between the particular assemblies and the penetrating rods during the installation and loading stages represent cohesionless soil - pile interaction in this part of the dissertation. During the model generation, the methods explained in Section 4.2 are utilized for decreasing computational time. These techniques are using a quarter of the sample and the pile, model upscaling, and particle refinement method. The first technique is already explained in Section 4.2.1. As discussed, considering only a quarter of the sample and

pile in the simulations is sufficient to quantitatively observe soil-pile interaction, since pile penetration is an axisymmetric problem. Here, the important point is that the measured forces should be multiplied by four to obtain the actual results. The second way for achieving a less computational cost is to use the up-scaled models. In this method, all components of a model become larger contrary to the particle upscaling. The important factor is to keep the ratio of the box width to the pile diameter and the ratio of the pile diameter to the particles size constant since the forces acting on the pile and the pile displacement are normalized to evaluate the results as shown in Section 4.2.2. The last technique is the particle refinement method. The main idea in the technique is that smaller particles are generated near the pile and larger ones further away as clarified in Section 4.2.3. In Section 4.2.3, the sample consists of three zones that contain particles of different sizes. In this chapter, one more zone is also added to the model in order to ensure that there is no boundary effect.

Accordingly, the DEM models include only a quarter of the samples which involve four zones with different particle sizes as shown in Figure 5.1. Here, each color represents particles of different sizes. All the zones are filled using the air-pluviation method. As emphasized in Section 4.2.3, the porosity should be the same for all the zones. It becomes possible to keep the porosity constant by adjusting inter-particle static friction for the particles of each zone during the filling stage.

The width of each zone (R_c) is determined using the calculation steps that are given in Table 5.1. The diameter and the color of the particles in each zone are also shown in Table 5.1. The model pile has a radius of 1 meter and the smallest particle in the model has a radius of 0.1 m. So, the ratio between the pile diameter and the diameter of the particles surrounding the pile (B/D_{50}) is 10 that is nearly the same as the maximum ratio used by Esposito *et al.* (2018). The ratio of the width of the quarter of the sample to the pile radius (R_c/R_{pile}) is 17.5 that is slightly higher than the ratio used in Falagush *et al.* (2015) and Chapter 3 of this study.

For modelling soil-pile interaction, the static friction coefficient between the particles and the pile is selected as 0.5. In addition, the pile length in the soil (D_p) and the

boundary distance from the pile bottom (after installation) to the bottom of the chamber is 10 times the pile diameter. This boundary condition is also used by Esposito *et al.* (2018).

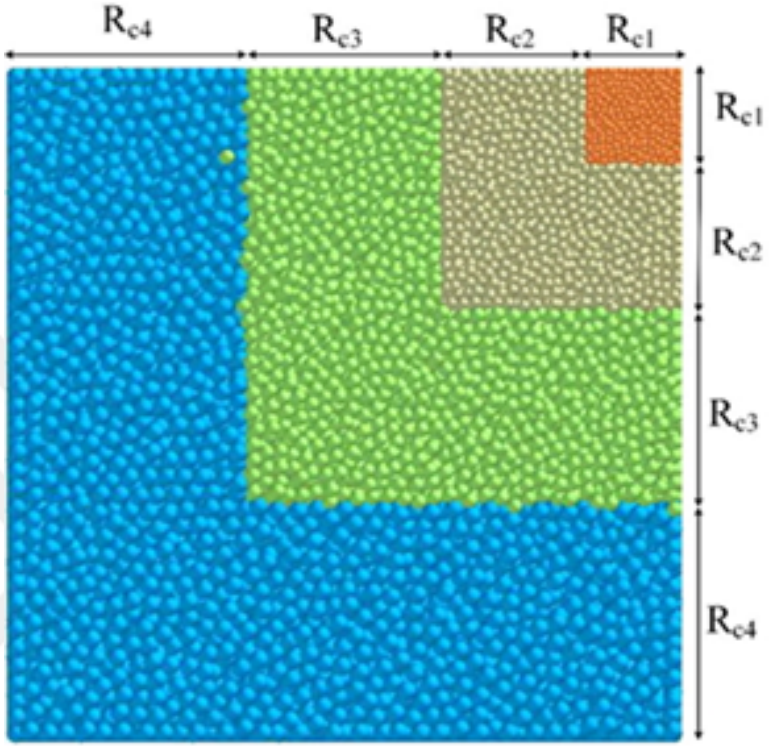


Figure 5.1. Soil sample prepared using particle refinement method (top view).

Table 5.1. Dimensions in Models 34 - 39.

Dimensions	**Calculation step**	**Value (m)**
d_p in Zone 1 (orange)	-	0.2
d_p in Zone 2 (yellow)	-	0.3
d_p in Zone 3 (green)	-	0.4
d_p in Zone 4 (blue)	-	0.5
R_{pile}	-	1
R_{c1}		2.5*R_{pile}
R_{c2}	$R_{c1} * \left(\frac{d_p \ in \ Zone \ 2}{d_p \ in \ Zone \ 1}\right)$	3.75
R_{c3}	$R_{c1} * \left(\frac{d_p \ in \ Zone \ 3}{d_p \ in \ Zone \ 1}\right)$	5
R_{c4}	$R_{c1} * \left(\frac{d_p \ in \ Zone \ 4}{d_p \ in \ Zone \ 1}\right)$	6.25
R_c	$R_{c1} + R_{c2} + R_{c3} + R_{c4}$	17.5
H_c	-	40

5.1.2. DEM Simulations Program

In this study, three unique samples, which are spherical - dense, non-spherical - dense, and non-spherical - loose, are prepared. These samples are utilized to investigate the effect of both particle shape and density state on soil-pile interaction. Additionally, in each sample, two installation methods (jacked and replacement) are applied separately (in total six cases are analyzed, as shown in Figure 5.2). Accordingly, this section will clarify the soil response to the construction and vertical loading of the piles installed with different techniques for different particle shapes and soil density states.

Model No	Pile Type	Particle Shape	Aspect Ratio	Density State	Porosity
34	Jacked		1	Dense	0.37
37	Bored				
35	Jacked		0.67	Dense	0.34
38	Bored				
36	Jacked		0.67	Loose	0.42
39	Bored				

Figure 5.2. Features of DEM models used for investigation of influences of pile installation methods.

5.1.3. DEM Model Setup of Pile Installation

5.1.3.1. Jacked Pile . Jacked piles, are generally placed into the soil by pushing with a constant speed. The penetration mechanism that is discussed in Chapters 3 and 4 illustrates the construction procedures of jacked piles. The installation steps in this part of the study are shown in Figure 5.3. The pile, with a diameter of 2 m, penetrates at the corner, where the smallest particles are located (orange-colored), as discussed in Section 4.2.3. The penetration depth is equal to 10 times the pile diameter. To eliminate the effect of pile velocity on the soil response, the upper limit velocity is determined using Equation 3.1 as in the work of Feng *et al.* (2019). In this chapter, the diameter of the particles surrounding the pile is 0.2 m. Consequently, the allowable penetration velocity is calculated as 0.198 m/s. As a result, the constant penetration velocity is selected as 0.2 m/s in this chapter.

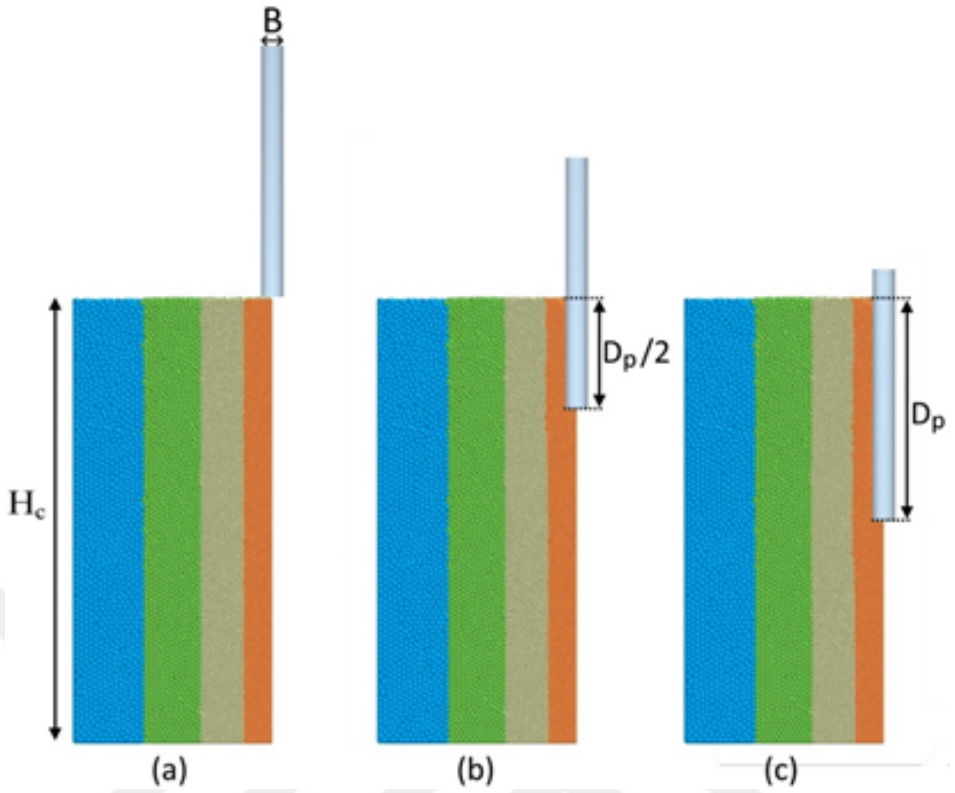


Figure 5.3. Installation steps of jacked piles.

5.1.3.2. Replacement Pile. The principle for the construction of a replacement pile is based on the replacement of the soil by the pile at the end of the installation. To apply this principle in the DEM models, the region where the pile will be located must be without particles. Therefore, a realistic procedure is followed to construct the replacement piles in a DEM simulation. According to this procedure, firstly, all the zones, except the core one, are filled with the designated particles. In the core zone, which is closest to the area where the pile will be located, the particles are only filled up to the level that coincides with the bottom of the pile (Figure 5.4a). With the use of dividing walls, which are used to separate the zones from each other, the height difference between the particle assemblies in the first zone and the others were preserved. As a second step, a pile cover, which is at the length of the pile but 10% wider than the pile, is created at the location where the pile is intended to be placed (Figure 5.4b). As the next step, it is continued to fill the surrounding area of the pile cover in the first zone with the particles until the assembly height in the core zone is the same as that in the others (Figure 5.4c). After that, all the frictionless dividing

walls between the zones are removed, then all the particles are allowed to settle until the system reaches equilibrium. As a final step, the pile cover is removed and the pile is positioned in the place of the cover (Figure 5.4d). After the cover is removed, due to the diameter difference between the cover and the pile, the particles surrounding the cover relocate to their new positions by moving towards the pile under gravity. After all the particles completely settle in their final positions, the pile installation phase is completed.

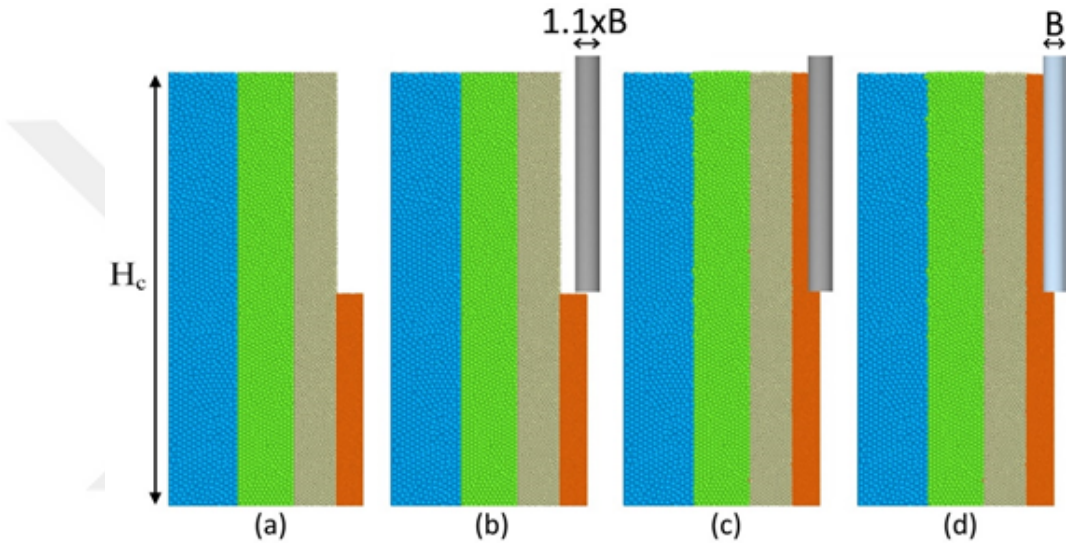


Figure 5.4. Installation steps of replacement piles.

5.1.4. DEM Model of Vertical Pile Load Tests

After the installation stages are completed, the vertical load tests are performed on the piles in Models 34 - 39. The aim is to assess the influences of pile installation method, soil density, and soil particle shape on the pile capacity under vertical loading. The loading tests allow the observation of the vertical pile displacement in response to each vertical load level. According to the loading procedure, the pile is pushed by increasing vertical load in a stepwise fashion, such as 0 kN, 2000 kN, 4000 kN, 6000 kN, and so on. Each load is applied until pile penetrates no more, at which stage nearly all particles lose their kinetic energies and the system reaches equilibrium. At the end of each loading step, the vertical pile displacement observed at that load level is measured.

5.2. Results and Discussions

5.2.1. Pile Installation Stage

5.2.1.1. Jacked Piles. Here, it is aimed to investigate the influences of both particle shape and soil density state on penetration resistance in three aspects which are total resistance, end bearing and, shaft friction. During penetration of a jacked pile, the soil particles both under the toe of the pile and around the pile show resistance to penetration together. The resistance of the particles which are under the pile toe is called "end bearing" while one developing due to friction between the particles and the pile shaft is known as "shaft friction". The DEM enables separate measure the penetration resistances that develop on the toe and shaft of the pile. As an example, it is sufficient to consider only the contact forces between the pile and the particles in contact with the surface area in the calculations to obtain just the shaft friction.

Accordingly, total resistance, end bearing and shaft friction are separately measured during the pile installation stage for different particle shapes and soil density states. The measured resistances and the penetration depths are normalized using Equation (4.1) and Equation (4.2), respectively. Figure 5.5 shows three different comparisons, which are between the total resistance, end bearing and, shaft resistance that are normalized, respectively, for Models 34 - 36. According to Figure 5.5, soil density has a significant effect on penetration resistance as presented in Section 3.4.2. This influence has validity for both end bearing and shaft friction. Clearly, the penetration resistance in the dense non-spherical sample is almost two times it in the loose one. In addition, it is seen that the particle shape also affects the penetration resistance as mentioned in Section 3.4.6. Although the spherical sample in Model 34 and the non-spherical sample in Model 36 are at dense and loose states, the resistance in the spherical-dense sample is just slightly higher than the non-spherical - loose one as shown in Figure 5.5a. However, the shaft frictions obtained in these samples completely coincide as illustrated in Figure 5.5c. It means that shaft friction highly contributes to the penetration resistance in the non-spherical sample as against the spherical one.

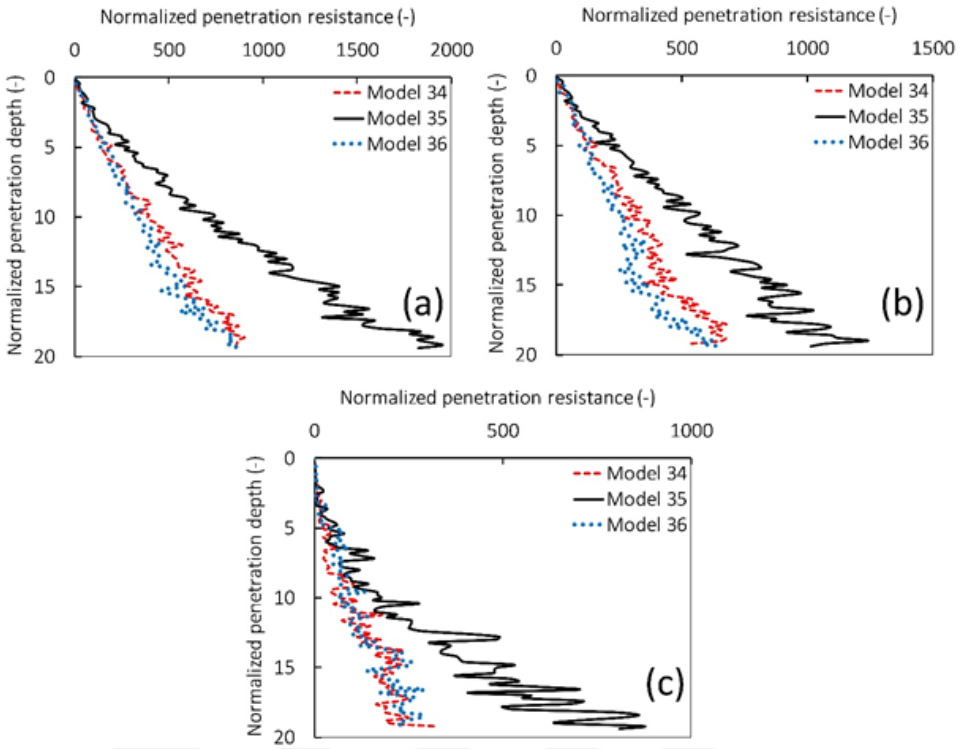


Figure 5.5. Penetration resistances in Model 34 [spherical - dense], Model 35 [non-spherical - dense], and Model 36 [non-spherical - loose] in terms of (a) total resistance (b) end bearing (c) shaft friction.

Coordination number is a micro-scale parameter that shows contact density within granular assemblies. It is defined as the average number of contacts per particle. Since this number reflects the micro-mechanical aspect of soil behavior, soil response to the pile installation can be also interpreted using this micro-scale indicator. However, it should be noted that the coordination number of a granular medium depends on techniques of sample preparation. It is a function of the inter-particle friction coefficient during the preparation stage as clarified in Section 3.4.2. Therefore, the initial coordination number of the assemblies in each zone is different from the others even before the pile installation in Models 34 - 36. Here it is focused on the variations in the average coordination number of the sample. Accordingly, these variations that are separately obtained for each zone in Models 34 - 36 are illustrated in Figure 5.6. According to Figure 5.6, the average coordination numbers in the last two zones do not show a significant change as against the other zones in all the models. It is not surprising because the penetration effect decreases further away from the pile. Though

the intensity is slightly higher for the first zone, they in the first two zones also show a similar tendency during the penetration in all the models. At the beginning of the penetration, the average coordination numbers in the first zones instantaneously decrease for all the situations as shown in Figure 5.6. However, the effects of particle shape and soil density state on the coordination number becomes apparent especially in the first zone as the pile continues to penetrate. Pile penetration has a deeper effect on the average coordination number of the non-spherical sample (Figure 5.6b) than that of the spherical one (Figure 5.6a). Nevertheless, it is seen that particle shape does not affect the tendency of the coordination number during penetration. In the first two zones, it continues to decrease in both situations where the particles are spherical and non-spherical, respectively. On the other hand, the soil density state directly affects the micro-mechanical aspect of soil response to pile penetration. The coordination number of the dense soil surrounding the pile consistently reduces (Figure 5.6b) while that of the loose one starts to increase (Figure 5.6c). This is because due to the penetration, the loose sample densifies while the dense one shows dilatant behavior.

The DEM can also give the illustration of all contact networks in a simulation (particle-particle and/or particle-geometry). Thus, the contact density of a granular assembly can be visually interpreted without any indicator, such as the coordination number. Here, it is aimed to visually observe the pile installation effect on the internal structure of the soil samples with different particle shapes and density states at the beginning of penetration. Accordingly, the contact networks before and immediately after penetration in Model 34 - 36 are shown in Figure 5.7. Since the penetration mostly affects the particles surrounding the pile, only the contacts between the particles in the first zones are observed in detail. As shown in Figure 5.7, before penetration, the contact networks are uniformly distributed in all three models. However, pile penetration leads to a break in uniform distribution of the contact network, therefore, a decrease in the number of force chains is seen. All three samples, that are with different particle shapes or density states, are exposed to a similar effect of penetration. As it is previously revealed that the coordination numbers of the assemblies in the first zones instantaneously decrease immediately after the pile penetrating. Thus, the findings given in Figure 5.7 are compatible with the variations in the coordination number

shown in Figure 5.6.

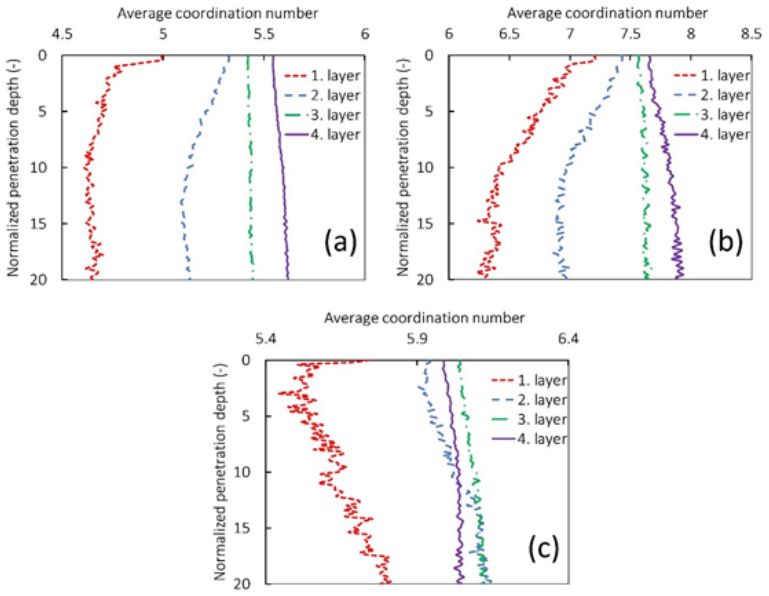


Figure 5.6. Variations in average coordination numbers during penetration stage (a) Model 34 [spherical - dense] (b) Model 35 [non-spherical - dense] (c) Model 36 [non-spherical - loose].

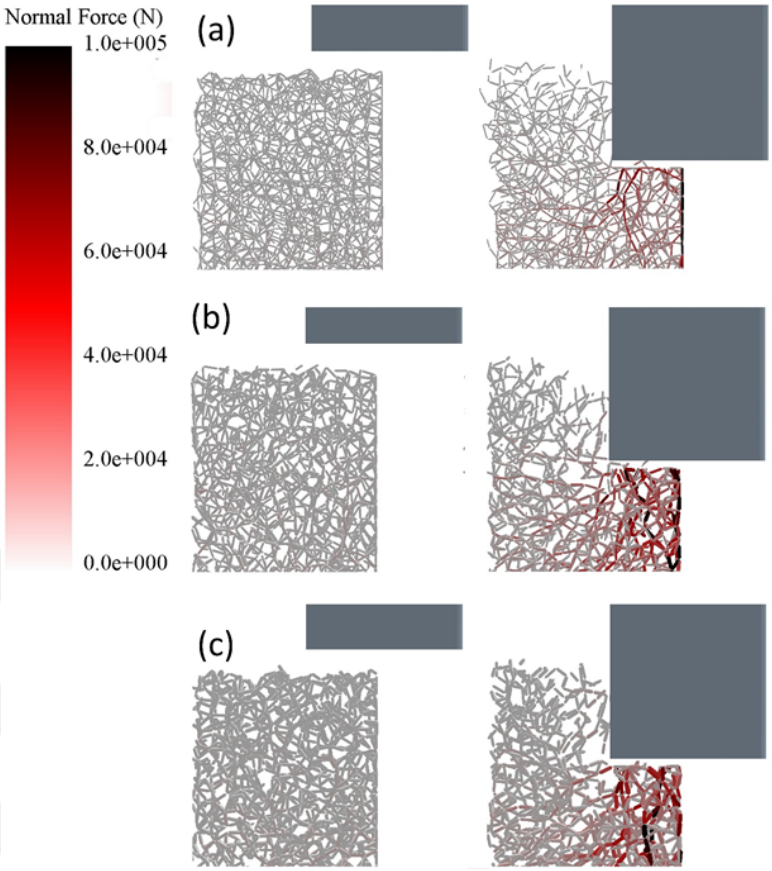


Figure 5.7. Contacts between the particles before and immediately after penetration in (a) Model 34 [spherical - dense] (b) Model 35 [non-spherical - dense] (c) Model 36 [non-spherical - loose].

5.2.1.2. Replacement Piles. Since replacement piles are not installed by pushing into the soil, soil resistance to the pile installation is not developed. Therefore, the soil response to pile installation can be observed in terms of only the contact intensity in the samples. Coordination numbers and contact networks are used to identify the contact intensity as clarified in Section 5.2.1.1. Accordingly, Figure 5.8 shows the variation in the average coordination number of the particles in each zone for the samples with different particle shapes and/or density states. However, the variation is versus the elapsed time, starting after the pile replaces with its cover, rather than the penetration depth because there is no penetration mechanism in this installation method. According to Figure 5.8, in all three models, the coordination numbers in the first zones decrease while those in the other zones do not show a considerable change during the installation stage. Thus, it can be reported that the installation

of a replacement pile causes a decrease in the average coordination number of the particles surrounding the pile irrespective of the particle shape or the soil density state. However, the comparison between Figure 5.8b and Figure 5.8c shows that the coordination number of the dense sample decreases more than that of the loose one.

In Models 37 - 39, the contact networks before and immediately after pile installation in the first zones are also obtained and shown in Figure 5.9. Before pile installation, the contact network is uniformly distributed around the pile cover in each model. At the beginning of the installation, the pile replaces with the cover and some contacts in the network disappear due to the instantaneous movement of the particles around the new geometry. Thus, the contact intensity decreases in all three models as shown in Figure 5.9. This finding is compatible with the results obtained from the coordination numbers presented in Figure 5.8. Also, the decrease in the network intensity observed in the dense sample is higher than it in the loose one, a similar finding with that obtained from the coordination numbers.

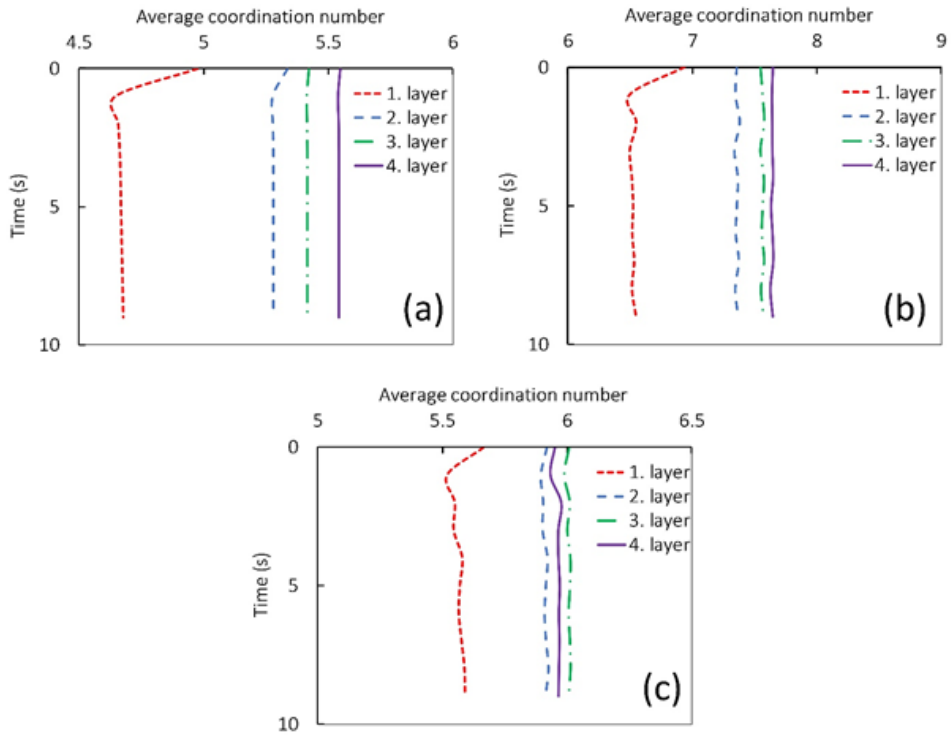


Figure 5.8. Variations in average coordination numbers during installation stage of replacement piles in (a) Model 37 [spherical - dense] (b) Model 38 [non-spherical - dense] (c) Model 39 [non-spherical - loose].

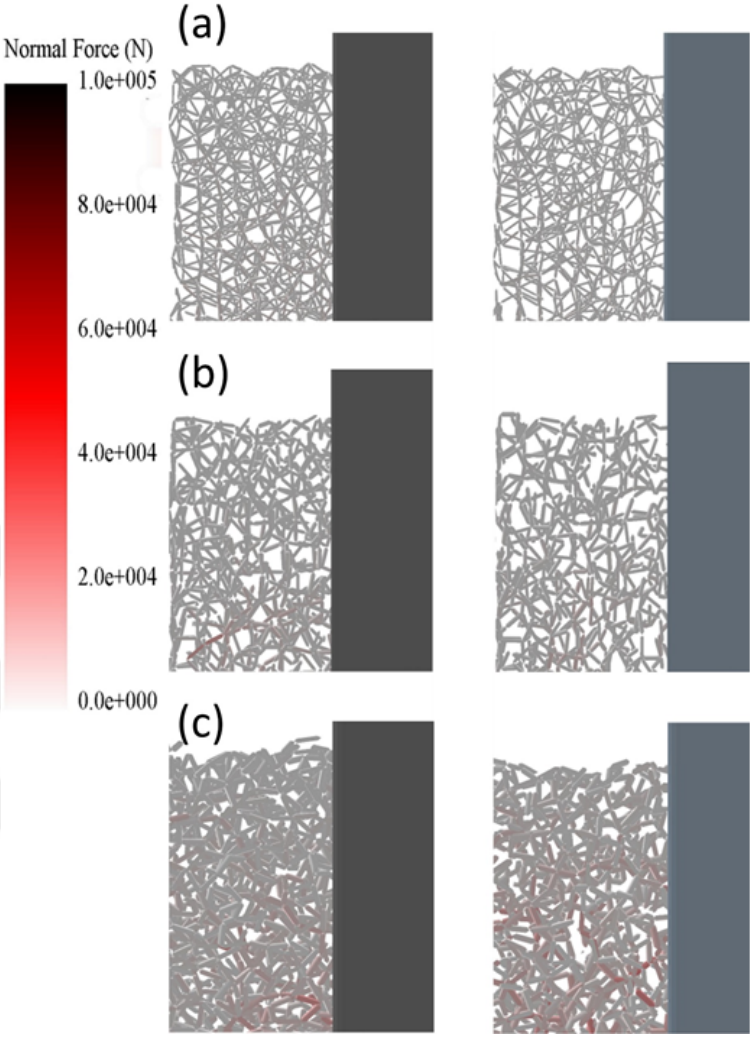


Figure 5.9. Contacts between the particles before and immediately after installation in (a) Model 37 [spherical - dense] (b) Model 38 [non-spherical - dense] (c) Model 39 [non-spherical - loose].

5.2.2. Pile Vertical Loading Stage

After the pile installation stage, both jacked and replacement piles are subjected to the loading tests in Models 34 - 39. The test procedure is explained in Section 5.1.4. Soil response to the load tests is classified into two major components that are end bearing and shaft friction. Total resistance is the product of these components. Determination of end bearing and shaft friction is explained in Section 5.2.1.1. The procedure is the same as that in the penetration stage. All the discussions of test results

given in the following are based on the total resistance, end bearing, and shaft friction. It should be noted again that all the forces and the displacements measured during the load tests are normalized using Equation (4.1) and Equation (4.2), respectively.

5.2.2.1. Jacked Piles. Figure 5.10 shows load-displacement curves that are obtained in terms of total resistance, end bearing, and shaft friction for each sample in Model 34 - 36. It is clear that for Model 34 (spherical) both end bearing and shaft friction show a similar trend with respect to load increments, as presented in Figure 5.10a. However, it must be noted that the gradual increase of both resisting components saturates at some point during the loading test. On the other hand, the loading test results for the non-spherical samples at dense and loose states are presented in Figure 5.10b and Figure 5.10c. It is seen that, contrary to the response of spheres, only the shaft friction reaches a saturation state while the end bearing continues to increase.

To have a better understanding regarding the influences of both particle shape and soil density state, the results from Figure 5.10 are individually compared in terms of total resistance (Figure 5.11a), end bearing (Figure 5.11b) and, shaft friction (Figure 5.11c) for Models 34 - 36. Compared to Models 34 and 35, it is observed that the total resistance is considerably higher for dense non-spheres (Model 35). Interestingly, it can be seen that the total resistances are almost similar for spherical dense (Model 34) and non-spherical loose (Model 36) samples. A similar conclusion can be drawn for the end bearing and the shaft friction. This indicates that both particle shape and soil density state must be considered as governing factors for soil-pile interaction in jacked piles.

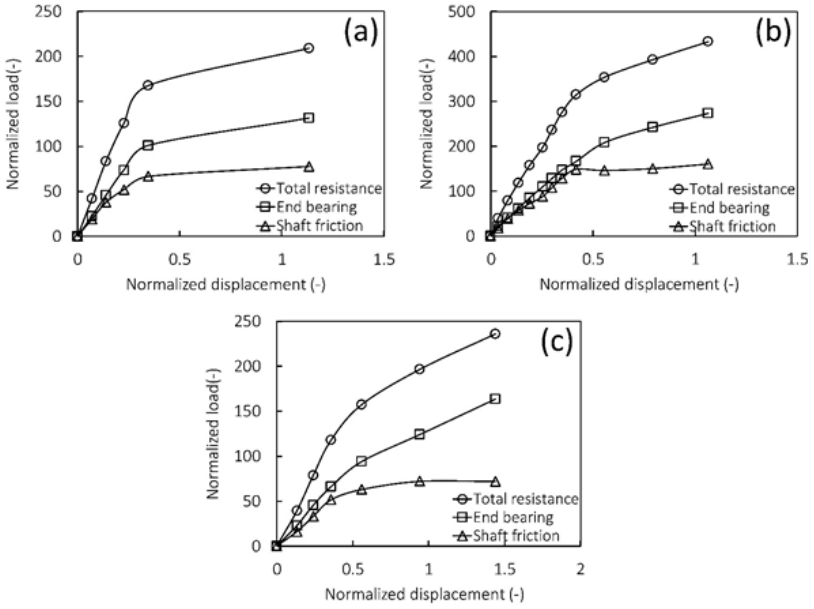


Figure 5.10. Jacked pile load test results, that show total resistance, end bearing, and shaft friction, in a) Model 34 (spherical - dense) b) Model 35 (non-spherical - dense) c) Model 36 (non-spherical - loose).

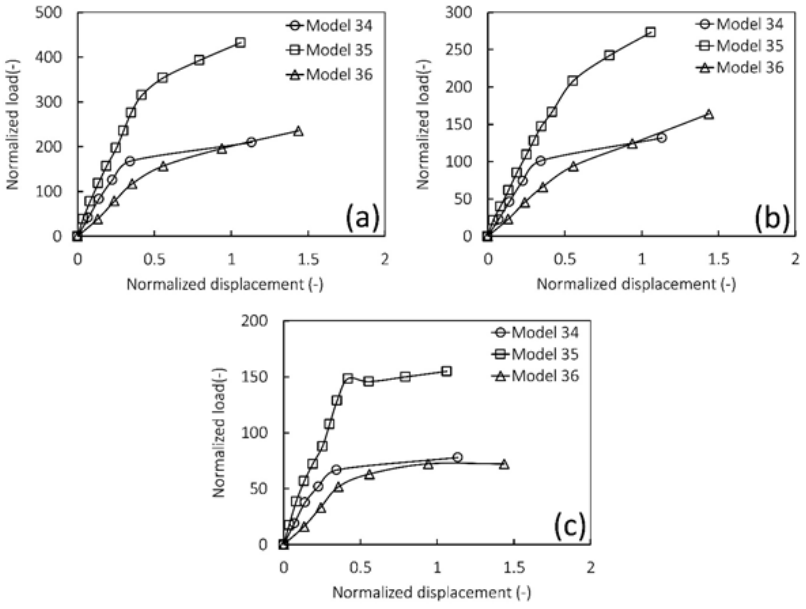


Figure 5.11. Comparison of load test results for jacked piles in Model 34 (spherical - dense), Model 35 (non-spherical - dense), and Model 36 (non-spherical - loose) in terms of a) total resistance b) end bearing c) shaft friction.

5.2.2.2. Replacement Piles. Similar investigations that are conducted for jacked piles are repeated for replacement piles as well and are shown in Figure 5.12 and Figure 5.13. It is seen in Figure 5.12 that while end bearing continuously increases for all cases, the shaft friction saturates for replacement piles independent of both particle shape and soil density state.

Furthermore, comparing different resisting components shown in Figure 5.13, it is shown that the non-spherical dense sample yields a higher bearing capacity. Additionally, it is seen that the non-spherical loose sample provides a higher loading capacity than the spherical dense sample, which is slightly different than the jacked pile. This indicates that in the case of the replacement pile installation method, spherical particles do not rearrange in the vicinity of the pile, and thus the pile has less interaction with the surrounding particles.

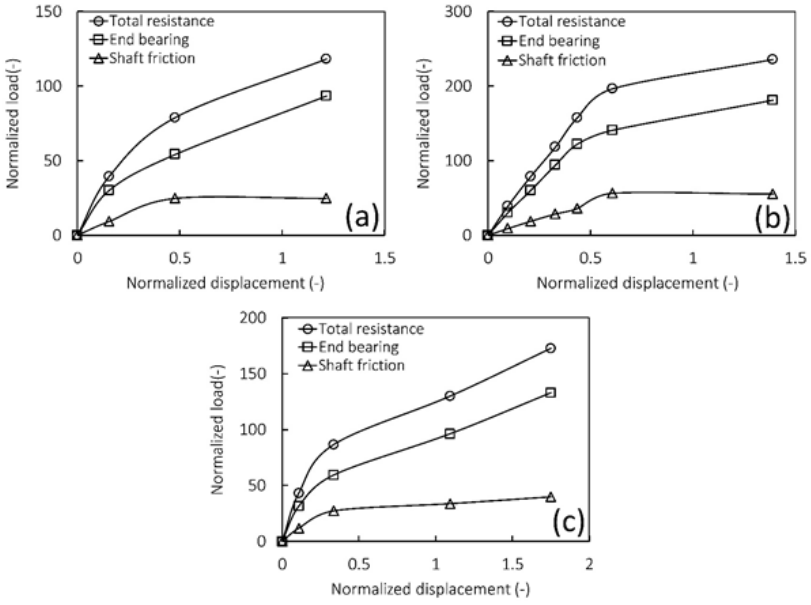


Figure 5.12. Replacement pile load test results, that show total resistance, end bearing and shaft friction in a) Model 37 (spherical - dense) b) Model 38 (non-spherical - dense) c) Model 39 (non-spherical - loose).

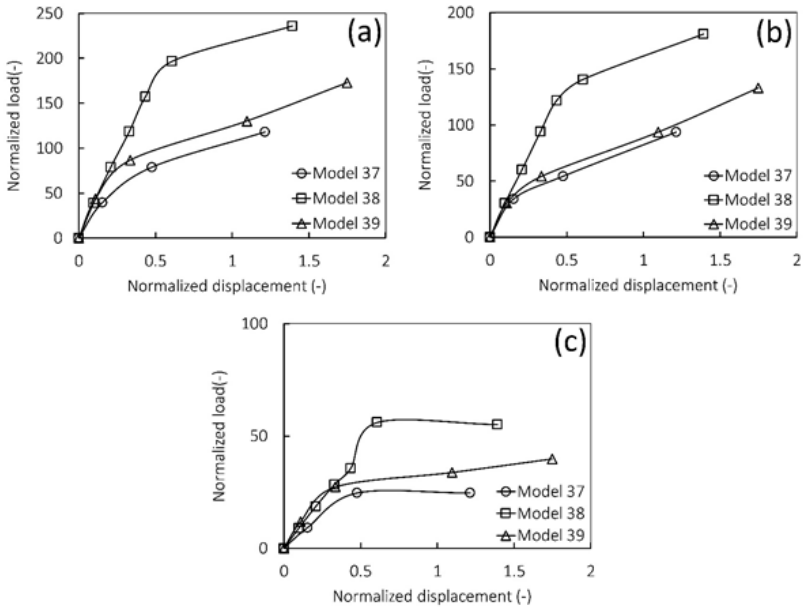


Figure 5.13. Comparison of load test results for replacement piles in Model 37 (spherical - dense), Model 38 (non-spherical - dense), and Model 39 (non-spherical - loose) in terms of a) total resistance b) end bearing c) shaft friction.

5.2.2.3. Soil Response based on Installation Methods. In Sections 5.2.2.1 and 5.2.2.2, the pile loading test is conducted for both pile installation methods. In these tests, the dependency of soil response to vertical load increment is investigated for samples with different particle shape and density states. However, it is also crucial to understand the differences in soil response for the two installation methods. Accordingly, using the load test results, here it is aimed to compare the jacked piles with the replacement piles in terms of end bearing and shaft friction for each sample.

Figure 5.14 shows the comparison between the end bearing curves of the jacked and replacement piles (including models 34 - 39). According to Figure 5.14, it is clear that the jacked pile has a higher end bearing capacity than the replacement one for all the models irrespective of particle shape and density state. The reason for this apparent difference is that a jacked pile compresses the soil particles both under its toe and along the shaft while penetrating. Additionally, this soil compaction leads to a higher shaft resistance for the jacked piles, as shown in Figure 5.15.

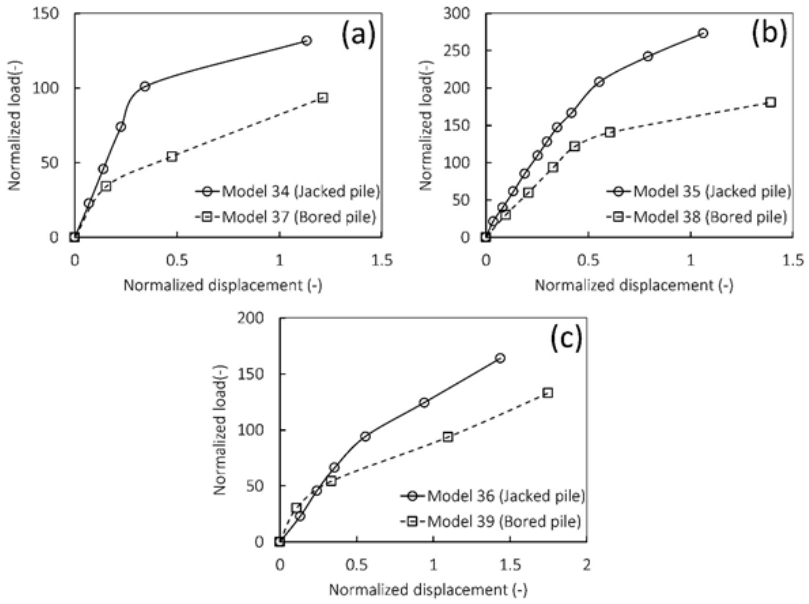


Figure 5.14. Effect of installation method (jacked and replacement piles) in terms of end bearing for a) dense sample with spherical particles (Models 34 & 37) b) dense sample non-spherical particles (Models 35 & 38) c) loose sample with non-spherical particles (Models 36 & 39).

It is observed in Figure 5.14 and Figure 5.15 that the installation method has a greater effect on the shaft friction than the end bearing. This is because the installation process of replacement piles loosens the surrounding soil, while soil compression is commonly observed on jacked piles. Consequently, it can be deduced that the shaft friction component of the pile loading resistance is significantly affected by the pile installation method.

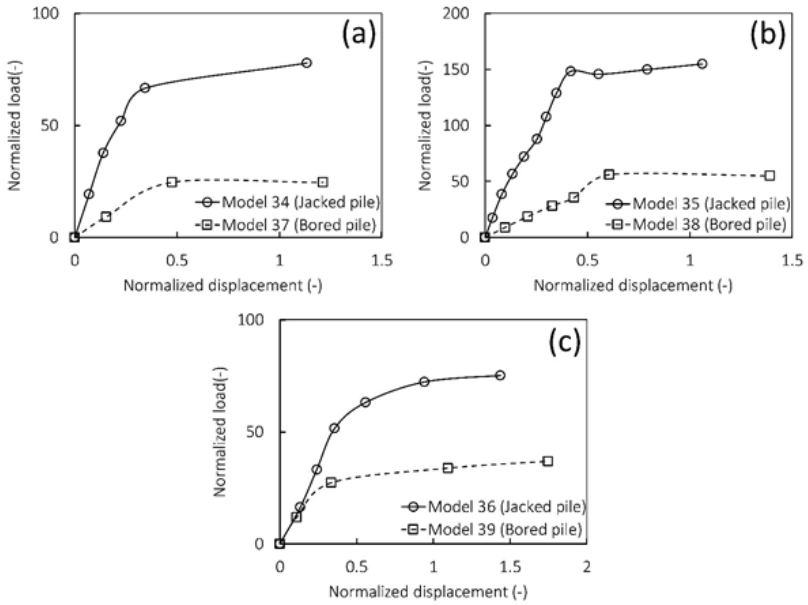


Figure 5.15. Effect of installation method (jacked and replacement piles) in terms of shaft friction for a) dense sample with spherical particles (Models 34 & 37) b) dense sample non-spherical particles (Models 35 & 38) c) loose sample with non-spherical particles (Models 36 & 39).

6. SUMMARY

This dissertation focuses on a multiscale investigation of soil-pile interaction with DEM modelling. This study has three main themes, which discuss soil-pile interaction from various perspectives. The following will summarize the outcomes for each chapter that contains numerical results.

6.1. Influence of Soil Characteristics on Pile Penetration

In Chapter 3, for various soil properties, the results of the DEM simulations for pile penetration are compared. A single parameter is varied in each model to observe its influence on penetration resistance uncoupled from the rest. This is achieved by comparing the variations of penetration resistances with depth for models that have only a single differing parameter. Based on the presented comparisons, the effect of each soil characteristic on penetration resistance is discussed. The main conclusions of this part of the dissertation can be summarized as follows:

- The minimum shear modulus that will not significantly alter penetration results is found to be 5 x 10^8 Pa.
- Models prepared at higher relative densities yield greater resistances to pile penetration, as expected.
- The average coordination number is dependent on the method of model preparation. Model preparation by air-pluviation with reduced inter-particle friction coefficient leads to higher coordination numbers (average number of contacts per particle) relative to model preparation by loading and unloading.
- Results show that resistance to penetration into dry cohesionless soils is independent of the average coordination number as resistance is controlled by void ratio and stress state. Therefore, the fabric does not influence penetration resistance as long as it does not affect density.
- The inter-particle friction coefficient has a major effect on pile penetration resistance until $\mu_{(s,particle)}$=0.5. However, this effect starts to saturate for$\mu_{(s,particle)}$ >0.5.

- It is observed that for the same size chamber and pile, models composed of larger particles produce greater resistance to penetration.
- Models with particle size distribution curves having greater coefficients of uniformity form denser granular arrangements; denser models have higher penetration resistances.
- In case two models have the same void ratio, grain shape and mean grain size, the one with particle size distribution curve resulting in a smaller coefficient of uniformity has higher penetration resistance.
- PSD curve with a greater coefficient of uniformity increases computational time even in case the void ratio is the same due to both smaller-sized particles and a larger number of particles in the model.
- When aspect ratio of particles in a model is concerned; a model composed of particles with smaller aspect ratios (having more elongated shapes) shows higher resistance to pile penetration compared to a model composed of particles with higher aspect ratios (having more rotund shapes).
- Models with rolling friction (discussed in Section 3.4.7) have higher resistances to penetration relative to those without when all particles are spherical. However, especially when the results of models with rolling friction are compared with the results of models with non-spherical particles, it is noticed that rolling friction cannot properly mimic the shape effect in case of penetration problems. Therefore, the use of rolling friction substituted for non-sphericity of particles in DEM simulations of penetration is not advised.

6.2. Validation of Dem Modeling of Penetration in Granular Materials and Methods to Reduce Computational Time

In Chapter 4, the DEM model is validated using the experimental results. For validation, the rolling friction coefficient is varied while other parameters are kept constant. After the validation, different methods are employed to reduce the computational time of the DEM simulations. The computational cost can be decreased using several strategies, where two simple ways are considered here, namely decreasing the number and increasing the sizes of particles. Therefore, in this part of the dissertation,

the micro- and macro-scale response of samples that are prepared using three different approaches are compared. In the first technique, only a quarter of the chamber is filled with particles, where the penetrating rod is only partially (one-fourth of its volume) contacting the prepared sample. By utilizing this method, the number of particles shrinks to a quarter. The results obtained from this model are compared with those acquired from the chamber that is fully filled with the particles. The comparison shows that the results for these models are similar. This observation was expected, since pile penetration is an axisymmetric problem.

The second technique is upscaling the whole model. Normally, particle upscaling is used to decrease the computational cost. However, this may lead to possible adverse effects on the accuracy of the simulation results. On the other hand, upscaling is carried on all of the model components, where the following ratios are kept constant: ratio of chamber width to the pile diameter, and that of the pile diameter to particle size. In this way, the particles get larger, and therefore, the time-step for DEM simulation is improved and computational cost reduces. However, the number of particles in contact with the pile remains unchanged (granular system is in a similar state as). To test the validity of this technique, a series of DEM simulations at different scales are generated. At the end of the simulations, the penetration resistances are obtained from the different scaled models and normalized to compare those with each other. The comparisons show that model upscaling can be adopted to decrease the computational cost of simulations.

The third technique to reduce computational time is the particle refinement method. This technique aims to decrease the total number of particles in a simulation with no change in the number of particles in contact with the pile. The principle of the particle refinement method is based on that the small particles in the simulation are located near the penetrating object while larger particles are further away. Accordingly, the model is divided into zones and each of those is filled with different-sized particles to employ this method. It should be considered that the porosity in each zone is the same as it is in the others. As a next step, the other sample that contains only the small particles is also prepared. Then both of these samples are subjected to

penetration and the resistances acquiring from those are compared. According to the comparison result, the penetration resistances that the refined and non-refined samples show are compatible with each other. This compatibility asserts the validity of the particles refinement method to decrease the computational cost of DEM simulations.

6.3. Multi-scale Analysis of Dependency of Soil - Pile Interaction Characteristics on Pile Installation Technique

In Chapter 5, the multi-scale effects of the particle shape and soil density state on the characteristics of the surrounding soil for both jacked and replacement piles are investigated. In addition, the influences of pile installation methods on the response of the soils with different density states and particle shapes are examined. Accordingly, three different samples that are spherical-dense, nonspherical-dense, and nonspherical-loose are prepared by using the techniques that are validated in Chapter 4. After sample preparation, both the jacked and replacement piles are installed into these samples. Thus, the six different soil-pile models (three with jacked pile and three with replacement pile) are considered in this part of the study. Consequently, the soil response to pile installation is evaluated based on the soil density state, particle shape, and installation method. The total penetration resistance is described as the sum of end bearing and shaft friction. Thus, all the comparisons are also made in terms of end bearing and shaft friction in addition to the total resistance. All the values of total resistance, end bearing, and shaft friction that are acquired during the installation are normalized to obtain dimensionless results. The conclusions from this chapter that are drawn in consequence of the DEM analyses of the pile installation can be summarized as follows:

- In the macro-scale investigation of the installation stages of jacked piles, it is observed that all types of penetration resistance in the dense-nonspherical sample are almost twice the ones in both the spherical-dense and nonspherical-loose those. On the other hand, the comparisons between the spherical-dense and the nonspherical-loose samples show that the end bearing is slightly higher in the former sample while the shaft frictions in these samples nearly coincide with each

other. Thus, it can be interpreted that shaft friction in the non-spherical sample is more effective than that in the spherical sample.

- Installation processes of the jacked piles are also investigated at the micro-scale by utilizing both average coordination numbers and contact networks. According to the observations on the variations in coordination numbers during the penetration, it can be deduced that the changes are mainly observed in the first two zones, especially the first (core) zone, for each sample type. It is also seen that the penetration process leads to a continuous decrease in the coordination number for the dense samples while causing an increase, after an instantaneous reduction at the beginning, in the loose sample. In addition, the particle shape does not affect the general trend of the variations in the coordination numbers, although the nonspherical particles lead to a more pronounced effect of the penetration process. At micro-scale, the contact networks for each sample type are assessed. The observations show that the contact networks are uniformly distributed before the penetration process. Then, at the beginning of the penetration, the networks are broken, therefore the contact intensity decreases in all the samples. The less intense contact networks due to pile penetration are compatible with the instantaneous reduction in average coordination numbers.
- In the micro-scale investigation of the installation stages of replacement piles, variations in both the average coordination numbers and the intensity of contact networks are monitored. According to the coordination number results, it is seen that the changes in those are mainly observed in the first zone and the installation process leads to a decrease in the average coordination number for all the samples. This indicates that there is no considerable effect of both soil density state and particle shape on the soil response. The observations for the contact networks in all the samples present a similar finding. The installation process of replacement piles causes an interruption in stability of uniformly distributed contact network that leads to less intense contact networks since that represent a decrease in the coordination number, in all the samples. It is just observed that the reduction in the intensity of the contact network in the dense sample is slightly higher than it in the loose one. This result is also compatible with that obtained from the changes in the coordination numbers.

After the pile installation stage is completed in each model, a vertical loading test is conducted on each pile installed into the soil samples with different soil density states and particle shapes. For all the simulations, load-displacement curves in terms of total resistance, end bearing, and shaft resistance are obtained. These resistance forces and the pile displacements are also normalized as those obtained in the installation stage. The normalized load - normalized displacement curves are compared with each other to reveal the effects of soil density state and particle shape for both jacked and replacement piles, as well as the influences of pile installation method. The main conclusions are summarized the following:

- Reviewing the loading test results obtained for the jacked piles, it is noticed that the shaft friction shows a similar trend with the end bearing, and therefore, the total resistance, in the spherical sample. On the other hand, in nonspherical samples (loose and dense), the shaft friction mobilizes at a certain normalized pile displacement, while the end bearing and total resistance continues a gradual increase. In addition, the load-displacement curves obtained from the spherical-dense, nonspherical-dense, and nonspherical-loose samples are compared in terms of the total resistance, end bearing, and shaft friction. The comparisons indicate that all the resistance components are considerably higher for the dense-nonspherical sample. However, the obtained results from spherical-dense and nonspherical-loose samples are similar to each other. It means that the spherical-dense sample can only show as much resistance as the nonspherical loose one. These results clarify that both the density state and particle shape have a considerable effect on the bearing capacity of jack piles.
- The replacement piles installed into the samples with different density states and particle shapes are also subjected to vertical loading tests. According to the test results, there is a similar trend in each sample so that the shaft friction saturates at a certain magnitude, while the end baring and the total resistance continue to increase. In addition, it is seen that the bearing capacity of the replacement pile, in the nonspherical dense sample, is clearly higher than the other ones. Interestingly, the bearing capacity of the replacement pile in the spherical-dense sample is even less than it is in the nonspherical-loose one.

- To investigate the effects of installation method, the curves for the end bearing and the shaft friction obtained from the jacked piles are compared with those from the replacement piles for each sample. According to the comparison results, it is clear that the jacked piles have higher bearing capacities than the replacement piles irrespective of the density state and the particles shape of the sample. This is because the build-up stresses are developed on the jacked piles due to the occurrence of soil compression during the penetration stage. However, it is also observed that the influence of installation method on the shaft resistance is stronger than it is on the end bearing for all samples. The reason for this difference is that the surrounding soil becomes looser during the installation of a replacement pile, whereas jacked pile installation makes the soil denser.

7. CONCLUSION

Pile installation process has different effects on the properties of the surrounding soil. However, these influences are not completely apparent and they need to be ascertained. For that reason, soil - pile interaction and the impact of pile installation on soil behavior are still investigated using different techniques, such as field tests, laboratory tests, and numerical analyses based on the finite element method. However, none of these approaches can provide micro-scale observation. At this point, the discrete element method (DEM) is an alternative numerical way to analyze soil - pile interaction. Unlike the other techniques, DEM enables the micro-scale investigation in addition to the macro-scale one. Therefore, recently, this method has been widely used to model the mechanisms of pile installation and loading. Accordingly, this dissertation purposes to present a multiscale investigation of soil - pile interaction, using the DEM modelling, by considering both soil characteristics and pile construction approaches. For this purpose, the dissertation is framed upon three major subjects. Firstly, the influences of the soil properties at the micro (i.e. particles stiffness, particles size, particle size distribution, particle shape, inter-particle friction, and rolling friction) and macro scales (i.e. soil void ratio) on the pile penetration resistance are investigated. The observed effects especially show the importance of particular characteristics of soils on their multi-scale response to pile penetration. Secondly, after validating a DEM model using the experimental results obtained from the literature, three novel techniques are used to decrease the computational costs of DEM simulations. Based on comparisons of the penetration resistances, the validity of each approach is evaluated. Lastly, the soil samples with different soil density states and particle shapes are prepared using the approaches that are considered to decrease computational cost in the second part of the thesis. Then, these samples are subjected to two installation methods, and their vertical bearing capacities are evaluated using loading tests. As a result of the DEM analyses, influences of the density state, particle shape and pile installation technique on soil response to pile installation and loading are verified with at multiscale.

REFERENCES

Abu-Farsakh M.Y. and H.H. Titi, 2004, "Assessment of Direct Cone Penetration Test Methods for Predicting the Ultimate Capacity of Friction Driven Piles", *Journal of Geotechnical and Geoenvironmental Engineering*, Vol. 130, No. 9, pp. 935-944.

Adejumo T.W. and I.L. Boiko, 2013, "Effect of Installation Techniques on the Allowable Bearing Capacity of Modeled Circular Piles in Layered Soil", *International Journal of Advanced Technology & Engineering Research*, Vol. 2, No. 8, pp. 1536-1542.

Alshibli K.A. and M.B. Cil, 2018, "Influence of Particle Morphology on the Friction and Dilatancy of Sand", *Journal of Geotechnical and Geoenvironmental Engineering*, Vol. 144, No. 3, pp. 04017118.

Arroyo M., J. Butlanska, A. Gens, F. Calvetti, and M. Jamiolkowski, 2011, "Cone Penetration Tests in a Virtual Calibration Chamber", *Géotechnique*, Vol. 61, No. 6, pp. 525-531.

Arshad M.I., F.S. Tehrani, M. Prezzi, and R. Salgado, 2014, "Experimental *Study of Cone Penetration in Silica Sand Using Digital Image Correlation", Geotechnique*, Vol. 64, No. 7, pp. 551-569.

Barreto D. and C. O'Sullivan, 2012, "The Influence of Inter-Particle Friction and the Intermediate Stress Ratio on Soil Response under Generalised Stress Conditions", *Granular Matter*, Vol. 14, No. 4, pp. 505-521.

Bolton M.D., 1986, "The Strength and Dilatancy of Sands", *Géotechnique*, Vol. 36, No. 1, pp. 65-78.

Bolton M.D., M.W. Gui, J. Garnier, J.F. Corte, G. Bagge, J. Laue, and R. Renzi, 1999, "Centrifuge Cone Penetration Tests in Sand", *Geotechnique*, Vol. 49, No. 4, pp. 543-552.

Broere W. and A.F. Van Tol, 2006, "Modelling the Bearing Capacity of Displacement Piles in Sand", *Proceedings of the Institution of Civil Engineers: Geotechnical Engineering*, Vol. 159, No. 3, pp. 195-206.

Butlanska J., M. Arroyo, A. Gens, and C. O'Sullivan, 2014, "Multi-Scale Analysis of Cone Penetration Test (CPT) in a Virtual Calibration Chamber", *Canadian Geotechnical Journal*, Vol. 51, No. 1, pp. 51-66.

Chakraborty T. and R. Salgado, 2010, "Dilatancy and Shear Strength of Sand at Low Confining Pressures", *Journal of Geotechnical and Geoenvironmental Engineering*, Vol. 136, No. 3, pp. 527-532.

Chen Y., A. Deng, F. Lu, and H. Sun, 2020, "Failure Mechanism and Bearing Capacity of Vertically Loaded Pile with Partially-Screwed Shaft: Experiment and Simulations", *Computers and Geotechnics*, Vol. 118, No. November 2019, pp. 103337.

Chen Y., A. Deng, A. Wang, and H. Sun, 2018, "Performance of Screw-Shaft Pile in Sand: Model Test and DEM Simulation", *Computers and Geotechnics*, Vol. 104, pp. 118-130.

Chung Y.C. and J.Y. Ooi, 2008, "Influence of Discrete Element Model Parameters on Bulk Behavior of a Granular Solid under Confined Compression", *Particulate Science and Technology*, Vol. 26, No. 1, pp. 83-96.

Cinicioglu O. and A. Abadkon, 2015, "Dilatancy and Friction Angles Based on In Situ Soil Conditions", *Journal of Geotechnical and Geoenvironmental Engineering*, Vol. 141, No. 4, pp. 06014019.

Coetzee C.J., 2019, "Particle Upscaling: Calibration and Validation of the Discrete Element Method", *Powder Technology*, Vol. 344.

Cundall, P.A. and O.D.L. Strack, 1979, "A Discrete Numerical Model For Granular

Assemblies", *Géotechnique*, Vol. 29, No. 1, pp. 47-65.

Dai B.B., J. Yang, and C.Y. Zhou, 2016, "Observed Effects of Interparticle Friction and Particle Size on Shear Behavior of Granular Materials", *International Journal of Geomechanics*, Vol. 16, No. 1, pp. 1-11.

De Borst R. and P.A. Vermeer, 1984, "Possibilities and Limitations of Finite Elements for Limit Analysis", *Geotechnique*, Vol. 34, No. 2, pp. 199-210.

Duan N., Y.P. Cheng, and X. Xu, 2017, "Distinct-Element Analysis Of An Offshore Wind Turbine Monopile Under Cyclic Lateral Load", *Proceedings of the Institution of Civil Engineers: Geotechnical Engineering*, Vol. 170, No. 6, pp. 517-533.

Duan Nuo, Y.P. Cheng, and J.W. Liu, 2018, "DEM Analysis of Pile Installation Effect: Comparing a Bored and a Driven Pile", *Granular Matter*, Vol. 20, No. 3, pp. 20-36.

EDEM, 2018, "EDEM 2018 User Guide".

Esposito R.G., R.Q. Velloso, E. do A.V. Jr, and B.R. Danziger, 2018, "Multi-Scale Sensitivity Analysis of Pile Installation Using DEM", *Computational Particle Mechanics*, Vol. 5, No. 3, pp. 375-386.

Falagush O., G.R. McDowell, and H.-S. Yu, 2015a, "Discrete Element Modeling of Cone Penetration Tests Incorporating Particle Shape and Crushing", *International Journal of Geomechanics*, Vol. 15, No. 6, pp. 04015003.

Falagush O., G.R. McDowell, H.S. Yu, and J.P. de Bono, 2015b, "Discrete Element Modelling and Cavity Expansion Analysis of Cone Penetration Testing", *Granular Matter*, Vol. 17, No. 4, pp. 483-495.

Feng Y., R. Blumenfeld, and C. Liu, 2019, "Support of Modified Archimedes' Law Theory in Granular Media", *Soft Matter*, Vol. 15, No. 14, pp. 3008-3017.

Gan J. and A. Yu, 2020, "DEM Simulation of the Packing of Cylindrical Particles", *Granular Matter*, Vol. 22, No. 1, pp. 1-19.

Gavin K., D. Cadogan, A. Tolooiyan, and P. Casey, 2013, "The Base Resistance of Non-Displacement Piles in Sand. Part I: Field Tests", *Proceedings of the Institution of Civil Engineers: Geotechnical Engineering*, Vol. 166, No. 6, pp. 540-548.

Gezgin A.T., B. Soltanbeigi, and O. Cinicioglu, 2020, "Discrete-element Modelling of Pile Penetration to Reveal Influence of Soil Characteristics", *Proceedings of the Institution of Civil Engineers: Geotechnical Engineering*, pp. 1-18.

Gezgin A.T., B. Soltanbeigi, A. Altunbas, and O. Cinicioglu, 2021, "Multi-scale Investigation of Active Failure for Various Modes of Wall Movement", *Frontiers of Structural and Civil Engineering*, Vol. 15, pp. 961-979.

Gong J., J. Zou, L. Zhao, L. Li, and Z. Nie, 2019, "New Insights into the Effect of Interparticle Friction on the Critical State Friction Angle of Granular Materials", *Computers and Geotechnics*, Vol. 113, No. March, pp. 103105.

Griffiths D. V., 1982, "Computation of Bearing Capacity Factors Using Finite Elements", *Geotechnique*, Vol. 32, No. 3, pp. 195-202.

Guo Y. and X.B. Yu, 2016, "Design and Analyses of Open-Ended Pipe Piles in Cohesionless Soils", *Frontiers of Structural and Civil Engineering*, Vol. 10, No. 1, pp. 22-29.

Hamann T., G. Qiu, and J. Grabe, 2015, "Application of a Coupled Eulerian-Lagrangian Approach on Pile Installation Problems under Partially Drained Conditions", *Computers and Geotechnics*, Vol. 63, pp. 279-290.

Huang A.B. and M.Y. Ma, 1994, "An Analytical Study of Cone Penetration Tests in Granular Material", *Canadian Geotechnical Journal*, Vol. 31, No. 1, pp. 91-103.

Huang X., K.J. Hanley, C. O'Sullivan, and C.Y. Kwok, 2014, "Exploring the Influence

of Interparticle Friction on Critical State Behaviour Using DEM", *International Journal for Numerical and Analytical Methods in Geomechanics*, Vol. 38, No. 12, pp. 1276-1297.

Janda A. and J.Y. Ooi, 2016, "DEM Modeling of Cone Penetration and Unconfined Compression in Cohesive Solids", *Powder Technology*, Vol. 293, pp. 60-68.

Jiang M.D., Z.X. Yang, D. Barreto, and Y.H. Xie, 2018, "The Influence of Particle-Size Distribution on Critical State Behavior of Spherical and Non-Spherical Particle Assemblies", *Granular Matter*, Vol. 20, No. 4.

Jiang M.J., Y. Dai, L. Cui, Z. Shen, and X. Wang, 2014, "Investigating Mechanism of Inclined CPT in Granular Ground Using DEM", *Granular Matter*, Vol. 16, No. 5, pp. 785-796.

Jiang M.J., D. Harris, and H.H. Zhu, 2007, "Future Continuum Models for Granular Materials in Penetration Analyses", *Granular Matter*, Vol. 9, No. 1-2, pp. 97-108.

Jiang M.J., H.S. Yu, and D. Harris, 2006, "Discrete Element Modelling of Deep Penetration in Granular Soils", *International Journal for Numerical and Analytical Methods in Geomechanics*, Vol. 30, No. 4, pp. 335-361.

Jiang M.J., H.H. Zhu, and D. Harris, 2008, "Classical and Non-Classical Kinematic Fields of Two-Dimensional Penetration Tests on Granular Ground by Discrete Element Method Analyses", *Granular Matter*, Vol. 10, No. 6, pp. 439-455.

Jin Y.F., Z.Y. Yin, Z.X. Wu, and A. Daouadji, 2018, "Numerical Modeling of Pile Penetration in Silica Sands Considering the Effect of Grain Breakage", *Finite Elements in Analysis and Design*, Vol. 144, pp. 15-29.

Kang W., Y. Feng, C. Liu, and R. Blumenfeld, 2018, "Archimedes' Law Explains Penetration of Solids into Granular Media", *Nature Communications*, Vol. 9, No. 1, pp. 1-9.

Khoubani A. and M.M. Ahmadi, 2014, "Numerical Study of Ground Vibration Due to Impact Pile Driving", *Proceedings of the Institution of Civil Engineers: Geotechnical Engineering*, Vol. 167, No. 1, pp. 28-39.

Klotz E.U. and M.R. Coop, 2001, "An Investigation of the Effect of Soil State on the Capacity of Driven Piles in Sands", *Geotechnique*, Vol. 51, No. 9, pp. 733-751.

Li H., S. Liu, and L. Tong, 2019a, "Evaluation of Lateral Response of Single Piles to Adjacent Excavation Using Data from Cone Penetration Tests", *Canadian Geotechnical Journal*, Vol. 56, No. 2, pp. 236-248.

Li L., W. Wu, M. Hesham El Naggar, G. Mei, and R. Liang, 2019b, "DEM Analysis of the Sand Plug Behavior during the Installation Process of Open-Ended Pile", *Computers and Geotechnics*, Vol. 109, pp. 23-33.

Lin J. and W. Wu, 2012, "Numerical Study of Miniature Penetrometer in Granular Material by Discrete Element Method", *Philosophical Magazine*, Vol. 92, No. 28-30, pp. 3474-3482.

Liu J., N. Duan, L. Cui, and N. Zhu, 2019, "DEM Investigation of Installation Responses of Jacked Open-Ended Piles", *Acta Geotechnica*, Vol. 14, No. 6, pp. 1805-1819.

Liu Q.B. and B.M. Lehane, 2012, "The Influence of Particle Shape on the (Centrifuge) Cone Penetration Test (CPT) End Resistance in Uniformly Graded Granular Soils", *Geotechnique*, Vol. 62, No. 11, pp. 973-984.

Liu S. and J. Wang, 2016, "Depth-Independent Cone Penetration Mechanism by a Discrete Element Method (DEM)-Based Stress Normalization Approach", *Canadian Geotechnical Journal*, Vol. 53, No. 5, pp. 871-883.

Lobo-Guerrero S. and L.E. Vallejo, 2005, "DEM Analysis of Crushing around Driven Piles in Granular Materials", *Géotechnique*, Vol. 55, No. 8, pp. 617-623.

Lobo-Guerrero S. and L.E. Vallejo, 2007, "Influence of Pile Shape and Pile Interaction on the Crushable Behavior of Granular Materials around Driven Piles: DEM Analyses", *Granular Matter*, Vol. 9, pp. 241-250.

Lommen S., D. Schott, and G. Lodewijks, 2014, "DEM Speedup: Stiffness Effects on Behavior of Bulk Material", *Particuology*, Vol. 12, No. 1, pp. 107-112.

McDowell G.R., O. Falagush, and H.S. Yu, 2012, "A Particle Refinement Method for Simulating DEM of Cone Penetration Testing in Granular Materials", *Geotechnique Letters*, Vol. 2, No. 3, pp. 141-147.

Mitchell J.K., 1993, *Fundamentals Of Soil Behavior*, Wiley New York, Wiley.

Miyai S., M. Kobayakawa, T. Tsuji, and T. Tanaka, 2019, "Influence of Particle Size on Vertical Plate Penetration into Dense Cohesionless Granular Materials (Large-Scale DEM Simulation Using Real Particle Size)", *Granular Matter*, Vol. 21, No. 4, pp. 1-21.

Mo P.Q., A.M. Marshall, and H.S. Yu, 2015, "Centrifuge Modelling of Cone Penetration Tests in Layered Soils", *Geotechnique*, Vol. 65, No. 6, pp. 468-481.

Ni Q., C.C. Hird, and I. Guymer, 2010, "Physical Modelling of Pile Penetration in Clay Using Transparent Soil and Particle Image Velocimetry", *Geotechnique*, Vol. 60, No. 2, pp. 121-132.

O'Sullivan C., 2011, *Particulate Discrete Element Modelling: A Geomechanics Perspective, London*, Tylor and Francis Group.

Peng Z., X. Xu, K. Lu, and M. Hou, 2009, "Depth Dependence of Vertical Plunging Force in Granular Medium", *Physical Review E - Statistical, Nonlinear, and Soft Matter Physics*, Vol. 80, No. 2.

Phuong N.T.V., A.F. van Tol, A.S.K. Elkadi, and A. Rohe, 2016, "Numerical Investigation of Pile Installation Effects in Sand Using Material Point Method", *Computers*

and Geotechnics, Vol. 73, pp. 58-71.

Pucker T. and J. Grabe, 2012, "Numerical Simulation of the Installation Process of Full Displacement Piles", *Computers and Geotechnics*, Vol. 45, pp. 93-106.

Qin Z., L. Chen, C. Song, and L. Sun, 2017, "Field Tests to Investigate the Penetration Rate of Piles Driven by Vibratory Installation", *Shock and Vibration*, Vol. 2017.

Qiu G., S. Henke, and J. Grabe, 2011, "Application of a Coupled Eulerian-Lagrangian Approach on Geomechanical Problems Involving Large Deformations", *Computers and Geotechnics*, Vol. 38, No. 1, pp. 30-39.

Salgado R., J.K. Mitchell, and M. Jamiolkowski, 1998, "Calibration Chamber Size Effects on Penetration Resistance in Sand", *Journal of Geotechnical and Geoenvironmental Engineering*, Vol. 124, No. September, pp. 878-888.

Schnaid F. and G.T. Houlsby, 1991, "An Assessment of Chamber Size Effects in the Calibration of in Situ Tests in Sand", *Geotechnique*, Vol. 41, No. 3, pp. 437-445.

Schneider J.A., X. Xu, and B.M. Lehane, 2008, "Database Assessment of CPT-Based Design Methods for Axial Capacity of Driven Piles in Siliceous Sands", *Journal of Geotechnical and Geoenvironmental Engineering*, Vol. 134, No. 9, pp. 1227-1244.

Sharif Y., M. Ciantia, M.J. Brown, J.A. Knappett, and D. Ball, 2019, *Jonathan, Numerical Techniques For the Fast Generation of Samples Using the Particle Refinement Method*, Proceedings of the 8th International Conference on Discrete Element Methods, Enschede, the Netherlands.

Sheng D., K.D. Eigenbrod, and P. Wriggers, 2005, "Finite Element Analysis of Pile Installation Using Large-Slip Frictional Contact", *Computers and Geotechnics*, Vol. 32, No. 1, pp. 17-26.

Shi D., Y. Yang, Y. Deng, and J. Xue, 2019, "DEM Modelling of Screw Pile Penetration in Loose Granular Assemblies Considering the Effect of Drilling Velocity Ratio",

Granular Matter, Vol. 21, No. 3, pp. 1-16.

Sloan S.W. and M.F. Randolph, 1982, "Numerical Prediction of Collapse Loads Using Finite Element Methods", *International Journal for Numerical and Analytical Methods in Geomechanics*, Vol. 6, No. 1, pp. 47-76.

Soltanbeigi B., A. Podlozhnyuk, J.Y. Ooi, C. Kloss, and S.A. Papanicolopulos, 2017, "Comparison of Multi-Sphere and Superquadric Particle Representation for Modelling Shearing and Flow Characteristics of Granular Assemblies", *EPJ Web of Conferences*, Vol. 140, pp. 4-7.

Susila E. and R.D. Hryciw, 2003, "Large Displacement FEM Modelling of the Cone Penetration Test (CPT) in Normally Consolidated Sand", *International Journal for Numerical and Analytical Methods in Geomechanics*, Vol. 27, No. 7, pp. 585-602.

Tan Y. and G. Lin, 2013, "Full-Scale Testing of Open-Ended Steel Pipe Piles in Thick Varved Clayey Silt Deposits along the Delaware River in New Jersey", *Journal of Geotechnical and Geoenvironmental Engineering*, Vol. 139, No. 3, pp. 518-524.

Tolooiyan A. and K. Gavin, 2011, "Modelling the Cone Penetration Test in Sand Using Cavity Expansion and Arbitrary Lagrangian Eulerian Finite Element Methods", *Computers and Geotechnics*, Vol. 38, No. 4, pp. 482-490.

Tolooiyan A. and K. Gavin, 2013, "The Base Resistance of Non-Displacement Piles in Sand. Part II: Finite-Element Analyses", *Proceedings of the Institution of Civil Engineers: Geotechnical Engineering*, Vol. 166, No. 6, pp. 549-560.

Tran Q.A., B. Chevalier, and P. Breul, 2016, "Discrete Modeling of Penetration Tests in Constant Velocity and Impact Conditions", *Computers and Geotechnics*, Vol. 71, pp. 12-18.

Vaid Y.P. and S. Sasitharan, 1992, "The Strength and Dilatancy of Sand", *Canadian*

Geotechnical Journal, Vol. 29, No. 3, pp. 522-526.

Vangla P. and G.M. Latha, 2015, "Influence of Particle Size on the Friction and Interfacial Shear Strength of Sands of Similar Morphology", *International Journal of Geosynthetics and Ground Engineering*, Vol. 1, No. 1.

Wang Y., S. Sang, M. Zhang, X. Liu, and S. Yang, 2021, "Field Test of Earth Pressure at Pile-Soil Interface by Single Pile Penetration in Silty Soil and Silty Clay", *Soil Dynamics and Earthquake Engineering*, Vol. 145, pp. 106666.

Wang J. and B. Zhao, 2014, "Discrete-continuum Analysis of Monotonic Pile Penetration in Crushable Sands", *Canadian Geotechnical Journal*, Vol. 51, No. 10, pp. 1095-1110.

Wensrich C.M. and A. Katterfeld, 2012, "Rolling Friction as a Technique for Modelling Particle Shape in DEM", *Powder Technology*, Vol. 217, pp. 409-417.

White D.J. and M.D. Bolton, 2004, "Displacement and Strain Paths during Plane-Strain Model Pile Installation in Sand", *Geotechnique*, Vol. 54, No. 6, pp. 375-397.

White D.J. and B.M. Lehane, 2004, "Friction Fatigue on Displacement Piles in Sand", *Geotechnique*, Vol. 54, No. 10, pp. 645-658.

Wu Y. and H. Yamamoto, 2014, "Numerical Analysis of the Effect of Pile Tip Shape on Soil Behavior around Pile", *Geotechnical Engineering*, Vol. 45, No. 2, pp. 78-89.

Yan Z., S.K. Wilkinson, E.H. Stitt, and M. Marigo, 2015, "Discrete Element Modelling (DEM) Input Parameters: Understanding Their Impact on Model Predictions Using Statistical Analysis", *Computational Particle Mechanics*, Vol. 2, No. 3, pp. 283-299.

Yang Z.X., R.J. Jardine, B.T. Zhu, and S. Rimoy, 2014, "Stresses Developed around Displacement Piles Penetration in Sand", *Journal of Geotechnical and Geoenvi-*

ronmental Engineering, Vol. 140, No. 3, pp. 1-13.

Yin F., Y. Xiao, H. Liu, H. Zhou, and J. Chu, 2018, "Experimental Investigation on the Movement of Soil and Piles in Transparent Granular Soils", *Geotechnical and Geological Engineering*, Vol. 36, No. 2, pp. 783-791.

Yu H.S. and J.K. Mitchell, 1998, "Analysis of Cone Resistance: Review of Methods", *Journal of Geotechnical and Geoenvironmental Engineering*, Vol. 124, No. 2, pp. 140-149.

Zarrabi M. and A. Eslami, 2016, "Behavior of Piles under Different Installation Effects by Physical Modeling", *International Journal of Geomechanics*, Vol. 16, No. 5, pp. 1-12.

Zhang C., G.D. Nguyen, and I. Einav, 2013, "The End-Bearing Capacity of Piles Penetrating into Crushable Soils", *Geotechnique*, Vol. 63, No. 5, pp. 341-354.

Zhang L.M. and H. Wang, 2009, "Field Study of Construction Effects in Jacked and Driven Steel H-Piles", *Geotechnique*, Vol. 59, No. 1, pp. 63-69.

Zhang Z. and Y.H. Wang, 2015, "Three-Dimensional DEM Simulations of Monotonic Jacking in Sand", *Granular Matter*, Vol. 17, pp. 359-376.

Zhao H., A.M. Asce, J. Zhang, P. Qiu, and S. Ji, 2019, "Hierarchical Modeling Method for DEM Simulation and Its Application in Soil - Pile - Cap Interaction and Impact Case", Vol. 19, No. 7, pp. 04019076.

Zienkiewicz O.C. and R.L. Taylor, 2000, *The Finite Element Method: Solid Mechanics*, Oxford, UK, Butterworth-Heinemann.